Journal of Energy Chemistry 62 (2021) 377–407

Contents lists available at ScienceDirect

Journal of Energy Chemistry

journal homepage: www.elsevier.com/locate/jechem

http://www.journals.elsevier.com/journal-of-energy-chemistry/

Review

Recent advances in catalytic systems for CO_2 conversion to substitute natural gas (SNG): Perspective and challenges

I. Hussain [a], A.A. Jalil [b,c,*], N.S. Hassan [b], M.Y.S. Hamid [b,c]

[a] Department of Chemistry, Faculty of Science, Universiti Teknologi Malaysia, 81310 UTM Johor Bahru, Johor, Malaysia
[b] School of Chemical and Energy Engineering, Faculty of Engineering, Universiti Teknologi Malaysia, 81310 UTM Johor Bahru, Johor, Malaysia
[c] Centre of Hydrogen Energy, Institute of Future Energy, 81310 UTM Johor Bahru, Johor, Malaysia

ARTICLE INFO

Article history:
Received 10 February 2021
Revised 19 March 2021
Accepted 22 March 2021
Available online 1 April 2021

Keywords:
CO_2 utilization
CO_2 methanation
SNG
Catalytic systems
Deactivation
Mechanism

ABSTRACT

It has been well established that carbon dioxide (CO_2) is one of the main greenhouse gasses and a leading driver of climate change. The chemical conversion of CO_2 to substitute natural gas (SNG) in the presence of renewable hydrogen is one of the most promising solutions by a well-known process called CO_2 methanation. There have been comprehensive efforts in developing effective and efficient CO_2 methanation catalytic systems. However, the choice of competitive and stable catalysts is still a monumental obstruction and a great challenge towards the commercialization and industrialization of CO_2 methanation. It is necessary to emphasize the critical understandings of intrinsic and extrinsic interactions of catalyst components (active metal, support, promoter, etc.) for enhanced catalytic performance and stability during CO_2 methanation. This study reviews the up-to-date developments on CO_2 methanation catalysts and the optimal synergistic relationship between active metals, support, and promoters during the catalytic activity. The existing catalysts and their novel properties for enhanced CO_2 methanation were elucidated using the state-of-the-art experimental and theoretical techniques. The selection of an appropriate synthesis method, catalytic activity for CO_2 methanation, deactivation of the catalysts, and reaction mechanisms studies, have been explicitly compared and explained. Therefore, future efforts should be directed towards the sustainable developments of catalytic configurations for successful industrial applications of CO_2 utilization to SNG using CO_2 methanation.

Dr. Ijaz Hussain was born in Lahore, Pakistan on 02 June 1986. He received a merit scholarship and graduated from Forman Christian College (A Chartered University) with a Bachelor of Science (Honor) major in chemistry. He remained at Forman Christian College (A Chartered University) to complete his Master of Philosophy (MPhil) in chemistry. He joined Pakistan Space & Upper Atmosphere Research Commission (SUPARCO) to conduct his research on satellite data application in net primary productivity under the supervision of Professor Dr. S.E. Benjamin. Then he joined different academic and research institutes as a lecturer to explore and innovate his skills. He moved to Malaysia in 2018 to continue his PhD in Chemistry. In 2020, he received his PhD in Chemistry under the supervision of Professor Dr. Aishah Abdul Jalil. His PhD thesis focused on the design of metal-loaded fibrous mordenite zeolite for carbon monoxide methanation. Currently, he is working as a research fellow under Professor Dr. Aishah Abdul Jalil, School of Chemical and Energy Engineering and Centre of Hydrogen Energy, Institute of Future Energy Universiti technology Malaysia. He has participated in many international seminars and conferences. He has published over 25 papers in local and international journals in the field of heterogeneous catalysis for energy and environmental applications. His current research focuses on designing heterogeneous catalytic materials for CO and CO_2 methanation, CO_2 photoreduction and CO oxidation, dry reforming of methane and photocatalysis for sustainable methane and hydrogen generation. In particular, his work is focused on CO_2 capturing and chemical conversion to valuable products.

* Corresponding author at: School of Chemical and Energy Engineering, Faculty of Engineering, Universiti Teknologi Malaysia, 81310 UTM Johor Bahru, Johor, Malaysia.
E-mail address: aishahaj@utm.my (A.A. Jalil).

https://doi.org/10.1016/j.jechem.2021.03.040

Professor Aishah Abdul Jalil received her B.Eng in Industrial Chemistry (1989) and M.Eng in Chemical and Environmental Engineering (1995) from Kitami Institute of Technology, Hokkaido, Japan. She worked for a year in a Japanese company before starting her career as a lecturer at Universiti Teknologi Malaysia (UTM), Johor in 1996. She returned to Japan two years later to pursue her PhD at Hokkaido University in Sapporo, sponsored by the Hitachi Scholarship Foundation and graduated in Molecular Chemistry in 2002. She has promoted to Senior Lecturer in 2005, perpetually involve in both teaching and research with the sole aim of guiding the next generation towards a higher level of education. Currently, Professor Aishah Abdul Jalil is one of the leading and prestigious scientists at the School of Chemical and Energy Engineering and Centre of Hydrogen Energy, Institute of Future Energy, UTM. With the research interest in syntheses of advanced and zeolitic materials, she utterly implementing "Chemistry for Green Applications" via electrochemistry, organic chemistry, adsorption, photocatalysis as well as gaseous catalytic reactions. To date, she managed to supervise more than 25 PhD students and postdoctoral research fellows as well as published more than 250 scientific papers in high-impact international and local journals. She has also coauthored of several book chapters and has licensed industrial patents and she is the Editor-in-chief of Malaysian Journal of Catalysis (eISSN: 0128-2581).

Dr Nurul Sahida Hassan received her PhD in Chemical Engineering from the Universiti Teknologi Malaysia in 2019 with a specialization in the synthesis and characterization of advanced material for heterogeneous solid acid catalysts, particularly in wastewater treatment. Previously, she has completed Master in Science (Chemistry) and degree in Bachelor of Science (Chemistry) from Universiti Teknologi Malaysia. Before pursuing her PhD study, she worked as a chemistry lecturer at Universiti Teknologi Mara Pahang and have gained much experience in the teaching field, especially in organic chemistry. At present, she is working as a postdoctorate fellowship in the School of Chemical and Energy Engineering at the Universiti Teknologi Malaysia. To date, she has published 29 ISI high-impact international journal articles in the field of heterogeneous catalysis for energy and environmental applications. Her area of expertise includes the development of advanced heterogeneous catalysis for energy and sustainability. In particular, her work is focused on carbon dioxide conversion and biomass volarization.

Dr Muhamed Yusuf Shahul Hamid was born in Penang, Malaysia in the year 1991. He received his bachelor's degree, majoring in chemical engineering from Universiti Malaysia Pahang, Malaysia. Through a fast-track program, he directly continued to pursue a doctoral degree in chemical engineering from Universiti Teknologi Malaysia, Malaysia under the scholarship from Malaysian government. His researched thesis focused on the development work of advanced silica material catalysts for combating greenhouse gasses emission. His scientific works were published in high-impact factor international journals and he graduated on time in 2018. Following that, Dr Yusuf continued to explore the potential industry for the application of his research niche. He worked at oil and gas-based company as a research and development engineer. He was assigned to lead a project for carbon dioxide capture using an ammonia absorption system. Two years later, in December 2020, he returned and became a senior lecturer at the Department of Chemical Engineering, School of Chemical and Energy Engineering, Universiti Teknologi Malaysia. He is also a research member at Green Technologi and Advanced Materials (GTAM) research group, Centre of Hydrogen Energy, Institute of Future Energy Universiti Teknologi Malaysia. His research interest is geared towards (but not limited to) acid-base catalysis and advance material for simultaneous renewable energy production and greenhouse gases elimination.

1. Introduction

Socioeconomic and scientific developments have increased the global energy demand due to the increasing human population, urbanization, modernization, and industrialization. Crude oil, coal, and natural gas, known as fossil fuels, are the main energy sources that have provided almost 85% of the world's primary energy in recent years. This high dependency on fossil fuels is escorted by a massive emission of anthropogenic greenhouse gases (GHGs) to the atmosphere, mostly in the form of carbon dioxide (CO_2). It has caused global warming, climate change, and various other associated environmental concerns, including acid rain, extreme weather events, imbalanced food distributions, disturbed nutrition, and mass migration of birds and animals [1–6]. According to recent scientific reports, atmospheric CO_2 can last from 100 to 10,000 years with related climate destruction consequences. The atmospheric CO_2 has been increased by 40% from 1750 to 2011 with > 400 million ppm. The same amount of CO_2 was released only in 2013, which is the worst in the global historical records so far; the most dangerous thing is that 50% of the total atmospheric CO_2 was released within 45 years. Before the industrial revolution, the concentration of atmospheric CO_2 was ~ 280 ppm, which has increased to ~ 410 ppm, and the global CO_2 emissions smashed 33 gigatonnes (Gt) in 2018 [7–10]. Recently, different techniques, such as photocatalysis, electrocatalysis, and thermocatalysis have been used to recycle atmospheric CO_2 into value-added chemicals and fuels, including methane, methanol, ethanol, syngas, as well as a number of other products [11–23].

In addition, the US Energy Information Agency (EIA) has projected a 48% increase in the world's energy consumption by 2040 from 549 to 815 quadrillions Btu. On the other hand, fossil fuels are being depleted very fast as predicted by Hubbert's curve. In such circumstances, CO_2 conversion into substitute natural gas (SNG) by CO_2 methanation is one of the promising ways to reduce atmospheric CO_2 and fulfill the high-energy demands. SNG has high calorific value (55.7 kJ g^{-1}) than coal (39.3 kJ g^{-1}) and petroleum (43.6 kJ g^{-1}); it produces a lower amount of CO_2 compared to coal and petroleum [24,25]. Due to the existing pipeline networks, filling stations, and storage facilities, SNG can be stored and distributed without additional costs [26–34].

In the last few decades, serval studies have been investigated to examine CO_2 methanation over various types of catalytic systems to produce SNG. From a thermodynamic perspective, it is still possible to boost catalytic efficiency by lowering temperatures, while simultaneously increasing the yield and selectivity of methane by reducing the effect of multiple side reactions. Coke is generated because of these multiple side reactions during CO_2 methanation, which may trigger catalyst deactivation by blocking active sites on the surface of catalysts (will be discussed in thermodynamic section). Furthermore, due to its exothermic nature, CO_2 methana-

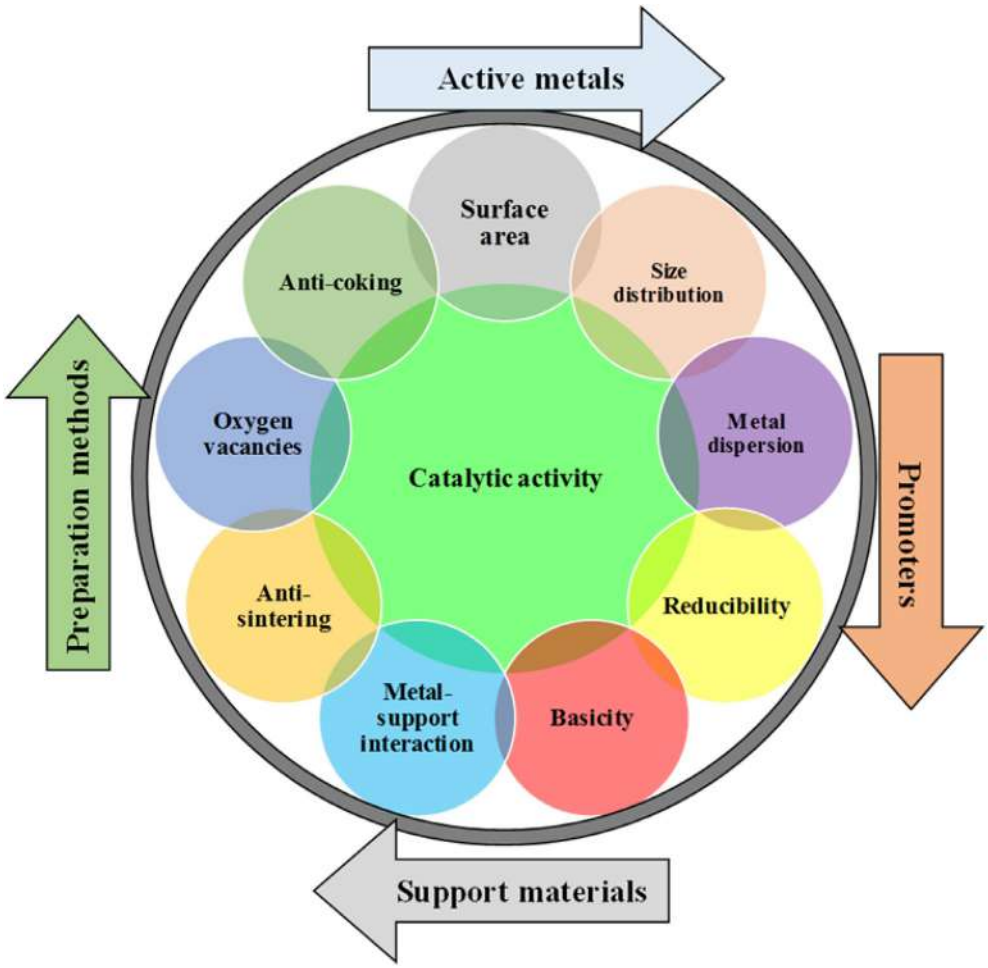

Fig. 1. Different catalytic properties for highly active catalytic systems for CO_2 methanation.

tion and other multiple side reactions emit a lot of heat, resulting in hotspots in the reactor and catalyst deactivation. Since different intermediates come from multiple side reactions, elucidating the reaction mechanism during CO_2 methanation is also a difficult task. These issues make the CO_2 methanation is a complicated reaction. Therefore, the development of highly efficient and stable catalysts is still a major challenge for the commercialization of CO_2 methanation [35–38].

In previous review studies, numerous CO_2 methanation issues and aspects have been analyzed and elucidated [35–49]. Nevertheless, there is still some gap in a state of the art knowledge devoted exclusively to synergistic interactions between the catalytic activity and catalytic characteristics. In an effort to fill this gap, this review updates and clarifies innovations for various latest developments in catalytic systems for CO_2 methanation with contemporary evaluation and synergistic relationship between oxygen vacancies, strong metal-support interaction, particle size, metal dispersion, chemical composition, acidity/basicity, reducibility, porosity, and surface area. The studies regarding the CO_2 conversion into methanol, hydrocarbons, higher alcohols, CO, dimethyl ether, formic acid, and formates by photo-/electrochemical processes are not focused in this review. Firstly, the thermodynamics and reaction chemistry of CO_2 methanation are addressed. Then the developments in catalytic systems for CO_2 methanation with active phase (metals), various types of supporting materials, promoters, and methods of preparation are deeply discussed, with an emphasis on their optimal synergistic relationships between surface area, electronic/redox properties, structural properties, basicity, metal-support interaction, oxygen vacancies, and reducibility during the catalytic activity (Fig. 1). We also summarize the recent improvements in metal-based catalysts, promoter-based catalysts of different supporting materials, including conventional, structural, zeolites, MOF, carbon, and other novel catalytic systems. Based on the theoretical and experimental studies, the deactivation of the catalysts and reaction mechanisms are also reviewed. Finally, the conclusions and outlook are provided.

2. A brief history of CO_2 methanation

The CO and CO_2 methanation techniques were discovered in 1902 by Paul Sabatier and Jean-Baptiste Senderens, and have been used in various applications for over 100 years [31,50,51]. During the late 1970 s oil crisis, methanation, or the hydrogenation of CO and CO_2, became very important for SNG production. In the 1980 s, basic studies on CO_2 methanation processes were conducted, with an emphasis on the use of blast furnace gas or coke oven gas for downstream methanation. However, due to the substantial effort needed to clean these gases, only a few of these ideas have made it to the commercial-scale [33,52,53]. Earth's fossil fuel reserves are limited in quantity and as the demand for fuel increases, these sources are being depleted. The need to switch from fossil fuels to renewable and sustainable energy sources was another big explanation for CO_2 methanation's recognition.

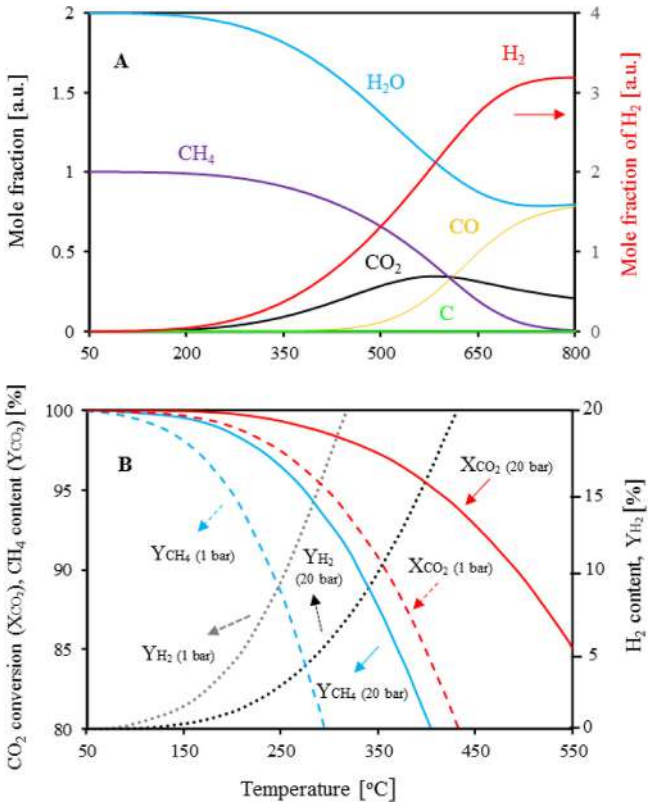

Fig. 2. (A) Product fraction of CO_2 methanation at equilibrium (1 bar and CO_2/H_2 = 1:4) obtained using HSC chemistry software 6.0 via Gibbs free energy minimizing method. The results are according with published data [56]. (B) Equilibrium conversion of CO_2, H_2 and formation of CH_4 in CO_2 methanation at temperatures and pressures using H_2/CO_2 = 4:1. Adapted from [43].

The CO_2 methanation process has received a renewed interest in research institutions and industries because of the growing demand for electricity storage, which has been fueled by rising wind and solar power share. Hashimoto et al. [54] suggested a combination of CO_2 methanation and seawater electrolysis as a way to avoid global warming and recycle CO_2 as early as the 1980 s. In 2009, Sterner et al. [55] resurrected this concept for the alleviation of climate change and the conservation of energy.

$$CO_2\ (g) + 4H_2\ (g)\ CH_4\ (g) + 2H_2O\ (g)\ \Delta H = -165\ kJ/mol \quad (1)$$

$$CO\ (g) + 3H_2\ (g)\ CH_4\ (g) + H_2O\ (g)\ \Delta H = -206.1\ kJ/mol \quad (2)$$

3. Thermodynamic considerations of CO_2 methanation

Thermodynamically, CO_2 methanation is a feasible reaction to produce CH_4 along with H_2O as a byproduct using the stoichiometric molar ratio of feed gases (H_2: CO_2; 4:1), according to Eq. (1) at relatively low temperature (200-250°C) and atmospheric pressure, as shown in Fig. 2A. On increasing the temperature (above 450°C) CO byproduct becomes more significant, which is produced by a side reaction called a reverse water gas shift reaction (RWGS; $H_2 + CO_2 \rightleftharpoons CO + H_2O$), and at the same time, unconverted H_2 and CO_2 also start to rise, with a significant drop in the CH_4 formation. As the CO_2 methanation is a strongly exothermic reaction along with a significant change in enthalpy (ΔH = -165 kJ/mol), thereby the CO_2 methanation activity is unfavorable at elevated reaction temperatures. The mole fraction of CO_2 reaches its maximum value when the temperature goes above 550°C and then falls due to RWGS, which dominates at high temperatures. Using a stoichiometric molar ratio of feed gases, no significant amount of carbon deposition is generated during CO_2 methanation [56–63].

3.1. Thermodynamic parameters and multiple side reactions during CO_2 methanation

CO_2 methanation involves several side reactions, as shown in Table 1, each with its own set of thermodynamic parameters. In Table 2, it can be seen that these all reactions are temperature-dependent and have a major influence on methane formation during CO_2 methanation [24,35]. Hussain et al. [35] performed experimental and thermodynamic analysis for CO_2 methanation; they studied the thermodynamic parameters, including equilibrium constant (ln (K)), Gibbs energy (ΔG), entropy (ΔS), and enthalpy change (ΔH) using different temperatures. Fig. 3 and Tables 1 display the ln (K) and Gibbs energy (ΔG) values for all potential reactions involved in CO_2 methanation. As can be seen that the reactions, including CO reduction (11), CO methanation (9), Boudouard reaction (7), CO_2 reduction (2), and CO_2 methanation (1) have positive ln (K), and negative ΔG and ΔH values, indicating their high spontaneity and exothermicity. It confirms that these are the most likely and dominant reactions during the methanation process. However, reverse water gas shift reaction (4), the reverse dry reforming of methane (6), and CH_4 cracking (8) have negative ln (K) and positive ΔG and ΔH values, indicating their infeasibility and endothermicity during methanation, particularly at low temperatures. As temperature increases, these reactions become significant and feasible, e.g., the cracking of CH_4 (8). It is noteworthy that the CO_2 hydrogenation (5) and CO hydrogenation (12) reactions are more significant and feasible in the range of 450–500 °C. However, these reactions decline and become infeasi-

Table 1
Possible reactions involved in CO_2 methanation with their corresponding equilibrium constant (ln(K)), Gibbs free energy (ΔG), entropy (ΔS) and enthalpy change (ΔH) values at T = 25°C and P = 0.1 MPa [35].

No.	Reactions	Chemical equations	ln(K)	ΔG	ΔS	ΔH
1	CO_2 methanation	CO_2 (g) + $4H_2$ (g) ⇌ CH_4 (g) + $2H_2O$ (g)	24.868	−141.932	−214.497	−164.747
2	CO_2 reduction	CO_2 (g) + $2H_2$ (g) ⇌ C + $2H_2O$ (g)	11.003	−62.800	−91.722	−90.147
3	CO_2 hydrogenation to CH_3OH	$2CO_2$ (g) + $3H_2$ (g) ⇌ CH_3OH (g) + $4H_2O$ (g)	−0.61	3.484	−177.109	−49.321
4	Reverse water gas shift	CO_2 (g) + $2H_2$ (g) ⇌ CO (g) + H_2O (g)	−5.011	28.602	42.045	41.138
5	CO_2 hydrogenation to C_2H_6	$2CO_2$ (g) + $7H_2$ (g) ⇌ C_2H_6 (g) + $4H_2O$ (g)	27.759	−158.43	−357.361	−264.978
6	Dry reforming of CH_4	CO_2 (g) + CH_4 (g) ⇌ 2CO (g) + $2H_2$ (g)	−29.879	170.535	256.542	247.023
7	Boudouard reaction	2CO (g) ⇌C + CO_2 (g)	21.026	−120.004	−175.812	−172.423
8	CH_4 cracking	CH_4 (g)⇌C + $2H_2$ (g)	−8.853	50.53	80.73	74.6
9	CO methanation	CO (g) + $3H_2$ (g) ⇌ CH_4 (g) + H_2O (g)	19.857	−113.330	−172.452	206
10	CO hydrogenation to CH_3OH	CO (g) + $2H_2$ (g) ⇌CH_3OH (g)	4.401	−25.118	−219.153	−90.459
11	CO reduction	CO (g) + H_2 (g) ⇌C + H_2O (g)	16.015	−91.402	−133.767	−131.285
12	CO hydrogenation to C_2H_6	2CO (g) + $5H_2$ (g) ⇌ C_2H_6 (g) + $2H_2O$ (g)	37.782	−215.635	−441.45	−347.254

Table 2
Interpretation of ΔG and ln (K) values in Fig. 4, for involved reactions in CO_2 methanation [35].

No.	Reaction name	Reaction equation	Remarks
1	CO_2 methanation	CO_2 (g) + $4H_2$ (g) $\rightleftharpoons CH_4$ (g) + $2H_2O$ (g)	Thermodynamically feasible and spontaneous for T < 600 °C, exothermic.
2	CO_2 reduction	CO_2 (g) + $2H_2$ (g) $\rightleftharpoons$ C + $2H_2O$ (g)	Thermodynamically feasible and spontaneous for T < 650 °C, exothermic.
3	CO_2 hydrogenation to CH_3OH	$2CO_2$ (g) + $3H_2$ (g) $\rightleftharpoons CH_3OH$ (g) + $4H_2O$ (g)	Thermodynamically feasible and spontaneous for T < 25 °C, exothermic.
4	Reverse water gas shift	CO_2 (g) + $2H_2$ (g) $\rightleftharpoons$ CO (g) + H_2O (g)	Thermodynamically feasible and spontaneous for T > 800 °C, endothermic.
5	CO_2 hydrogenation to C_2H_6	$2CO_2$ (g) + $7H_2$ (g) $\rightleftharpoons C_2H_6$ (g) + $4H_2O$ (g)	Thermodynamically feasible and spontaneous for T < 425 °C, exothermic.
6	Dry reforming of CH_4	CO_2 (g) + CH_4 (g) $\rightleftharpoons$ 2CO (g) + $2H_2$ (g)	Thermodynamically feasible and spontaneous for T > 625 °C, endothermic.
7	Boudouard reaction	2CO (g) $\rightleftharpoons$ C + CO_2 (g)	Thermodynamically feasible and spontaneous for T < 700 °C, exothermic.
8	CH_4 cracking	CH_4 (g) $\rightleftharpoons$ C + $2H_2$ (g)	Thermodynamically feasible and spontaneous for T > 525 °C, endothermic.
9	CO methanation	CO (g) + $3H_2$ (g) $\rightleftharpoons CH_4$ (g) + H_2O (g)	Thermodynamically feasible and spontaneous for T < 625 °C, exothermic.
10	CO hydrogenation to CH_3OH	CO (g) + $2H_2$ (g) $\rightleftharpoons$ CH_3OH (g)	Thermodynamically feasible and spontaneous for T < 150 °C, exothermic.
11	CO reduction	CO(g) + H_2 (g) $\rightleftharpoons$ C + H_2O (g)	Thermodynamically feasible and spontaneous for T < 675 °C, exothermic.
12	CO hydrogenation to C_2H_6	2CO (g) + $5H_2$ (g) $\rightleftharpoons C_2H_6$ (g) + $2H_2O$ (g)	Thermodynamically feasible and spontaneous for T < 500 °C, exothermic.

ble after 500 °C. The hydrogenations of CO and CO_2 to CH_3OH (numbers 10 and 3) are more significant at low temperatures and vice versa. Based on the foregoing findings, it was proposed that CO_2 methanation is a complex process involving multiple competitive side reactions that affect overall methane yield. As a result, in order to achieve high selectivity and methane yield during CO_2 methanation, reaction conditions must be optimized. According to Le Chatelier's principle, changing the different parameters (e.g., temperature, H_2/CO_2, and pressure) thermodynamically can boost the CO_2 methanation activity. For example, using high pressure can increase the CO_2 methanation activity, as previously reported [43], shown in Fig. 2B. They found that 1 bar (below 225 °C) or 20 bar (300 °C) pressure is required to achieve at least 98% of CO_2 conversion during the CO_2 methanation reaction.

3.2. Effect of H_2/CO_2 ratio on CO_2 methanation

Several studies have stated that the change in H_2/CO_2 ratio has a major impact on CO_2 methanation activity [57–59,64–67]. For example, Ahmad et al. [59] reported that H_2/CO_2 played an important role in the equilibrium conversion of CO_2, methane yield, the selectivity of CO and methane, as shown in Fig. 4. It is noteworthy that the molar ratio of H_2/CO_2 has a significant impact on the equilibrium conversion of CO_2 (Fig. 4A). Using the H_2/CO_2 ratio of 2:1, the CO_2 conversion is lower than that of H_2/CO_2 of 4:1 at the same pressure, indicating that H_2 acted as a limiting reactant during CO_2 methanation (Eq. (1)). The higher H_2/CO_2 ratio (≥4) results in excess H_2 molecules on the catalyst surface to reduce the available active sites on the catalytic surface during CO_2 methanation, resulting in increased product yield and improved CH_4 selectivity (Fig. 4B, Fig. 4C). In addition, the selectivity of CO during CO_2 methanation is an important factor for high methane yield; the higher H_2/CO_2 ratio significantly reduces CO formation (Fig. 4D). Similar results were reported by other studies of CO_2 methanation [57,68]. Hussain et al. [35] also explained the effect of the H_2/CO_2 ratio on the selectivity of methane and CO_2 conversion during CO_2 methanation. They reported that at low temperatures, the main products are H_2O, CO_2, and C with lower H_2:CO_2 of 1:1. The RWGS: CO_2 (g) + $2H_2$ (g) $\rightleftharpoons$ CO (g) + H_2O (g) produces more CO as the temperature rises above 400 °C. As the temperature increases, the CH_4 selectivity decreases, suggesting that CO_2 methanation is unfavorable at high temperatures. As the H_2/CO_2 ratio continues to increase, the CH_4 selectivity and CO_2 conversion are significantly enhanced (100%) using H_2/CO_2 of 4:1.

3.3. Effects of pressure on CO_2 methanation

It is generally accepted that if one or more of the reactants are gas then increasing pressure will effectively increase the concentration of the reactant molecules and speed up the reaction. The particles are, therefore on average, closer together and collisions between the particles will occur more frequently. Several studies have documented that increasing pressure dramatically improves the conversion of CO_2, selectivity, and yield of methane [38,40,57,69,70]. For example, Ahmad et al. [59] found that pressure was a significant factor in achieving high selectivity and yield of CH_4 during the equilibrium conversion of CO_2, as shown in Fig. 5. It is clear to notice that the equilibrium conversion of CO_2 to methane has enormously enhanced when pressure was increased from 1 to 100 bar (Fig. 5A). A similar trend was observed for methane yield and selectivity during CO_2 methanation (Fig. 5B, Fig. 5C) In contrast, CO selectivity decreased rapidly as the pressure increased from 1 to 100 bar (Fig. 5D). It should be noted that during CO_2 methanation at various pressures, there are no major improvements in CH_4 selectivity at low temperatures (below 700 K). As the temperature is raised, the CO_2 conversion, selectivity, and yield of methane at high pressures all increase noticeably. However, from an industrial and economical perspective, CO_2 methanation should be carried out at a low pressure using high temperature. Since the high-pressure equipment is dangerous to use, low temperatures during the chemical phase are not appropriate for accelerating the reaction rate [35].

4. Reaction chemistry of CO_2 methanation

From a thermodynamic perspective, CO_2 methanation is a reversible, exothermic, and favorable reaction at room temperature and atmospheric pressure; however, experimental CO_2 methanation does not produce significant methane yield using these conditions. Even though CO_2 appears to be a simple molecule, it has a linear, highly inert, stable, and diamagnetic molecule. According to molecular orbital theory, there are formal double bonds between O and C; two combination orbitals (O2s + O2s and O2s-O2s) of O and the carbon 2 s and 2p(z) orbitals combine to make two sigma bonding orbitals and two sigma antibonding orbitals, as shown in Fig. 6. The carbon 2p(y) combines with the group orbital O2p(y) + O2p(y) and the carbon 2p(x) combines with the group orbital O2p(x) + O2p(x). This generates two π^* antibonding molecular orbitals and two π bonding molecular orbitals. The other four p orbitals on the oxygen atoms are non-bonding molecular orbitals.

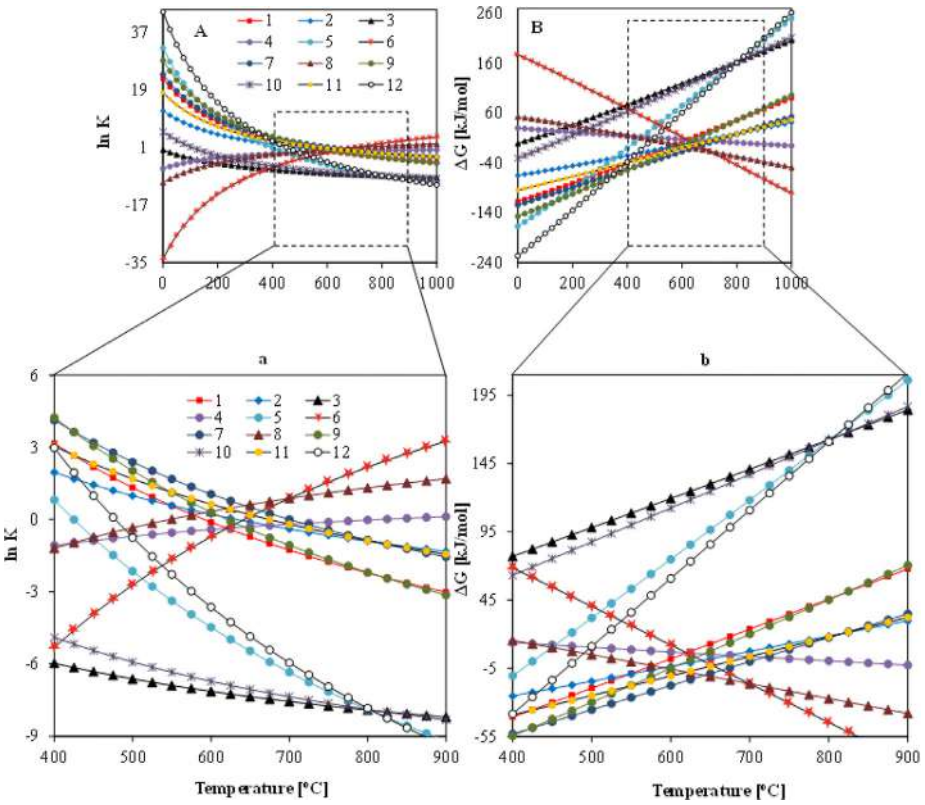

Fig. 3. (A) Equilibrium constants and (B) Gibbs free energy of possible multiple side reactions during CO2 methanation activity. Fig. 3 (a, b) for better view. Reprinted with permission from [35]. Copyright 2021 Elsevier.

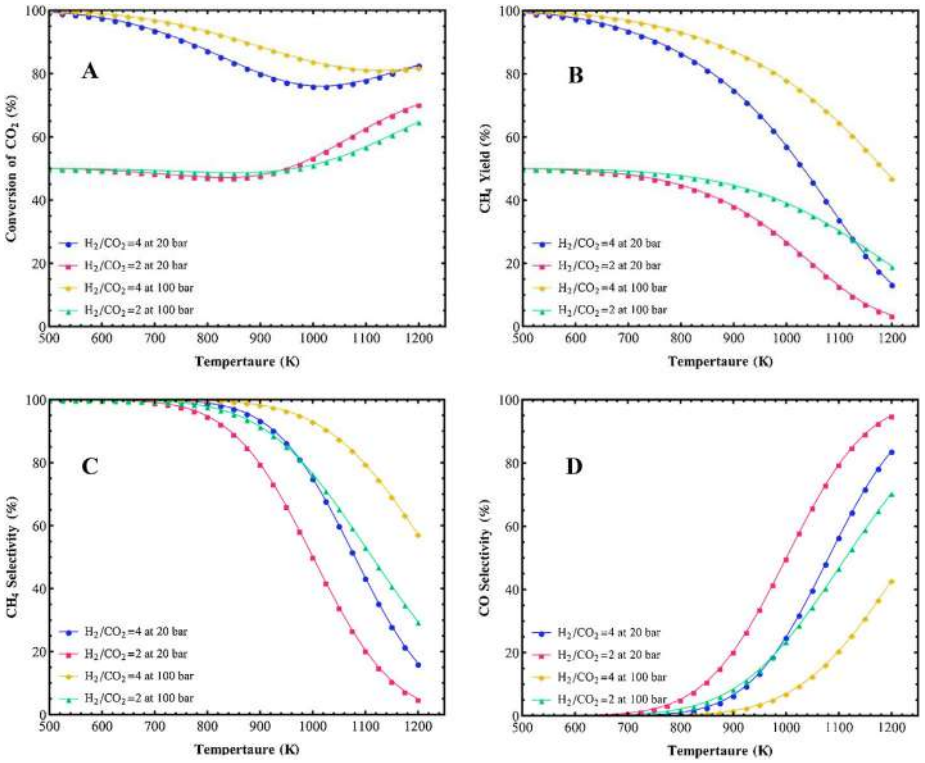

Fig. 4. Effect of H_2/CO_2 ratio on (A) CO_2 conversion, (B) CH_4 yield, (C) CH_4 selectivity and (D) CO selectivity. Reprinted with permission from [59]. Copyright 2016 Elsevier.

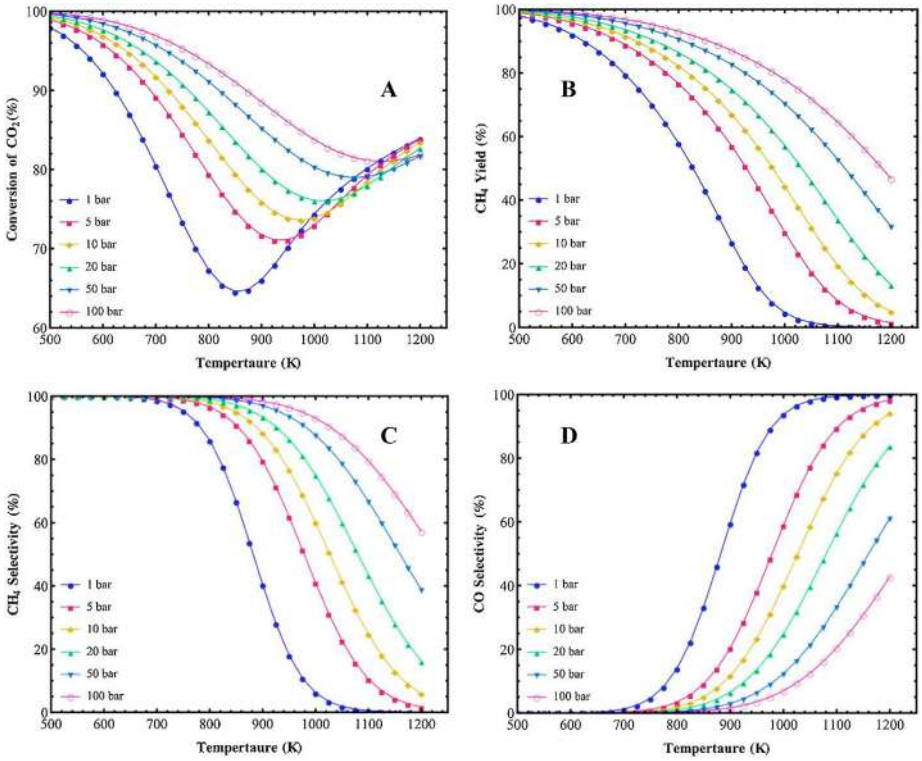

Fig. 5. Effect of pressure on (A) CO_2 conversion, (B) CH_4 yield, (C) CH_4 selectivity and (D) CO selectivity. Reprinted with permission from [59]. Copyright 2016 Elsevier.

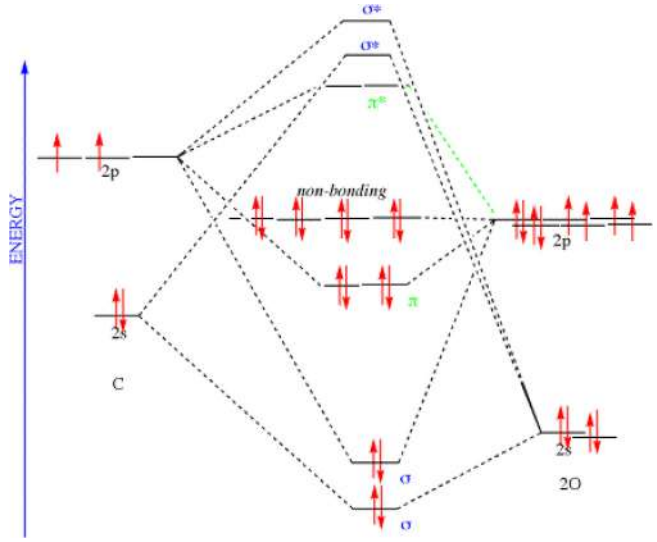

Fig. 6. The molecular orbital diagram of carbon dioxide.

This entire configuration creates CO_2 very stable, making it very difficult to convert into other products. The dissociation of CO_2 into O_2 and CO is a highly endothermic process at room temperature with ΔH of 293 kJ/mol. When CO_2 is used as a single reactant at 2000 °C, just 2% of it transforms into CO (g) and O_2 (g), demonstrating its high chemical stability. In addition, the Lewis CO_2 structure indicates that both oxygen and carbon atoms have completed their octet by sharing electrons. Thus, the reduction of the fully oxidized carbon (C^{4+} of CO_2) to methane (C^{4-} of CH_4 ($CO_2 + 8e^- \rightarrow CH_4$)) has a large kinetic barrier due to the high chemical stability of the CO_2 molecule as discussed above [42,72]. As a result, a substantial energy input, an adequate catalytic system, and optimized reaction conditions are needed to energize the chemical conversion of CO_2 to methane [11]. It should be noted that the addition of H_2 as a co-reactant in the methanation reaction allows the conversion of CO_2 thermodynamically feasible with a ΔH of − 167 kJ/mol due to higher Gibbs free energy [13,71]. Therefore, for CO_2 dissociation and reaction with hydrogen in order to generate methane, it is mandatory to have an efficient and highly active catalyst. Recent catalytic developments for CO_2 methanation reaction to methane production are carried out in the following sections.

5. Catalyst developments for CO_2 methanation

Regardless of the thermodynamically favored CO_2 methanation reaction, the presence of a catalyst is essential to achieve an acceptable reaction rate and selectivity; a suitable and active catalyst is indispensable due to the chemically inert nature of CO_2 [73]. Over the last few decades, numerous research works and reviews have been produced to design and investigate the efficient conversion of CO_2 into methane through CO_2 methanation [4,9,74–78]. Typically, the catalysts used in CO_2 methanation are made of active metals (active phase: e.g., Co, Fe, Ni, Pd, Ru, Rh, Pt, Mo or W) and supporting materials (e.g., SiO_2, Al_2O_3, CeO_2, TiO_2, SiC, and ZrO_2) [45,79]. In the following sections, many types of active metals and supporting materials, which are widely used in CO_2 methanation studies, have been explained.

5.1. Active metals (active phase)

It was found that the transition metals of groups 8–10 in the periodic table have a great capacity to activate CO/CO_2 during methanation reactions. Fischer et al. [79] investigated these metals and applied for methanation reactions as unsupported metal catalysts. The reactivity results obtained from respective metals catalysts have been shown in Fig. 7 (1). In another study, a new order of activity and selectivity of these metals was reported by

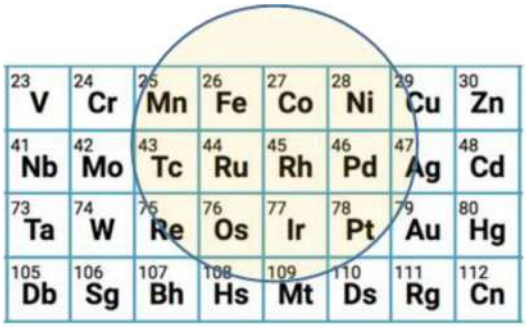

1 **Reactivity:** Ru > Ir > Rh > Ni > CO > Os > Pt > Fe > Mo >Pd > Ag

2 **Reactivity:** Ru > Fe > Ni > Co > Rh > Pd > Pt > Ir

Selectivity: Pd > Pt > Ir > Ni > Rh > Co > Fe > Ru

3 **Reactivity:** Ru > Fe > Ni > Co > Mo

Selectivity: Ni > Co > Fe > Ru

Fig. 7. Important active metals for methanation reactions.

Vannice et al. [80] for methanation reactions, as shown in Fig. 7 (2). Mills et al. [73] also investigated these metals to establish an activity order of five metals, as shown in Fig. 7 (3). It is noteworthy that these orders of reactivity for metals present only a general trend; in most cases, these differ and depend on several other factors, including metal-support interactions, reduction temperatures, or activation temperatures. The widely used active metals in methanation reactions with their pros and cons have been summarized in Table 3.

A volcano-shaped curve was observed when the activity of different supported transition metals was plotted against their reaction energies for dissociative CO chemisorption, which was associated with the catalyst surface's ability to form chemical bonds with either products, reactants, or reaction intermediate, as shown in Fig. 8 [96]. This relationship can help to find new catalysts for methanation reactions. The far-right side metals had high dissociative CO adsorption energies with the rate of methanation limited by the high resistance to CO dissociation, which stated that these metals were not appropriate for methanation reactions. It was suggested that the metals in the middle (e.g., Ru) had optimum chemisorption energy in the region of -150 kJmol^{-1}, and this could explain why Ru had higher activity than all the other metals of groups 8–10 in the methanation reaction. The other metals, including Rh, Ni, and Co, also have high activity for methanation reactions [97–100]. Active metals play a decisive role in the formation of methane by tuning selectivity towards CH_4 and CO products during methanation or hydrogenation of CO_2. For this purpose, several studies have been carried out to improve the formation of methane by selecting appropriate active metals. Previously, several studies have shown that different transition metals exhibit a broad range of methane selectivity for CO_2 hydrogenation during the catalytic performance of monometallic catalysts. For example, Mutschler et al. [101] examined a series of pristine transition metals for CO_2 hydrogenation and found that Co and Ni exhibited high activity and selectivity towards methane formation with less CO production. Fe, on the other hand, was mainly involved in the formation of CO by the RWGS reaction. Cu did not show any catalytic activity as a pristine metal for CO_2 hydrogenation. It was found that the observed activation energies on Co and Ni are 77 kJ/mol 74 kJ/mol, respectively. Garbarino et al. [102] investigated the efficiency of unsupported Co and Ni nanoparticles for CO_2 hydrogenation. The unsupported metallic cobalt nanoparticles displayed a substantial involvement in methane production but deactivated after time on stream due to rapid sintering and the formation of encapsulating carbon. On the other hand, they retain more stable activity in the RWGS reaction, producing CO as the main product. In another study, CO_2 hydrogenation was carried out for the production of methane using the Ni/Al_2O_3 catalysts. The catalysts containing very small Ni particles have been found to be very selective to methane without a significant formation of CO [103]. Bersani et al. [104] performed CO_2 hydrogenation and modeling predictions based on density functional theory (DFT) simulations of the CuO system. CH_4 was produced with the formation of the Cu-Phase and in correspondence with the decomposition of the Cu-Phase format, with a maximum conversion rate of CO_2 (2.8%) at 470 °C (on fully reduced copper), supporting the indication of independent reaction pathways for the conversion of CO_2 to CH_4 and CO. Panagiotopoulou et al. [105] conducted CO_2 hydrogenation over supported noble metal catalysts. They found that the Rh- and Ru-based TiO_2-supported catalysts favored methane formation and CO_2 conversion was followed the order of Rh > Ru > Pt > Pd over the TiO_2-supported catalysts. While the Pd- and Pt-based catalysts mainly produced CO as the major product. In general, methane and CO formation are highly dependent on the choice of metal and pressure, as shown in Fig. 9. Using the Pd [72,106], Fe [107–109], Pt [110–112], and Cu-based catalysts produce CO as the main product via RWGS reaction. While Rh [113,114], Ru [101,115–117], Co and Ni-based [118–120][121] catalysts produce methane as the main product during atmospheric-pressure CO_2 -hydrogenation. In the next sections, we will evaluate the catalytic

Table 3
Summary of characteristics of different transition metals with their pros and cons.

Metal	Advantages	Disadvantages
Ru	• Ruthenium (Ru) is considered the most efficient and active metal for methanation reactions. • Ru also shows high catalytic activity at low temperatures [67,81]. • Ru-promoted catalysts show long-term thermal stability compared to the other methanation catalysts [82,83].	• Ru is very expansive metal; it is more than 100 times costly compare to Ni. • • Using Ru is not economically viable for industrial-scale methanation reactions [37,81].
Ni	• Nickel (Ni) is undeniably known as the reference for methanation benchmark due to higher activity and low price. • Nickel is applied active metal for commercial methanation applications [84]. • The recovery rates of Ni is 50%, which is higher than 25% of Ru. Therefore, from environmental and industrial point of view, Ni is more prominent than Ru for many chemical reactions [85].	• However, the catalyst instability, caused by carbon deposition and Ni sintering, are the major limitations of nickel catalysts [86]. • • Ni easily can form Ni-carbonyls species, which are toxic and have serious concerns on environment and health [84,87,88].
Fe	• Iron (Fe) is highly active and efficient metal for methanation reaction. • Fe is more active than Ni and has considerable lower price than Ni [85]. • Fe-based catalysts can be used at elevated temperatures (700–950 °C). • • Fe is generally used as a second metal to Ni to prepare alloy or bimetallic catalysts for the Fischer-Tropsch synthesis (FTS) and ammonia production [84,89,90].	• Fe based catalysts have low selectivity towards methane. More prone to carbon deposition in CO methanation [85]. • • Fe- based catalysts form Fe_2O_3, Fe_3O_4 and FeO structural changes during methantion reactions. Fe0 and different phases, including θ-Fe_3C, ε-Fe_2C, ε'- χ-Fe_5C_2, and $Fe_{2.2}C$ might coexist [87,91].
Mo	• Molybdenum (Mo) is well known for highest sulphur tolerance during methanation reactions compared to all other metals. • It is widely used for hydrodesulfurization and hydrodenitrogenation [92]. • Mo are used as promoters for Ni catalysts to improve the interaction between support and Ni species in the Ni-Mo alloy, which can hinder the sintering of Ni particles at high temperature [93].	• Mo metal has a low methanation activity than Ru, Fe, Co, and Ni. • • Mo exhibits a higher selectivity towards higher hydrocarbons, which effects the possible methane yield during methantion reactios [95].
Co	• • Cobalt (Co) shows similar catalytic activity to Ni for methanation reactions [94].	• • Co is also expensive metal compared to others Fe and Ni. Therefore, Co-based catalysts are not commonly used for industrial scales applications as nickel catalysts [94].

performance of different supporting materials coupled with active metals, promoters, and methods of preparation for CO_2 methanation.

5.2. Supporting materials

The catalysts' activity does not only depend on the metal phases, but the supporting materials also contribute greatly to enhance the catalytic performance during the chemical reactions in heterogeneous catalysts. The supporting materials provide certain physicochemical properties, including high surface area, high dispersion of metal particles, electron mobility, and the additional active sites on the catalysts [42,45,51,122,123]. Several types of supporting materials, including SiO_2, Al_2O_3, TiO_2, CeO_2, ZrO_2, structured metal oxide, perovskite, solid solution, hexaaluminate, zeolites, and carbon materials have been prepared using different preparation methods for CO_2 methanation [36,46,69,124,125]. In this study, we focused on various types of supporting materials that have been extensively used in recent studies of CO_2 methanation.

5.2.1. Conventional supporting materials

Conventional supporting materials such as aluminium oxide (Al_2O_3) is one of the most commonly used support for CO_2 methanation and many other industrial reactions. Al_2O_3 has different types of crystallographic modifications, including α, γ, κ, δ, and θ phase, which make it more complicated than other metal oxides [45]. Typically, α-Al_2O_3 is not considered proper support in nickel-based catalysts for CO_2 methanation, whereas γ-Al_2O_3 has been extensively employed for CO_2 methanation catalysts due to its well-developed pore structure and high textural and surface acidic/basic properties [126,127]. Zheng et al. [128] used γ-Al_2O_3 as support to perform CO_2 methanation. They found a stable catalytic performance under cyclic operating conditions due to high surface area and larger average pores of γ-Al_2O_3. However, γ-Al_2O_3 supported catalysts are susceptible to carbon formation (coke), agglomeration of metal particles, and sintering at elevated reaction temperatures [45]. Therefore, γ-Al_2O_3 supports are modified using promoters or additives to increase the catalytic performance for CO_2 methanation. The promoters will be discussed in the following section 5.3.

Reducible metal oxides such as TiO_2, ZrO_2, and CeO_2 have been widely employed as supporting materials for numerous chemical reactions. TiO_2 is regarded as the most efficient defect-rich semiconductor supporting material for heterogeneous catalysis; it has been found that the TiO_2 supported Ni catalysts exhibited higher catalytic performance towards CO_2 methanation because the partial substitution of Ni particles could create oxygen vacancies in the TiO_2 lattice. TiO_x could provide electrons to Ni atoms on the catalyst surface, which facilitated the hydrogen adsorption on Ni nanoparticles and spilled-over to support, which sequentially could improve the activation and dissociation of CO_2, leading to a comparatively higher CO_2 methanation activity at low temperatures [129,130]. Jia et al. [130] used ZrO_2 as supporting material to synthesize a Ni/ZrO_2 catalyst for CO_2 methanation. A superior low-temperature CO_2 methanation activity was achieved with CO_2 conversion and CH_4 yield of 71.9% and 69.5%, respectively over the plasma-decomposed catalyst at 300 °C. The high catalytic activity was due to lattice oxygen vacancies, basicity, and highly dispersed Ni nanoparticles at the Ni/ZrO_2 interface. They concluded that higher basicity and oxygen vacancies have improved CO_2 adsorption and activation. While rapid dissociative adsorption of H_2 was occurred at Ni nanoparticles particles to generate hydrogen atoms, which spilled-over onto ZrO_2 support to form methane, as depicted in Fig. 10. Like TiO_2 support, CeO_2 and ZrO_2 have been widely used in CO_2 methanation due to their redox property that could enhance the activation and dissociation of CO_2 by electron transfer from supporting material to metal atoms [120,123,131]. Tada et al. [123] conducted a CO_2 methanation study over different Ni-promoted support materials, including Ni/α-Al_2O_3, Ni/MgO, Ni/TiO_2, and Ni/CeO_2. They found that the Ni/CeO_2 catalyst exhibited higher CO_2 conversion compared to other catalysts due to high basicity and oxygen vacancies on CeO_2 support.

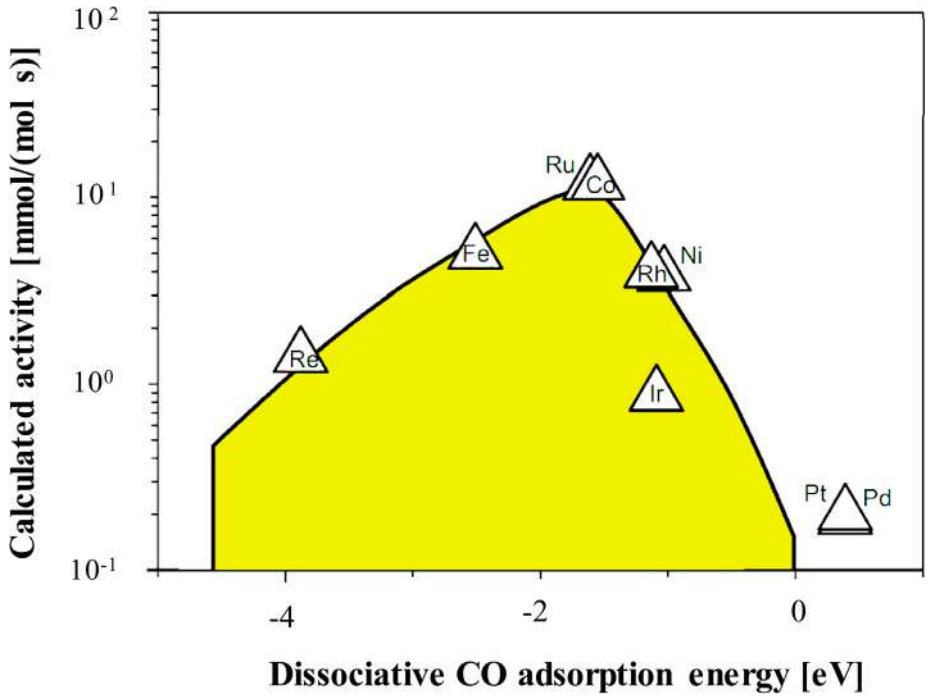

Fig. 8. Volcano-shaped curve of dissociative CO chemisorption for different transition metals at 550 K. Adapted from [96].

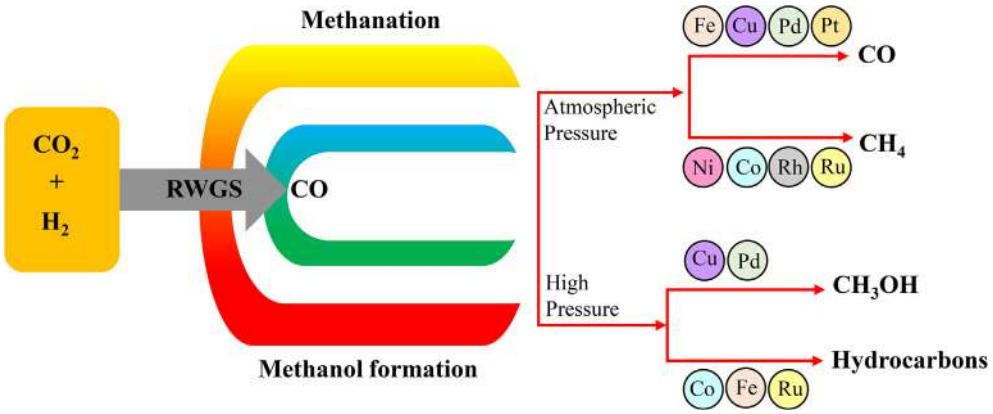

Fig. 9. Schematic showing possible products and potential catalysts for CO_2 hydrogenation.

5.2.2. Nanostructured porous support materials

The nanostructured porous materials represent a promising choice to replace the conventional supported catalysts due to their tailorable pore size, high surface area, short-range order, higher number of dangling bonds, and a great variety in the valence band electron structure. These nanostructured porous materials have also been used as host materials to synthesize nano-sized catalysts for CO_2 methanation and many other chemical reactions [132–137]. One potential candidate as new supporting material is mesostructured silica nanoparticles (MSN), which have attracted a great deal of attention due to unique features such as well-ordered structures, nanosized dimensions, high surface area, tunable pores size (1.5–10 nm), and tailorable pores diameters. Therefore, MSN-based materials have been used in many applications, including biomedical imaging, drug delivery, and catalysis [51,138–143]. Aziz et al. [51] investigated CO_2 methanation over a Ni/MSN catalyst to compare with other catalysts. They observed that a large amount of intra- and inter-particle porosity and oxygen vacancies in the Ni/MSN catalyst had increased the catalytic performance compared to other catalysts. In another study, Aziz et al. [143] examined different metal-promoted MSN catalysts for CO_2 methanation. Among all the catalysts, the Rh/MSN catalyst exhibited superior catalytic performance due to an extensive number of oxygen vacancies, basic sites, and large surface area. They have explained the active role of the MSN support during CO_2 methanation activity by conducting in-situ FTIR observations, as depicted in Fig. 11. It was found that CO_2 and H_2 were adsorbed and activated on Rh (metal phase of catalyst) to form CO, O, and H atoms, which migrated onto the MSN surface by spilled-over phenomena to form methane via linear/bridged carbonyl intermediate species. They reported that the oxygen vacancies rich MSN support played a crucial role in providing strong interaction to form carbonyls spices, which were important reaction intermediates in methane formation during CO_2 methanation.

5.2.3. Metal-organic framework (MOF) supporting materials

Another class of crystalline materials contains multidentate organic linkers and transition-metal cations via coordination

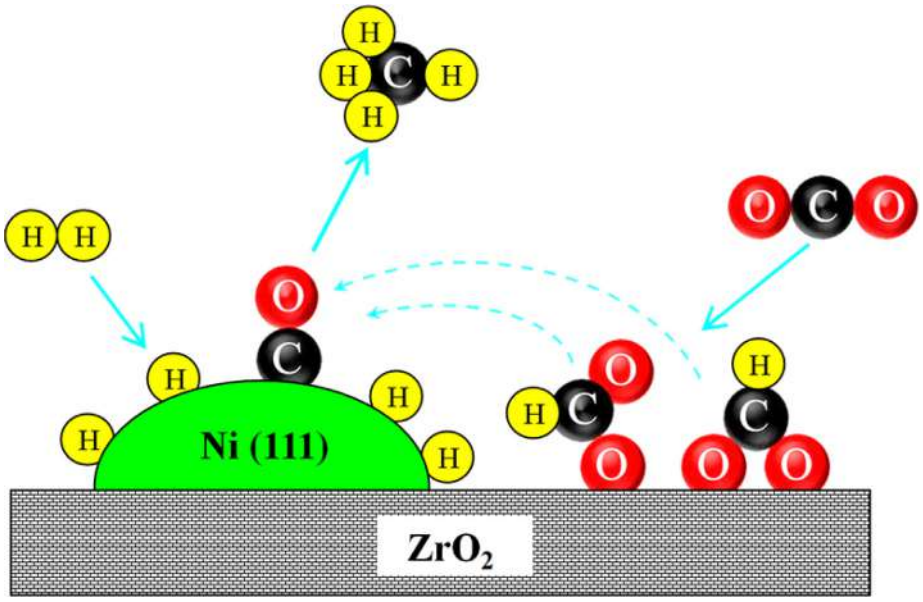

Fig. 10. Schematic demonstration of mechanistic reaction between CO_2 and H_2 over Ni/ZrO_2 catalyst. Modified from [130].

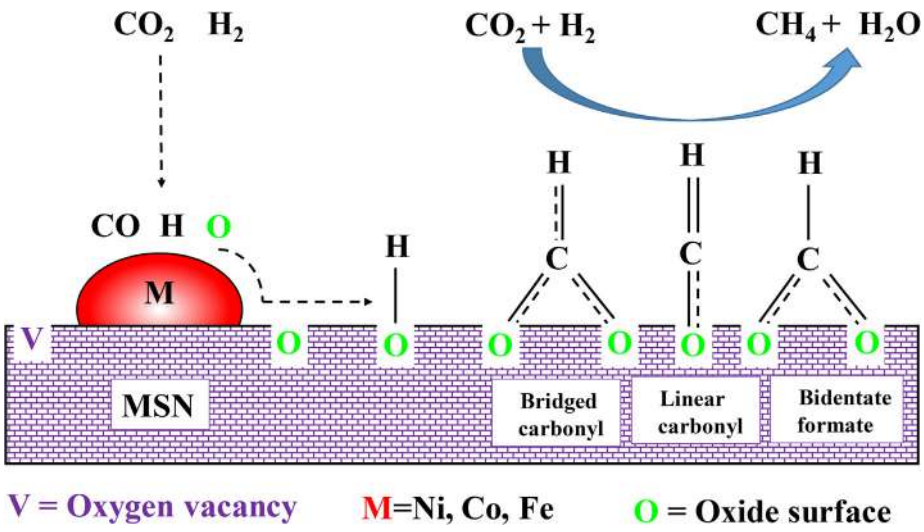

Fig. 11. Propose mechanism of CO_2 methanation on metal supported MSN. Adapted from [143].

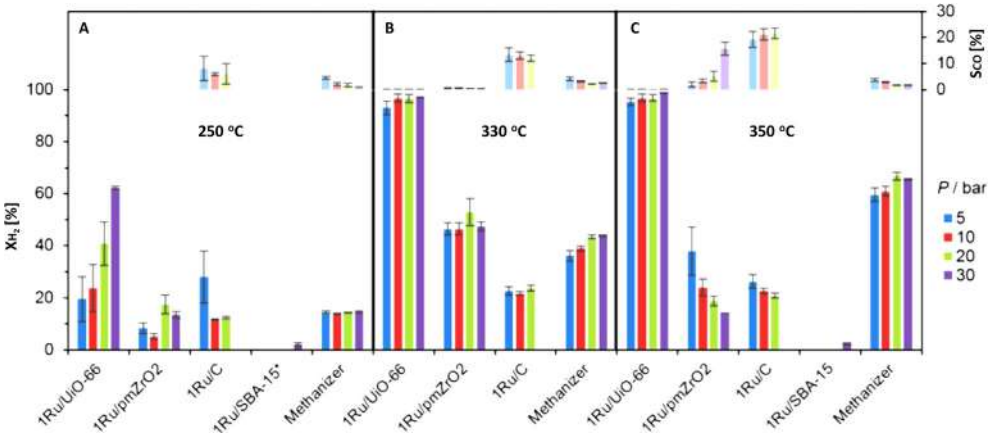

Fig. 12. CO_2 methanation activity in terms of H_2 conversion (X_{H2}) and selectivity for CO (S_{CO}) over different catalysts at 250, 330 and 350 °C with increasing pressure (left to right). Adapted from [149].

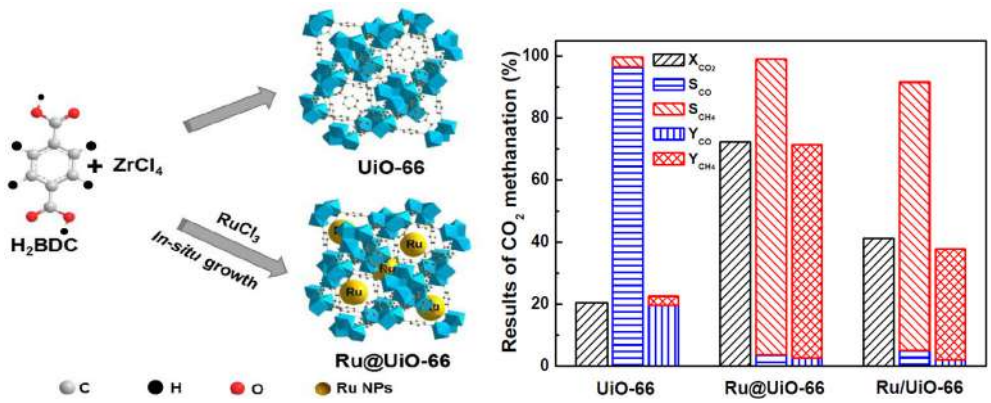

Fig. 13. Preparation of UiO-66 and Ru@UiO-66 and their catalytic performance towards dielectric barrier discharge plasma-assisted CO_2 conversion. Reprinted with permission from [154]. Copyright (2019) American Chemical Society.

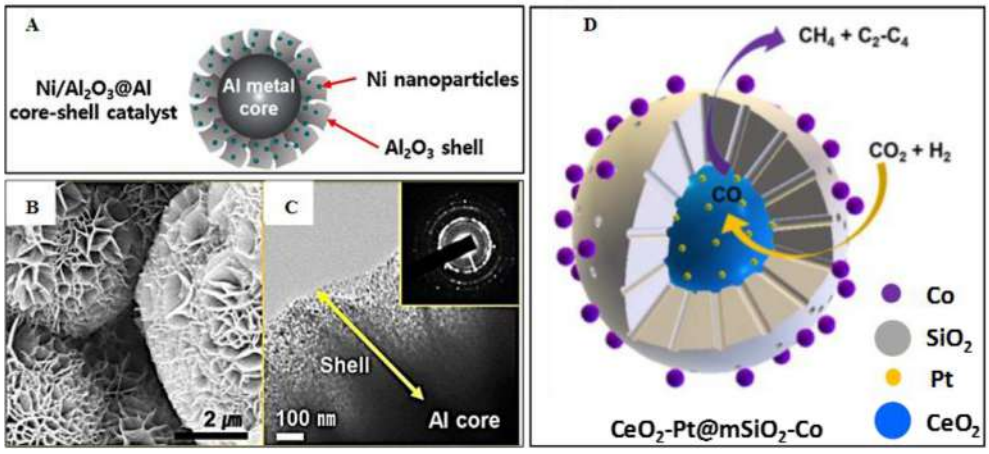

Fig. 14. (A) Core-shell structure of Ni/Al_2O_3@Al catalyst reduced at 673 K. (B) SEM of Ni/Al_2O_3@Al), (C) TEM of Ni/Al_2O_3@Al with SAED pattern, formed by exolution from NiAl-LDH shell. Reprinted with permission from [172]. Copyright 2017 Elsevier. (D) Core-shell CeO_2-Pt@mSiO_2-Co. Reprinted with permission from [173]. Copyright (2019) American Chemical Society.

bonds are called metal–organic frameworks (MOFs), which are considered porous materials with the open framework. MOFs have recently gained a great deal of interest as supporting materials due to their high surface area (1000–10000 $m^2\ g^{-1}$), controlled structure, confined pore space, unique structural features of the skeleton, and functional organic linkers. Therefore, MOFs have attracted global interest in various applications such as catalysis, sensors, molecular separation, and gas absorption [144–150]. The MOFs are considered marvelous catalyst templates; thermal removal of water ligands resulting in free coordination sites in metals situated at the nodes of the MOFs structure such as Cu, Mn, or Cr [151–154]. The Lewis acidic sites are produced in the MOFs catalysts due to coordinatively unsaturated metal sites and act as tremendous active sites in synergy with encapsulated NPs or by themselves. The catalytic active metal sites can be promoted in MOFs either during the MOFs synthesis or post-synthesis modification through the metalation of ligands situated on the MOF linkers.

Recently, MOFs-based catalysts have been used in several CO_2 methanation studies. Zhen et al. [146] studied CO_2 methanation over the Ni@MOF-5 catalyst. It was found that the well-dispersed, uniform Ni nanoparticles state and stronger metal supporting interactions between the MOF-5 and Ni atoms resulted in high catalytic activity (CH_4 selectivity; 100%) and high thermal stability. Lippi et al. [149] executed CO_2 methanation over a highly active 1Ru/UiO-66 catalyst derived from a MOFs template. The 1Ru/UiO-66 catalyst demonstrated marvelous activity towards CH_4 selectivity with a lower amount of CO at 330°C, as shown in Fig. 12B. It was suggested that the catalytic activity of the 1Ru/UiO-66 was greatly affected by the unique morphology of the UiO-66 MOFs template, which provided a well-ordered distribution of Ru nanoparticles (Ru-NPs) throughout the framework of the UiO-66 template. In a similar study, Xu et al. [154] prepared a Ru@UiO-66 catalyst using the UiO-66 MOFs. The Ru-NPs were encapsulated during the synthesis of the UiO-66 MOFs through a solvothermal method and applied for plasma-assisted catalytic CO_2 methanation. It was found that the Ru@UiO-66 catalyst revealed a superior activity with 72.2% CO_2 conversion and 95.4% of CH_4 selectivity due to the excellent dispersion of Ru-NPs on its unique framework structure, as shown in Fig. 13. Li et al. [155] synthesized MOFs-derived catalysts and investigated the effect of different particle sizes and morphologies on CO_2 methanation. It was found that the ZIF-67-templated porous carbon, along with Co-NPs, exhibited excellent CO_2 methanation activity (CH_4 selectivity; 99.2%) at low reaction temperatures. The high catalytic performance was due to the highly dispersed Co-NPs (with a size of 7–20 nm) inside the carbon matrix, separated by the graphite-like carbon, which also prevented the metal from sintering effectively. In addition, several CO_2 methanation studies were conducted over MOFs catalysts [156–165].

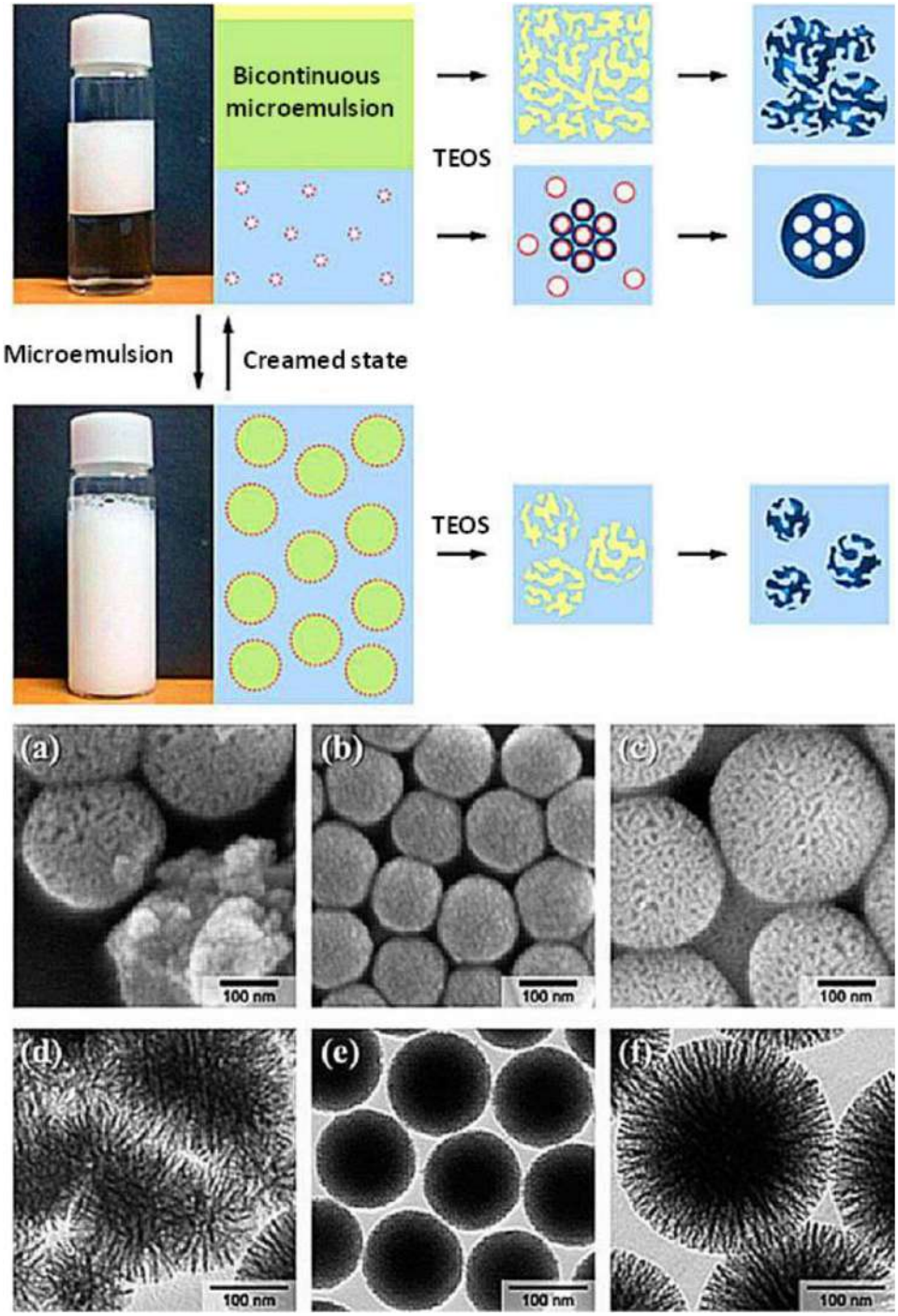

Fig. 15. Schematic phases in synthesis of silica nanoparticles with SEM (a, b and c), TEM (d, e and f). Upper microemulsion layer (a and d), lower aqueous layer (b and e), and macroemulsion system (c and f). Reprinted with permission from [192]. Copyright (2012) American Chemical Society.

5.2.4. Core-shell structured supporting materials

It is a great challenge to avoid metal sintering and carbon deposition on active sites of catalysts during CO_2 methanation catalytic performance. Recently, to overcome this issue, a new core–shell configuration has gained much interest due to the encapsulation of metallic particles by a porous shell, including alumina or silica; it is also called a yolk-shell structure, typically prepared using the modified Stöber method [166–168]. The core–shell configuration prevents coking, sintering, and agglomeration of metal particles by the encapsulated metal particles. This unique configuration is developed by adding different reagents [169–174] as a protective shield to cover the active metal particles. Lee et al. [172] synthesized a Ni/Al_2O_3@Al core–shell microstructure consisting of an Al core and a NiAl layered double hydroxide (LDH) shell with petal-like surface morphology, as illustrated in Fig. 14(A-C). The catalytic properties of the Ni/Al_2O_3@Al core–shell catalysts were studied towards CO_2 methanation to compare with those of the conventional Ni/Al_2O_3 catalysts. They examined CO_2 methanation and found that the Ni/Al_2O_3@Al exhibited a three times higher turnover rate (TOF) than the Ni/Al_2O_3 catalyst developed by conventional filtration methods, reflecting the marked internal catalytic properties of the Ni/Al_2O_3@Al catalyst. The superior catalytic activity was due

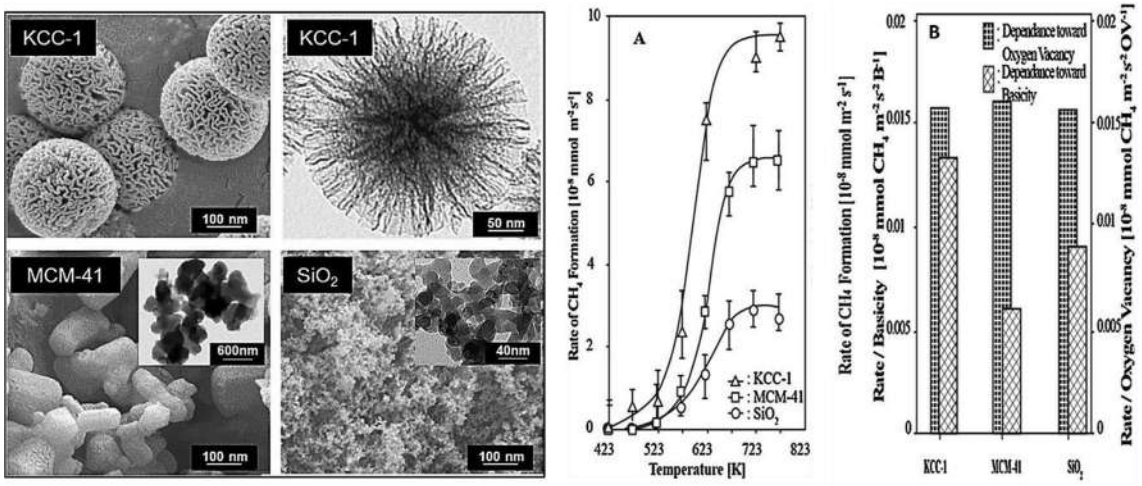

Fig. 16. FESEM and TEM images of KCC-1, MCM-41 and SiO_2 along with their catalytic performance towards CO_2 methanation. (A) Rate of CH_4 formation and (B) dependence study of catalysts. Reprinted with permission from [194]. Copyright 2017 Elsevier.

to fine nickel nanoparticles (Ni-NPs) dispersion on the thin nanosheets comprising the Ni/Al_2O_3@Al core–shell microstructure, which topologically retarded the aggregation of Ni-NPs to provide facile transport of reactant and product species through the catalyst microstructure. Xie et al. [173] developed a well-defined nanostructured catalyst (CeO_2-Pt@mSiO_2-Co) using two metal-oxide interfaces, including CeO_2-Pt as a core and mesoporous silica as a shell, which was further decorated with cobalt nanoparticles as shown in Fig. 14D. It was found that the CeO_2-Pt@mSiO_2-Co catalyst showed high selectivity (60%) towards C_2-C_4 due to this unique core–shell configuration of catalyst. Le et al. [174], synthesized a Ni-promoted unique aluminate spinel substrate Al@MAl_2O_4 (M = Zn, Mg or Mn) core–shell catalyst for CO_2 methanation. It was found that the core–shell spinel structures of Ni-Al@$MnAl_2O_4$ have performed outstanding CO_2 methanation activity due to the creation of the moderate basic and improved dispersion of Ni-NPs. Kirchner et al. [175] prepared a silica-based core–shell catalyst for CO_2 methanation and achieved a 20% of CO_2 conversion. Though the CO_2 conversion was low, the core–shell configuration exhibited pronounce resistance against thermal sintering, particle attrition, and coke deposition during CO_2 methanation. Several other CO_2 methanation studies were conducted over the core-shell catalysts [176–185].

5.2.5. Fibrous supporting materials

In recent years, Polshettiwar and co-workers discovered a new class of fibrous nano-silica (KCC-1) of unique fibrous morphology in 2010 [186]. KCC-1 has emerged as an effective supporting material for several chemical reactions such as drug delivery system, the adsorbent in removing drugs, and heavy metals in wastewater streams due to exceptional physical properties, including larger pores volume, high surface area, and thermal/hydrothermal mechanical properties. In contrast to the closed two-dimensional porous silica materials of cylindrical pore structured materials (SBA-15 and MCM-41), KCC-1 has open silica fibrous and dendritic-like structures, which are easily accessible for reactants molecules [187–192]. Moon et al. [192] synthesized and investigated the formation mechanism of hierarchical mesoporous silica nanoparticles with a bicontinuous microemulsion phase, as shown in Fig. 15. They suggested that the inner wrinkle distances of wrinkled silica nanoparticles (WSNs) could be accurately tuned to enhance the pore's size volume and surface area.

Motivating by this innovative fibrous morphology of the spherical silica nanoparticles, Patil et al. [193] applied KCC-1 in CO_2 adsorption, and better adsorption was found on KCC-1 compared to MCM-41. Hamid et al. [194] also prepared mesoporous silica KCC-1 using the microemulsion method and obtained uniform microspheres with unique, well-defined fibrous morphology compared to MCM-41 and SiO_2, as shown in Fig. 16. They conducted the CO_2 methanation reaction and noticed that CH_4 selectivity was 83% with a rate of CH_4 formation of 9.0×10^{-8} mmol $m^{-2}s^{-1}$, which were higher than MCM-41 and SiO_2 (Fig. 16A and B). They concluded that the high catalytic performance was due to fibrous morphology, which provided higher accessibility of CO_2 and H_2 in the activation process. They reported that a higher amount of oxygen vacancies and basicity in KCC-1 played a critical role in enhancing the catalytic performance towards CO_2 methanation activity. Singh et al. [187] executed CO_2 adsorption over the KCC-1 and compared the results with MCM-41. They found that the KCC-1 showed higher CO_2 adsorption capture capacity compared to MCM-41 due to the fibrous morphology, which provided great accessibility sites for the CO_2 adsorption. In another study, Mishra et al. [195] developed metal-free-ligand-free fibrous nanocatalysts that convert CO_2 to methane at significant rates, scales, and stabilities. In another study, Hamid et al. [196] investigated CO_2 methanation over metal promoted fibrous silica KCC-1 and found the highest catalyst performance for the Ni/KCC-1 due to high surface area, small particle size, and high dispersion of Ni nanoparticles.

5.2.6. Zeolites as supporting materials

Zeolites are aluminosilicates (AlO_4^{5-} and SiO_4^{4-}) of the family of microscopic mesoporous solids called molecular sieves, consisting primarily of Si, Al, O, and metals such as Ti, Sn, and Zn. They have been applied mainly as catalysts in many industrial reactions because of the high large surface area, thermal stability, shape selectivity, and high tailorable acid-base properties [197]. In recent times, several CO_2 methanation studies have been conducted over zeolites-based catalysts [198–200]. It was reported that the zeolites' capacity to adsorb CO_2 molecules and their catalytic properties are impressively influenced by the Si/Al ratio, which can affect CO_2 methanation performance. Bacariza et al. [201] reported that catalytic performances towards CO_2 methanation were highly dependent on Si/Al ratio, regardless of the compensating cation in zeolites. They also reported that sintering and loss of crystallinity were not detected after the catalytic tests. Quindimil et al. [202] synthesized Ni-supported Y- and BETA-zeolites to study CO_2 methanation. They found that Na^+ ion-exchanged zeolites, mainly BETA zeolite showed enhanced CO_2 conversion (65%) due to high reducibility.

Table 4
Summary of catalytic performance of CO_2 methanation catalysts.

No	Catalyst	Active metal /ion	Promotor/ Si/Al ratio	SynthesisProtocol	P (atm)	Reactor	T (°C)	XCO_2 (%)	SCH_4 (%)	Ref.
1	Ni/MSN	Ni	-	Sol-gel method	1	fixed-bed	300	64	99.9	[51]
2	Ni/CeO_2	Ni	-	Wet impregnation	1	fixed-bed	300	90	100	[123]
3	Ni@ MOF-5	Ni	-	Impregnation	1	-	280	48	100	[146]
4	γ-Fe_2O_3	-	-	PVA route	1	fixed-bed	400	67	87	[175]
5	KCC-1	-	-	Microemulsion	1	fixed-bed	450	48.7	-	[194]
6	1Ru/UiO-66	Ru	-	Incipient Wetness Impregnation	30	fixed-bed	250	60	100	[197]
7	Ni-MgO/ZrO_2	Ni	Mg	Impregnation	1	fixed-bed	300	90	100	[210]
8	Ni-Ca/AC	-Ni	Ca	Impregnation	1	fixed bed	360	76	100	[211]
9	Ni-xCeO_2/MCM-41	Ni	-	Deposition precipitation	1	fixed-bed	380	85.6	99.8	[212]
10	Ru/CeO_2	Ru	-	Impregnation	1	fixed-bed	300	80	99	[116]
11	Ru–CeO_2/Al_2O_3	Ru	-	Impregnation	1	fixed-bed	300	60	99	[116]
12	Ru-Mn-Ni/Al_2O_3	Ni	Ru-Mn	Impregnation method	1	microreactor	400	99.74	72.36	[213]
13	Pd–Mg/SiO_2	Pd	Mg	Reverse microemulsion	1	fixed-bed	450	59	95	[72]
14	Pd-Ni/SiO_2	Ni	-	Microemulsion	1	fixed-bed	450	50.5	89	[72]
15	Pd-Li/SiO_2	Li	-	Microemulsion	1	fixed-bed	450	42.6	88.5	[72]
16	Co/KIT-6	Co	-	Impregnation	1	fixed-bed	360	52.6	94.5	[214]
17	MesoporousNi-Al_2O_3	Ni	-	EISA	1	fixed bed	400	83	97	[215]
18	Ni/Υ-Al_2O_3	Ni	-	Incipient wetness impregnation	1	spinning-basket	210	80	99.5	[216]
19	Fe-Ni/Al_2O_3	Ni	Fe	Incipient wetnessimpregnation	1	down-flow tubular	250	22.1	99.5	[217]
20	Fe/Al_2O_3	Fe	-	Incipient wetnessimpregnation	1	down-flow tubular	250	11.4	96.5	[217]
21	Ni/ZrO_2	Ni	-	Impregnation method	5	fixed-bed	250	90	90	[218]
22	Co-Ni/ZrO_2	Ni	CO	Impregnation method	5	fixed-bed	250	93	90	[218]
23	Rh-Ba/Al_2O_3	Rh	Ba	Two-nozzle flame spraypyrolysis	1	fixed-bed	450	55	94	[219]
24	Rh-K/Al_2O_3	Rh	K	Pyrolysis	1	fixed-bed	450	25	0	[219]
25	NiRu/SiO2-P	Ni	Ru	PEG-free method	10	fixed-bed	320	10	80	[220]
26	Ni-CeO_2/γ-Al_2O_3-Plasma treated	Ni	-	DBD plasma method	1	fixed-bed	300	80	100	[221]
27	Ni-Meso ZrO_2	Ni	-	Ultrasound-assisted method	1	fixed-bed	300	70	100	[222]
28	Mg-Ni/USY	Ni	Mg	Impregnation	1	pyrex reactor	400	63	93	[223]
Zeolites supported catalyts										
29	FS@ZSM-5	-	-	Microemulsion	1	fixed-bed	500	-	66	[50]
30	ZSM-5	-	-	Microemulsion	1	fixed-bed	500		37	[50]
31	Ni/Y	H^+	-	Impregnation	1	fixed-bed	300	48.5	96.4	[51]
32	Ni/USY	Na^+	3	Impregnation	1	flow tubular	400	65	94	[198]
33	Ni/USY	Na^+ / Cs^+	38	Impregnation	1	fixed-bed	400	73	97	[201]
34	Zeolite 13X	-	1.0	Impregnation	1	fixed-bed	320	79	100	[208]
35	Ni/USY zeolites	Mg^{2+}	3.7	Ion-exchanging	1	fixed-bed	350	80	15	[209]
36	Ni/USY zeolites	Cs+	3.7	Ion-exchanging	1	fixed-bed	350	40	15	[209]
37	Ni-Ce/USY	Cs^+	38	Co-impregnation	1	pyrex reactor	305	78	99	[224]
38	Mg-Ni/USY	Na^+	3	Impregnation	1	pyrex reactor	400	63	93	[223]
39	Zeolite silicalite-1	-	-	Impregnation	1	fixed-bed	450	60	-	[225]
40	BETA zeolite	NH_4^+	25	Ion exchange	-	DBD plasma reactor	400	84	97	[226]
41	Rh-Y	Na^+	2.4	Ion exchange	30	fixed-bed	150	6	100	[227]
42	Ni/BEA	Na^+ / Cs^+	38	Impregnation	1	fixed-bed	400	70	96	[228]
43	Ni/BEA	Na^+	243	Impregnation	1	Fixed-bed	400	71	97	[228]
44	Ni/MOR	Na^+ / Cs^+	47	Impregnation	1	fixed-bed	400	66	95	[228]
45	Ni/ZSM-5	Na^+ / Cs^+	40	Impregnation	1	fixed-bed	400	65	96	[228]
46	Ru/ZSM-5	H^+	15	Impregnation	1	tubular microreactor	350	100	100	[229]
47	Pt-Co-MOR	Na^+	5	Ion exchange	I	microreactor	350	41	15	[230]
Carbonaceous supported catalysts										
48	Rh/γ-Al_2O_3 + Ni/AC	Ni	Ni	Incipient wetness Impregnation	-	fixed-bed	125	50	100	[231]
49	Rh/γ-Al_2O_3 + Ni/AC	Ni	Ni	Incipient wetness Impregnation	-	fixed-bed	125	50	100	[231]
50	Fe@CNT	Fe	-	aerosol assisted chemical vapour deposition (AACVD)	1	fixed-bed	370	45.1	29.3	[232]
51	Ni-Ce/CNT	Ni	Ce	Co-impregnation	1	fixed-bed	350	83.8	100	[233]
52	Ni/CNT	Ni	-	Co-impregnation	1	fixed-bed	350	61.1	96.6	[233]
53	Ni-Ce/Al_2O_3	Ni	Ce	Co-impregnation	1	fixed-bed	350	64.5	97.5	[233]
54	Ni/Al_2O_3	Ni	-	Co-impregnation	1	fixed-bed	350	30.2	86.4	[233]
55	NiMn/(SGO)-CNT	Ni	Mn	-	1	micro-reactor	350	78	100	[234]
56	Ni/N-CNT	Ni	-	Chemical vapourdeposition	1	fixed-bed	360	90	99	[235]
57	Fe/N-CNT	Fe	-	Dry impregnation	25	-	360	25	40	[236]
58	Fe/CNT	Fe	K^+	-	2	fixed-bed	340	35	26	[237]
59	Ru/N-CNF	Ru	-	-	-	porous frit	375	63	100	[238]
60	Ru/N-ABC	Ru	-	Wet impregnation	10	fixed-bed	380	94	100	[239]
61	Ru-N/ABC-600	Ru	N	In-situ pyrolysis	10	fixed-bed	380	93.8	99.7	[239]
62	Ru/N-ABC-500	Ru	N	In-situ pyrolysis	10	fixed-bed	400	92.8	91.8	[239]
63	Ni-Ce/CNT	Ni	Ce	Impregnation	1	fixed-bed	350	55	85	[240]
64	Ni/OCF	Ni	-	Incipient wetness Impregnation	1	fixed-bed	320	74	97	[240]

(*continued on next page*)

Table 4 (*continued*)

No	Catalyst	Active metal /ion	Promotor/ Si/Al ratio	SynthesisProtocol	P (atm)	Reactor	T (°C)	XCO_2 (%)	SCH_4 (%)	Ref.
65	Ni/MgAl-MMO	Ni	Mg	Impregnation	1	fixed-bed	250	97.9	97.5	[241]
66	Ni-Ca/AC	Ni	Ca	Impregnation	1	fixed-bed	360	76	100	[211]
67	Ru-Co/C	Co	Ru	Impregnation	5	fixed-bed	300	29.9	54.3	[242]
68	FeK/MWNTs	Fe	K	Ultrasonication	20	fixed-bed	340	43.6	27.1	[243]
69	FeK/SWNTs	Fe	K	Ultrasonication	20	fixed-bed	340	52.7	13.5	[243]

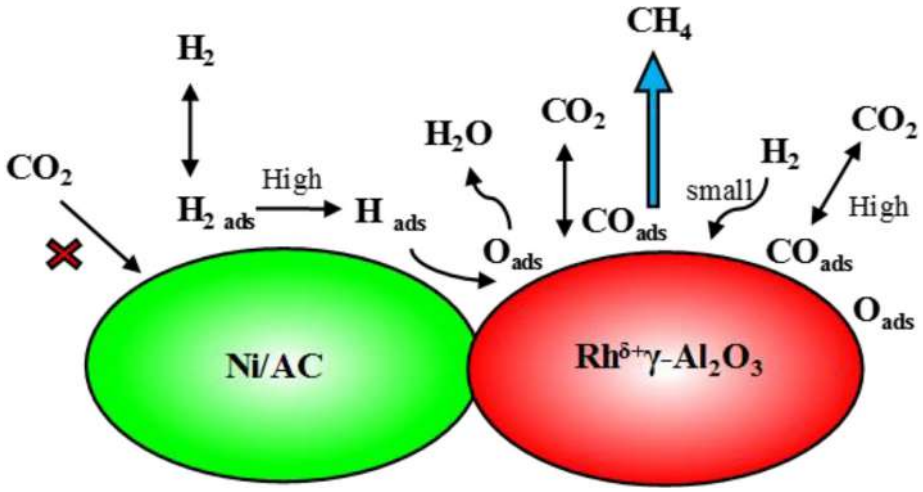

Fig. 17. CO_2 methanation activity over activated carbon and Rh/γ-Al_2O_3 catalysts. Adapted from Swalus [231].

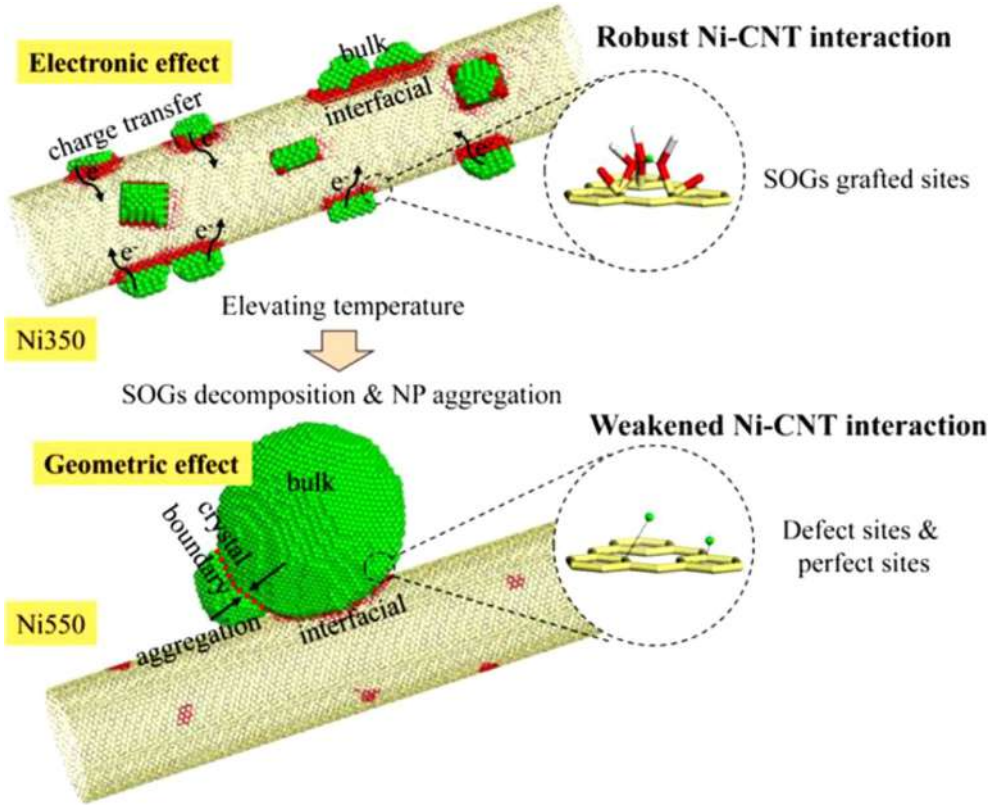

Fig. 18. Proposed interface-bonding mechanism in the Ni-CNT catalytic system. Reprinted with permission from [234]. Copyright (2018) American Chemical Society.

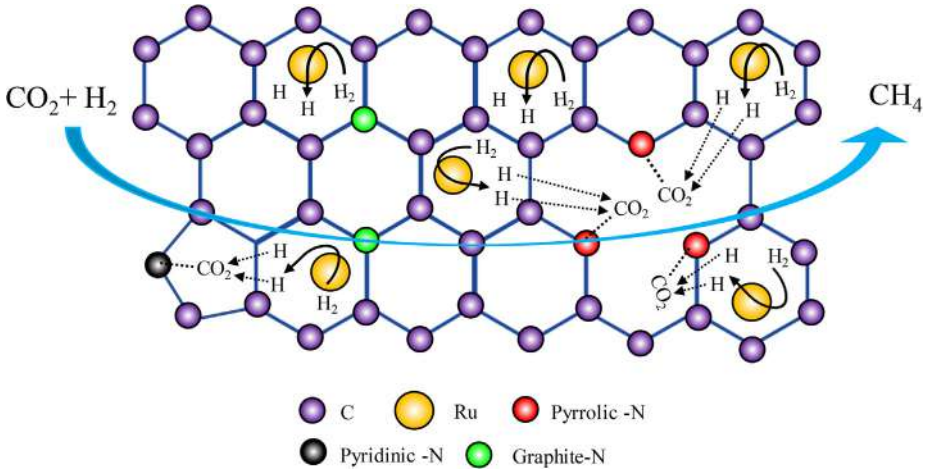

Fig. 19. N-doped biochar supported Ru as efficient catalyst for CO_2 methanation. Adapted from [239].

Intrinsic basicity is one of the most critical factors, which improves the catalytic performance of the zeolite-based catalysts to attract more acidic CO_2. The basicity of zeolites can be enhanced by adding more basic compensation cations, including Mg, Ce, and La or promoters. These are the most widely used compensation cations that increase the basicity of zeolites and provide the new active sites for the absorption and activation of CO_2 molecules. The development of a suitable zeolite catalyst for well-defined and controlled types of active sites increases the capacity of various metal species to stabilize. In addition, the confinement effects boost the activity of the catalyst in zeolite's channels and cages, which act like nanoreactors [203–206]. Borgschulte et al. [207] studied hydrogenation of CO_2 over different zeolites supported Ni catalysts. They found that the selectivity for methane is significantly boosted if the size of the pores of the support is larger than 5 Å. In comparison, the size of the pores less than 3 Å reduced the overall conversion rate and the selectivity for methane. Wei et al. [208] prepared zeolite 13X, and 5A supported Ni catalysts and applied them for CO_2 methanation. They found that the zeolite 13X was proved the best catalyst with a superior catalytic performance due to larger pores size. Bacariza et al. [209] studied CO_2 methanation by adding the compensating cations on Ni/USY zeolites. They found that larger alkaline compensation cations (Mg^{2+}) enhanced the CO_2 adsorption and CO_2 methanation activity. They concluded that the catalytic activity of zeolites was improved by tuning the catalytic properties through the exchanged cation. All these features of zeolite materials make them suitable, selective, and stable catalytic materials for CO_2 methanation. As shown in Table 4, the most performant zeolite-based leading catalysts tend to have higher catalytic performance, particularly methane selectivity during CO_2 methanation.

5.2.7. Carbon as supporting materials

It is well established that the presence of hydrogen is essential; it must be supplied at the surface of the catalyst for methanation reaction. Several studies have proved that the activated carbon materials could provide high adsorption sites for hydrogen. After the activation process, hydrogen could migrate at the surface by a spillover mechanism to promote the hydrogenation of CO_2. Although carbon as a supporting material provides high active sites for adsorbed hydrogen, they are unable to activate CO_2. These are promising supporting materials in other perspectives, such as less coking tendency tunable physicochemical and textural properties, and high thermal conductivity.

Numerous carbon-supporting materials, such as activated carbons [231,244], carbon nanotubes [232–234,237–239], nanocarbon nanofiber [245], biomass [239] and carbon felt [240] have already been used for CO_2 methanation reaction. Swalus et al. [231] prepared composite material of nickel promoted activated carbon (Ni/AC) and Rh/γ-Al_2O_3 to examine CO_2 methanation. They noted the enormous increase in CO_2 methanation activity over synthesized catalysts. They concluded that high catalytic performance was due to the Ni/AC's capacity to absorb and activate H_2 to H atoms, which spilled over to the active Rh sites for chemical reaction with adsorbed CO_2, as shown in Fig. 17. O'Byrne et al. [232] synthesized CNTs supported iron catalysts (Fe@CNT and Fe decorated CNT) and applied them for methanation reaction. They noticed that the Fe@CNT was proved a superior catalyst for methanation reaction in methane selectivity and CO_2 conversion due to the high hydrogen spillover process on Ni-promoted CNTs. Wang et al. [233] prepared a Ni-based catalyst modified with carbon nanotubes (CNTs) and promoted with cerium (12Ni4.5Ce/CNT) to study the CO_2 methanation activity. They reported that among all the catalysts, the 12Ni4.5Ce/CNT demonstrated high activity and thermal stability. It was suggested that the confinement effect produced between Ce and well-dispersed Ni-NPs on CNTs, has greatly enhanced the catalytic activity for CO_2 methanation. In another study, Wang et al. [237] conducted hydrogenation of CO_2 over different support materials including, SiO_2, TiO_2, ZrO_2, and Al_2O_3. Among all, carbon nanotubes, mesoporous carbon illustrated the highest catalytic activity for CH_4 selectivity. The chemical and physical properties, such as electronic state or binding energy (BE) and thermal stability of CNTs, can be effectively tuned by adding oxygen and nitrogen [234,236,239]. Li et al. [234] investigated CO_2 hydrogenation over oxygen functionalized Mn-promoted Ni-CNTs and found higher catalytic performance (nearly 100% CH_4 selectively) at low reaction temperatures compared to other unprompted catalysts. They reported that high performance was due to the surface oxygen groups (SOGs) on CNTs, which could act as a channel between CNTs and Ni NPs. This promoted a strong interaction by forming interfacial covalent bonding between them SOGs-CNTs and Ni atoms, as shown in Fig. 18. Thereby, the thermal stability of the catalyst was improved when the Ni-CNTs interactions were established by donating electrons (electronic effect) from Ni to the CNTs. Wang et al. [235] examined CO_2 methanation over prepared Ni-NPs grown on the N-doped carbon nanotubes (Ni/N-CNTs), which presented high CO_2 methanation activity due to improvements in the binding-sites for Ni-NPs with minimum metallic

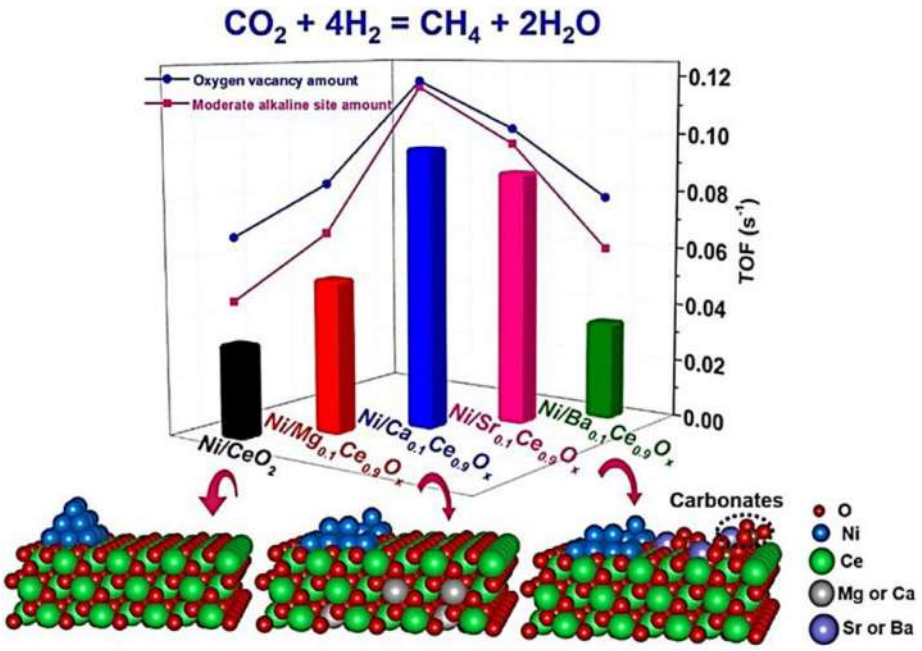

Fig. 20. Promotional effects of alkaline earth metal oxides on Ni/CeO_2 for CO_2 methanation. Reprinted with permission from [241]. Copyright 2020 Elsevier.

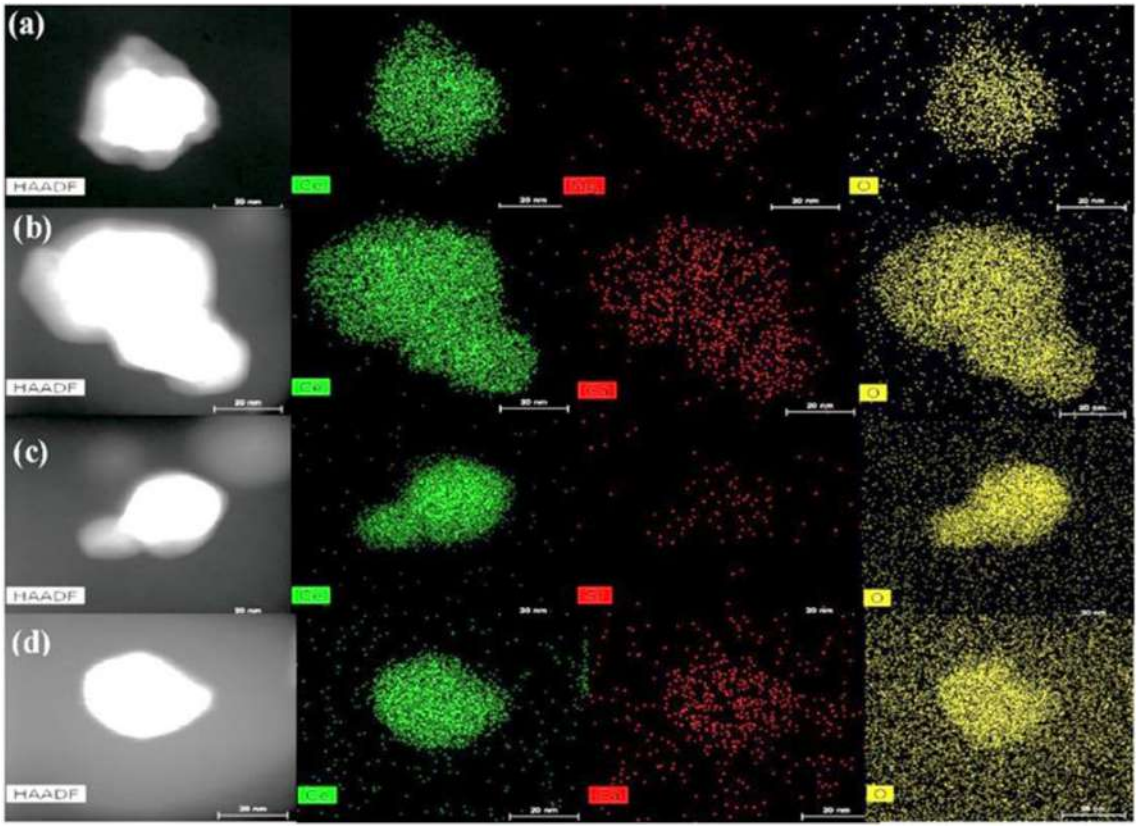

Fig. 21. STEM-mapping images of the catalysts: (a) $Mg_{0.1}Ce_{0.9}O_x$; (b) $Ca_{0.1}Ce_{0.9}O_x$;(c) $Sr_{0.1}Ce_{0.9}O_x$; (d) $Ca_{0.1}Ce_{0.9}O_x$-IMP. Reprinted with permission from [241] Copyright 2020 Elsevier.

aggregation. Chew et al. [236] prepared iron catalysts supported on oxygen and nitrogen-functionalized multi-walled carbon nanotubes (CNTs) and on silica to examine hydrogenation of CO_2. It was observed that the prepared O-CNTs and N-CNTs demonstrated higher activity than the SiO_2 support due to the well dispersed Fe-NPs metallic, high reducibility, and metal-support interactions, and hydrophilicity. Wang et al. [239] synthesized the N-doped biochar catalysts with different pyridinic-N content to study CO_2 methanation. They reported that the Ru/N-ABC-600 catalyst showed a high CH_4 selectivity of 99.7% and CO_2 con-

version of 93.8% because the basic N species could act as an anchor for CO_2 capture, as shown in Fig. 19. Although the existing studies of structured carbon materials for CO_2 methanation showed promising results, their applications for CO_2 methanation are scarce [246–248].

5.3. Effect of promoters on CO_2 methanation

A promising concept for improving the catalytic activity and thermal stability of the catalysts is promoters or additives, which increase the resistance of catalysts towards sintering and coking. Generally, the promoters are categorized into chemical (electronic) and textural (structural). Chemical promoters are used to provide new additional active sites to improve the chemical properties related to the activity of the catalysts such as redox property or basicity. Textural promoters are usually applied to delay and avoid the sintering of active species by improving the textural properties of the catalysts. Typically, alkali metals, alkaline earth metals, transition metals (Fe, Ru, Co, Mn, Zr, La, Ce, Y, etc.), and metal oxides are used as promoters for the development of CO_2 methanation catalysts [27,45,249].

5.3.1. Addition of alkali metals

The addition of alkali cations is a very successful approach to increase the catalytic efficiency and thermal stability for CO_2 methanation. For example, Petala et al. [115] synthesized a Ru/TiO_2 catalyst to study CO_2 methanation activity. They used different alkali metals, including Na, K, Li, and Cs as promoters to enhance CO_2 methanation. Among all the catalysts, the Na-promoted catalyst (Ru/Na-TiO_2) exhibited higher catalytic performance compared to unpromoted Ru/TiO_2 catalysts and other catalysts (about three times higher). Small quantities of alkalis were suggested to replace the portion of costly metals, lower the price and increase the performance of the CO_2 methanation reaction. In another study, Cimino et al. [250] synthesized alkali promoted based Ru/Al_2O_3 catalyst for CO_2 methanation. They found that the addition of Li on Ru/Al_2O_3 could improve both the CO_2 capture capacity and methanation activity due to the formation of a mixed Li-Aluminate spinel phase. However, surface K and Na carbonates reduced the CO_2 methanation activity and selectivity. Panagiotopoulou et al. [251] examined methanation of CO_2 over alkali-promoted Ru/TiO_2 catalysts. The activity and the selectivity of CH_4 were found to increase with the promotion of 0.5%Ru/TiO_2 with alkalis. The alkali promotion of 0.5%Ru/TiO_2 catalyst favored the dissociative adsorption of CO during CO_2 methanation. Several other studies also used alkali metals as promoters to enhance the CO_2 methanation [252–256].

5.3.2. Addition of alkaline earth metals

The catalytic performance of CO_2 methanation catalysts can also be increased by alkaline earth metals, usually considered as structural promoters. Liu et al. [241] investigated different alkaline sites by modifying CeO_2 with different alkaline earth metal oxides (e.g., Mg, Ca, Sr, Ba) for CO_2 methanation. Among all the catalysts, Ca promoted catalyst (Ni/$Ca_{0.1}Ce_{0.9}O_x$) illustrated the higher catalytic activity than other catalysts, as shown in Fig. 20. It was concluded that the high catalytic performance was due to the formation of the solid solution in the $Ca_{0.1}Ce_{0.9}O_x$ sample after doping Ca^{2+} cations into the CeO_2 lattice. While other cations were dispersed on the CeO_2 surface, STEM-mapping confirmed that promoting Ca to Ni/CeO_2 could effectively improve Ni dispersion with moderate alkaline sites. The high amount of surface oxygen vacancies was the major reason for enhanced catalytic performance during CO_2 methanation, as depicted in Fig. 21. In order to improve the CO_2 methanation activity of the USY zeolite, Bacariza et al. [209] also added Mg. It was noticed that the presence of Mg in the prepared catalyst improved the CO_2 methanation activity. The addition of Mg (up to 2.5%) produced basic sites and enhanced the dispersion and size of Ni-NPs, which has increased the activation of CO_2. The concentrations of Mg were an essential factor in structural changes of the USY zeolite; a high amount of defective surfaces with oxygen atoms of low-coordination numbers were produced in USY zeolite using the lower concentrations of Mg. Nevertheless, the Ni nanoparticles' reducibility and the crystallinity of the support have been decreased by high Mg concentrations due to the formation of solid solution, e.g., NiO-MgO, which has reduced the CO_2 methanation activity. Liang et al. [257] examined the alkaline earth metals as promoters for the Ni/Al_2O_3 catalyst towards CO_2 methanation activity. The promotion of Mg and Ca has negative effects on the catalytic efficiency of Ni/Al_2O_3 in CO_2 methanation by promoting the RWGS reaction. In converse, the methanation activity has been increased drastically, especially in the low-temperature region with the addition of Sr or Ba. It was reported that the Sr species generated the oxygen vacancies, which have increased the activation of CO_2 to improve CO_2 methanation. Tan et al. [210] prepared Ni/ZrO_2 catalysts with different Ni loadings for study CO_2 methanation. They found that the catalytic activity and thermal stability of the Ni/ZrO_2 catalyst were significantly improved on adding the MgO as a promoter due to highly dispersed Ni NPs and confinement effect. Meanwhile, all promoters are not equally favorable for CO_2 methanation. It has been reported that some promoters have acted differently, depending on the supporting material used. For example, Le et al. [258] found that the Na addition to Ni/CeO_2 catalyst has a negative impact on the catalytic performance for CO_2 conversion. While the Ni/SiO_2 catalyst showed a high catalytic performance towards CO_2 methanation on Na addition as a promoter, they suggested that the addition of Na to the catalyst was closely linked to chemisorb CO_2 on the surface of support materials during CO_2 methanation. In another study, Iloy et al. [259] observed a negative effect of potassium metal for CO_2 hydrogenation activity over silica-supported cobalt due to a decrease of reducibility of Co-NPs during the calcination of catalyst. Other studies also reported similar results [260–263].

5.3.3. Addition of zirconium oxide (ZrO_2)

ZrO_2 has also been used extensively as a promoter in many catalysts to improve catalytic performance for CO_2 methanation due to its superior advantages, including rich oxygen vacancy sites and high thermal stability. Cai et al. [126] used ZrO_2 as a promoter to improve the catalytic performance of synthesized Ni/ZrO_2-Al_2O_3 catalysts for CO_2 methanation. It was found that the addition of ZrO_2 to Ni/Al_2O_3 catalyst has enhanced the catalytic performance (six times higher methane yield) and thermal stability compared to the un-promoted Ni/Al_2O_3 catalyst. They suggested that the high catalytic performance was mainly due to well-dispersed ZrO_2, which suppressed the incorporation of Ni-NPs into the crystal lattice of γAl_2O_3. In another study, high performance has resulted from a synergistic effect by a doped element, ZrO_2 modified clays, and nickel species [264]. Lin et al. [265] studied CO_2 methanation; they found that the addition of ZrO_2 into Ni/Al_2O_3 has increased the oxygen vacancies and active Ni sites to present excellent CO_2 methanation stability.

5.3.4. Addition of cerium oxide (CeO_2)

Cerium, in the form of CeO_2, is another one of the most favorable promoters used in CO_2 methanation to enhance the catalysts' catalytic performance. So far, numerous CO_2 methanation studies have been conducted over ceria-promoted catalysts [131,145,266–268]. Liu et al. [131] synthesized a Ni/Al_2O_3 catalyst and added CeO_2 on it as a promoter to study the CO_2 methanation. They found that the catalytic activity was strongly dependent on the CeO_2 content in all Ni-CeO_2/Al_2O_3 catalysts for CO_2 methana-

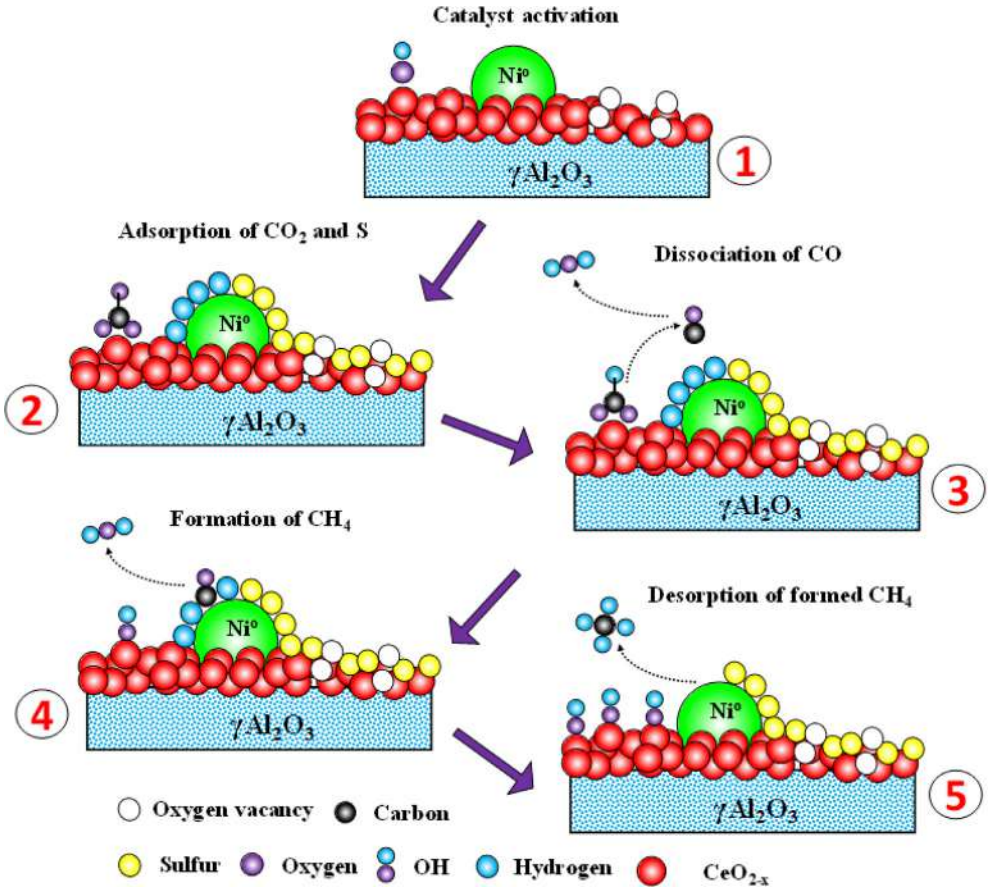

Fig. 22. Schematic representation of the proposed reaction mechanism of CO_2 methanation under H_2S poisoning for Ni-CeO_2 catalyst. Adapted from [268].

tion. Among all the catalysts, the Ni-CeO_2/Al_2O_3 with CeO_2 (2wt%) had the highest catalytic activity and thermal stability due to the high reducibility of Ni-NPs species. They reported that the addition of CeO_2 has lowered the reduction temperature and improved the catalyst's reducibility by altering the interaction between Al_2O_3 and Ni-NPs. Bacariza et al. [224] investigated the effect of incorporating the metal in the Ni/zeolites catalysts for CO_2 methanation. The highest CH_4 selectivity and CO_2 conversion were obtained for the 5Ni-3Ce/Na-USY (3) catalyst, most likely as a result of the combined effect of good dispersion of the NPs and the small size and, their easier reducibility due to interaction with CeO_2 and the good CO_2 adsorption capacity. Recently, Guo et al. [266] synthesized a Ni-Al layered double hydroxide (LDHs), used as catalyst precursors, and modified it by CeO_2 for CO_2 methanation. It was found that the synthesized NiAl-MO/CeO_2-5 catalyst exhibited the highest CO_2 conversion of 91% at low temperature (250 °C). The addition of CeO_2 was beneficial to provide appropriate and oxygen vacancies and basic sites, well dispersion of NPs, which were conducted the activation CO_2 to form methane. Wang et al. [212] investigated CO_2 methanation on the CeO_2 promoted Ni/MCM-41 catalyst. They found high CH_4 selectivity and CO_2 conversion over the CeO_2 promoted Ni/MCM-41 due to well-dispersed Ni particles by synergetic effect among Ni active sites, CeO_2 and MCM-41. Rynkowski et al. [267] synthesized a Ru/Al_2O_3 catalyst and modified it with CeO_2 to improved CO_2 methanation. They observed that the creation of new active sites at the interface between the partially reduced ceria and the Ru metal particles via the Ce-AlO_3 structure had improved catalytic performance of CeO_2 promoted Ru/Al_2O_3 catalyst. The catalytic performance was linked with high reduction temperatures, which indicated larger ruthenium crystallites on the CeO_2 promoted catalyst. They concluded that the Ce (III) atoms present in the $CeAlO_3$ structure were the major factor in improving the CO_2 methanation. Alarcon et al. [268] synthesized the Ni-CeO_2/γ-Al_2O_3 modified catalyst using CeO_2 as a promoter for the CO_2 methanation study. They found that the modified catalyst exhibited higher tolerance to sulfur poisoning due to the presence of CeO_2, which minimized the formation of non-active NiS sites on the catalyst during CO_2 methanation activity, as shown in Fig. 22. In addition, the CeO_2-promoted catalyst showed high thermal stability, while the non-promoted catalyst suffered from nickel sintering. In another study, Tada et al. [116] also used CeO_2 in the modification of synthesized Ru/Al_2O_3 catalyst to examine CO_2 methanation. They found that the CeO_2 promoted Ru/Al_2O_3 showed a high CO_2 conversion rate with high sulfur tolerance due to partial surface reduction, which contributed to decompose formate species.

5.3.5. Addition of lanthanum oxide (La_2O_3)

La_2O_3 is one of the most active promoters used to modulate the surface basicity of the catalysts for CO_2 methanation. Quindimil et al. [202] prepared Ni supported on beta and Y zeolites to test CO_2 methanation. They also used La_2O_3 as a promoter to improve the catalytic activity of the catalysts. It was noted that the beta zeolites performed higher CO_2 methanation activity than the Y zeolites due to the high dispersion of Ni particles. The Ni dispersion was enhanced due to the addition of La_2O_3, which has further boosted the Ni/BETA zeolite catalyst's basic properties to improve the activity and selectivity to CH_4. The La_2O_3 promoted Ni/BETA catalyst performed CO_2 conversion of 65% and CH_4 selectivity of ca. 100%, twofold compared to unpromoted Ni/BETA catalyst without La_2O_3. Zhang et al. [269] prepared the La-doped Ni/Mg-Al catalysts with different La loadings to study CO_2 methanation. They

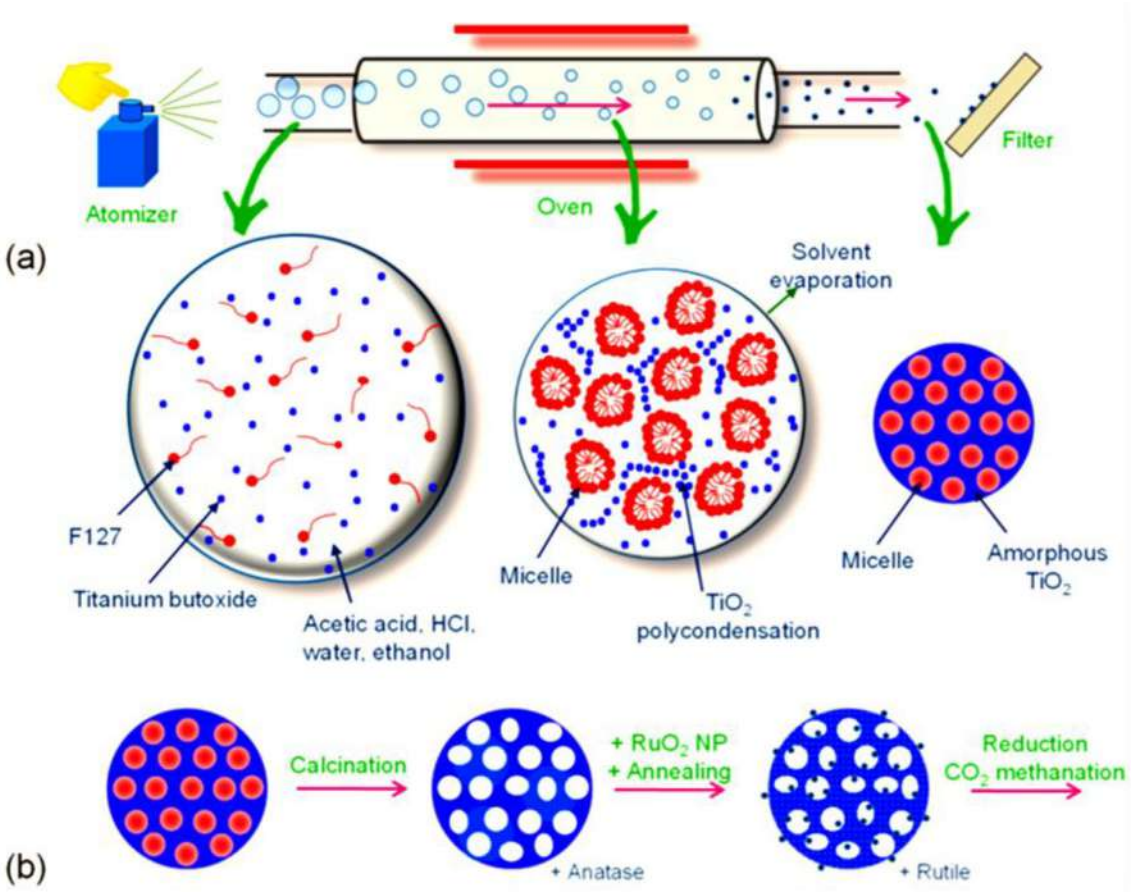

Fig. 23. (a) Systematic synthesis steps involved in mesoporous Ru promoted TiO_2 support. The precursor solution was atomized. Then the aerosol mist paced in a tubular furnace. The obtained dried particles of surfactant micelles and amorphous TiO_2 were collected on an absolute filter. (b) The particles were calcined in air to generate the porosity and NPs of RuO_2 were impregnated onto the mesoporous TiO_2 supports. Reprinted with permission from [287]. Copyright (2018) American Chemical Society.

discovered that the 2% La prompted Ni/Mg-Al catalyst achieved the high CO_2 conversion (61%) and CH_4 selectivity (nearly 100%) due to high basicity. Zhi et al. [270] investigated the effect of La_2O_3 on the catalytic performance of the Ni/SiC for CO_2 methanation. It was found that the La_2O modified Ni/SiC exhibited high activity and thermal stability than pure Ni/SiC due to high dispersion Ni-NPs. Wang et al. [271], investigated CO_2 methanation over a La-modified Ni/SBA-15 catalyst. They found that the La-modified Ni/SBA-15 catalyst exhibited decent catalytic performance, high stability, and anti-sintering due to the high dispersion of Ni-NPs and strong metal-support interaction.

5.3.6. Addition of vanadium oxide (VO_x)

VO_x, as a promoter, has recently been studied in various CO_2 methanation catalysts. Lu et al. [272] investigated CO, and CO_2 methanation over the VO_x promoted Ni catalysts supported catalysts. They reported that adding a proper amount of VO_x could enhance methanation activities with superior anti-sintering and anti-coking properties. It was attributed that high catalytic activity was due to the well-dispersed active Ni-NPs, which have improved the interaction with bentonite support by VO_x. In another study, Hamid et al. [273] examined CO_2 methanation over vanadium promoted Ni/KCC-1 catalyst. They reported that the addition of V_2O_5 to Ni/KCC-1 catalyst had improved the CO_2 methanation activity due to high basicity and well-dispersed Ni species, which provided additional adsorption sites for CO_2 activation at a lower temperature. Wang et al. [274], conducted CO_2 hydrogenation over Rh-0.3VO_x/MCM-41catalysts, modified using vanadium oxide as a promoter. They found that higher CO_2 hydrogenation activity was due to a higher number of nanoparticles of Ru and the VO_x-Rh interface sites on the MCM-41.

5.3.7. Addition of other promoters

Recently, Burger et al. [275] prepared a modified $NiAlO_x$ catalyst using two promoters Mn and Fe, and applied it for CO_2 methanation. It was reported that the combination of both dopants enhanced the catalytic activity. Moghacidam et al. [276] synthesized the mesoporous supported nickel-based catalysts on nanocrystalline alumina using different types of promoters, including Fe, Zr, Co, La, and Cu. Among all, Fe promoted Ni-based catalyst presented the highest CO_2 methanation activity due to the high reducibility of NiO, which was occurred at lower temperatures. Zhao et al. [277] investigated Mn-promoted Ni/Al_2O_3 catalysts for CO and CO_2 methanation and found that the high Ni nanoparticles dispersion and reducibility have improved the catalytic performance of Mn-Ni/Al_2O_3 (60%) three times higher compared to the unpromoted catalyst (ca. 20%). The well-dispersed Ni particles and the high number of basic sites also contributed to improving the catalytic performance of Mn-promoted catalyst with anti-sintering properties during the methanation reaction. Vrijburg et al. [278] studied the promotional effect of MnO on Ni catalysts supported on a silica-modified γ-Al_2O_3 (SA) to execute CO_2 and CO methanation. Significantly higher methanation rates and CH_4 selectivities were obtained for Mn-promoted compositions compared to Ni-only catalysts. The Mn addition has increased the dispersion and the reducibility of Ni particles, which enhanced the CO_2 adsorption and activation. Bakar et al. [213] prepared the Ni/Al_2O_3 catalysts and modified them with Mn and noble metals to

study CO_2 methanation. Among all the catalysts, the Ru promoted Ni/Al_2O_3 showed superior CO_2 conversion of 99.74% and CH_4 formation of 72.36% due to the high reducibility of Ru nanoparticles. Guo et al. [279] prepared a Co modified Ni/SiO_2 catalyst and applied it in CO_2 methanation. The catalytic activity has been observed to increase significantly over Ni-Co/SiO_2 catalysts due to Co/Ni molar ratios and high Co loading. In another study, the CO_2 methanation reaction was performed using Co as a promoter and it was found that the appropriate addition of Co metal on Ce_x-$Zr_{1-x}O_2$ could remarkably enhance the catalytic activity and thermal stability [280]. Isah et al. [281] executed the CO_2 methanation reaction over a zeolite-promoted Ni/Al_2O_3 nanocatalyst and found that the addition of zeolite (2%) has exhibited superior CO_2 conversion of 99% and CH_4 selectivity of 56% towards CO_2 methanation reaction due to high the surface area.

5.4. Effect of preparation methods on CO_2 methanation

One of the most significant considerations for developing catalysts for methanation reactions is an optimized preparation process. The metal dispersion, catalytic activity, crystal structure, and allowable metal loadings on the supports can be affected by chemical and physical techniques used to combine metals and supports. Some of the commonly used preparation methods are discussed in the following sections.

5.4.1. Sol-gel method

The sol–gel is one of the most versatile chemical methods, which has been used for the preparation of solids catalysts for various chemical reactions. Typically, this method is employed to synthesize a porous solid catalyst using small metal alkoxide molecules, sulfides, or nitrides, or specific metal salts [282–285]. Different processes, including aqueous and non-aqueous routes and preparation methods, are used to produce methanation catalysts, following the basic sequence: (1) the precursor's solution is converted into an active state, (2) the activated precursors are converted to nanoclusters through polycondensation, (3) gelation; formation of gel which encapsulates the solvent, (4) aging process (typically 1–5 days; 50–100 °C), (5) calcination process, (6) washing process, and (7) stabilization/drying. Thus, the synthesized catalysts are stable enough and can be used for methanation reactions up to 500 °C [286,287]. Kim et al. [287] synthesized mesoporous Ru promoted TiO_2 based CO_2 methanation catalyst via the aerosol-assisted self-assembly process, as depicted schematically in Fig. 23. They reported that the catalytic activity depends greatly on the large surface area, small RuO_2 crystals, and the strong interaction between rutile TiO_2 and RuO_2.

5.4.2. Impregnation method

When a precursor of an active phase is contacted with the solid support using a specific volume and then dried subsequently to remove the imbibed solvent is called impregnation, which is prominent in two ways: wet impregnation (WI) and incipient wetness impregnation (IWI). In the first one, the solution volume is used in excess amount. The solid particles are separated after some particular interval of time, and the heating or drying process detaches the excess solvent [288]. The latter one is also called capillary impregnation or dry impregnation. Typically, the active metal's precursor is mixed in an organic or aqueous solution of incipient wetness amount. Several heterogeneous metal catalysts for methanation reactions have been synthesized using this technique because it is easy and straightforward to control metal loadings without liquid waste. However, the impregnation method generally results in the formation of large, aggregated particles on the external surface of the mesoporous silica [289,290].

Pan et al. [291] examined the CO_2 methanation reaction over different nickel-promoted catalysts synthesized by impregnation, deposition–precipitation, and urea combustion techniques. They reported that the $Ni/Ce_{0.5}Zr_{0.5}O_2$ catalyst prepared by the impregnation method had displayed the highest activity due to a large number of oxygen vacancies, basic sites, high Ni surface area, and high Ce (III) atoms. Dong et al. [292] synthesized a Ni/3DSBA-15 catalyst using the incipient wetness impregnation method to examine CO_2 methanation. It was reported that the phyllosilicate catalyst presented superior catalytic performance and stability. In another study, Guo et al. [293] conducted CO_2 methanation over the Mg-modified Ni/SiO_2 catalysts prepared by different impregnation methods and found that the co-impregnation method could significantly improve the activity and thermal stability of synthesized catalysts compared to other prepared catalysts.

5.4.3. Microemulsion method

Typically, industrial processes are performed under harsh conditions, making it difficult to achieve the long-term thermal stability of the catalysts. To design high thermally, stable catalysts for methanation reactions has been a great challenge. The microemulsion process, which is regarded as the best way to achieve high thermal stability, high pores volume, high surface area, and high dispersed metal nanoparticles, can develop organic or inorganic nanomaterial catalysts, which play a critical role in increasing CO_2 methanation [50,294]. Generally, the combination of the water phase, oil phase, surfactant, and co-surfactants are used in the microemulsion process. Primarily, the aqueous phase consists of the metal salt and other ingredients, while the oil is a complex mixture of olefins and hydrocarbons. There are three types of microemulsion: (i) water-in-oil or reverse microemulsion, (ii) oil-in-water microemulsion, and (iii) bicontinuous microemulsion [295–297]. Park et al. [72] studied CO_2 methanation over monometallic and bimetallic catalysts prepared by a reverse microemulsion process. They reported that the nanoparticles of palladium, magnesium, nickel, and lithium were highly dispersed and aggregated on the surface of silica support. The superior CO_2 methanation activity was noticed due to the synergistic effect between well-dispersed nanoparticles of Pd, Mg, and Si oxide. During the microemulsion process, the surfactant might be nonionic or ionic, which defines the stabilizing interactions between the aqueous phase and the hydrophilic end of the surfactant [298–301]. Hussain et al. [50] studied CO_2 methanation over a metal-free fibrous silica ZSM-5 (FS@ZSM-5) catalyst synthesized using a microemulsion process. They found higher CO_2 methanation activity (formation of methane of 0.108 mmol $m^{-2}s^{-1}$ and CH_4 selectivity of 66%) than commercial ZSM-5 (rate of formation of methane 0.067 mmol $m^{-2}s^{-1}$ of CH_4 selectivity of 37%). In another study, Hussain et al. [185] prepared fibrous silica-mordenite (FS@SiO_2-MOR) and fibrous silica-beta zeolite (FS@SiO_2-BEA) using the microemulsion method and applied these as metal-free catalysts for CO_2 methanation. They found that high surface area, oxygen vacancies, and basicity improved the catalytic performance for CO_2 methanation.

5.4.4. Other preparation methods

Hwang et al. [302] employed a co-precipitation method to synthesize the mesoporous NiFe-Al-X catalysts using different types of precipitation agents such as $(NH_4)_2CO_3$, Na_2CO_3, NH_4OH, and NaOH. They applied these synthesized catalysts for CO_2 methanation and found that among all, the NiFeAl-NaOH catalyst exhibited high CO_2 methanation activity. The catalytic performance of the catalysts was found to rely on the nature of the precipitation agents used in the synthesis process. In recent times, another type of material consists of anion intercalated inorganic linkage, which is also known as hydrotalcite-like compounds, anionic clays, or lay-

Table 5
Types and nature of catalyst deactivation in methanation activity.

No.	Mechanism	Description	Example	Nature	Ref.
1	Fouling	The blockage of the sites and pores onto the catalyst active surface due to carbon deposition that results in activity loss.	$2CO\ (g) \leftrightarrow CO_2\ (g) + C\ (s)$	Physical	[308,309]
2	Attrition or crushing	The crushing of the catalyst particles due to mechanical fluidization, which reduces the internal surface area of catalytic materials.	In a fluidized-bed or slurry-bed reactors, the catalyst particles are crushed into fines powder, which may block the active sites is carried away with the product flow.	Physical	[308]
3	Thermal degradation (Sintering)	The loss of active surface of catalysts due to crystallite growth of either the active phase or support material by sintering, chemical transformations or evaporation.	Thermal degradation is usually occurs during reduction or calcination of synthesized samples at high temperatures.	Physical	[310]
4	Poisoning	Strong chemisorption of pollutants species on the catalytic active sites due to unwanted chemical reactions.	• $H_2S\ (g) + NiO\ (s) \leftrightarrow NiS\ (s) + H_2O\ (g)$ • $2H_2\ (g) + C_4H_5S\ (g) \leftrightarrow H_2S\ (g) + C_4H_{10}\ (g)$ • Tars • Ammonia • Chlorine compounds • Alkalis	Chemical	[311]
5	Vapours solids reactions	Formation of inactive phases on catalytic actives sites due to chemical reactions with, support materials, promoter or fluid.	Carbon monoxide react with active phase of Ni-based catalysts to form nickel carbonyls species at temperatures below 230 °C. $Ni_{(S)} + 4CO_{(g)} \leftrightarrow Ni\ (CO)_{4(g)}$	Chemical	[312]

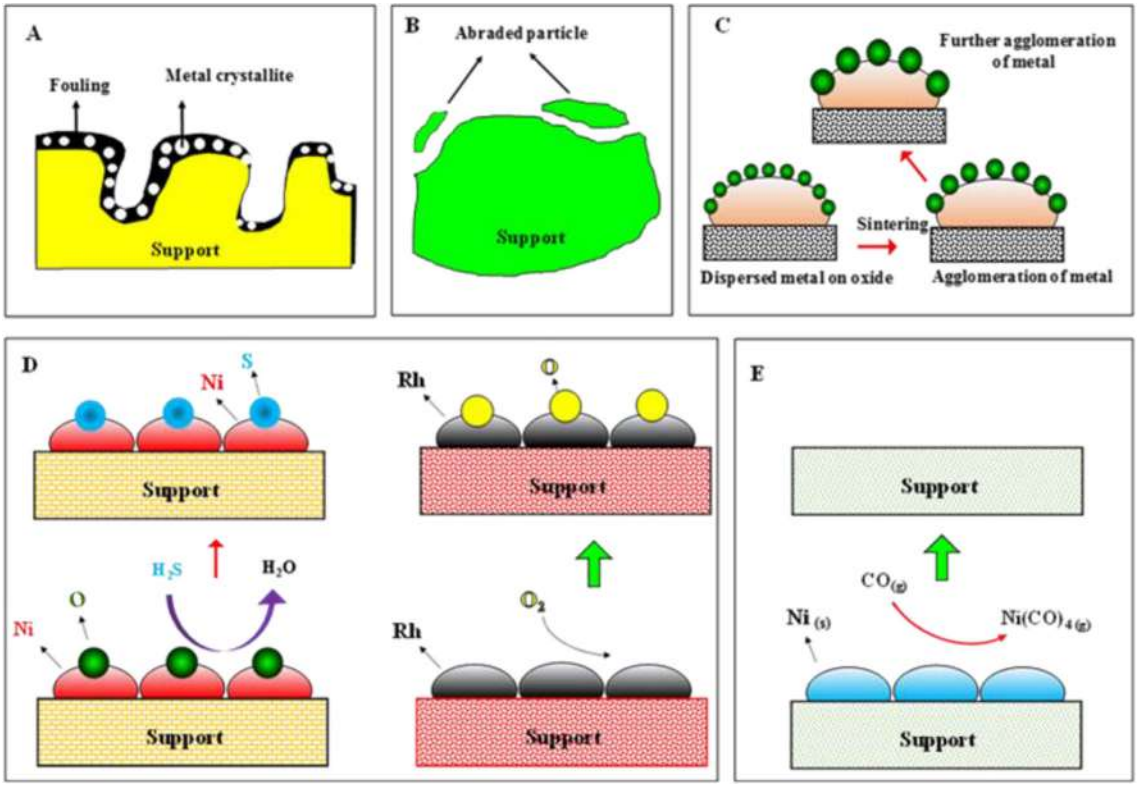

Fig. 24. Different types of catalyst deactivation in methanation (A) fouling, (B) attrition, (C) sintering, (D) poisoning, and (E) vapours solids reactions. Adapted from [42].

ered double-hydroxide materials (LDHs). These materials have gained much interest as precursors or heterogeneous catalysts due to their high dispersion of metallic particles and large specific surface area. He et al. [303] used a facile method to synthesize the NiAl-LDH precursor using a hierarchical Al_2O_3 matrix and applied it for CO_2 methanation. They reported that high catalytic performance was achieved (over 90% CO_2 conversion) over the synthesized catalyst. It was found that the activity was correlated to high dispersion of fastened Ni clusters, and a large number of surface vacancies, which severed as the active sites during CO_2 methanation. In another study, the Ni-Al_2O_3-HT catalysts were prepared using Al hydrotalcite as a precursor for CO_2 methanation. It was reported that the high catalytic performance of both catalysts was due to highly dispersed Ni particles and basic sites; these results were consistent with another CO_2 methanation study [304].

Dielectric barrier discharge plasma (DBD) is another crucial and new method, which is used to enhance the catalytic activity by plasma generation that requires a dielectric barrier material between the electrodes [305,306]. Very recently, the nickel precursors are decomposed by DBD to prepare the Ni/$MgAl_2O_4$ catalysts with well-dispersed Ni nanoparticles (Ni-NPs) [307]. It was reported that using this method, the CO_2 methanation activity could improve significantly. In another study, Jwa et al. [213] used a DBD reactor filled with Ni/zeolite pellets to examine the hydrogenation of CO and CO_2 to produce CH_4. It was found that after the plasma-assisted reaction, smaller and well-dispersed Ni-NPs

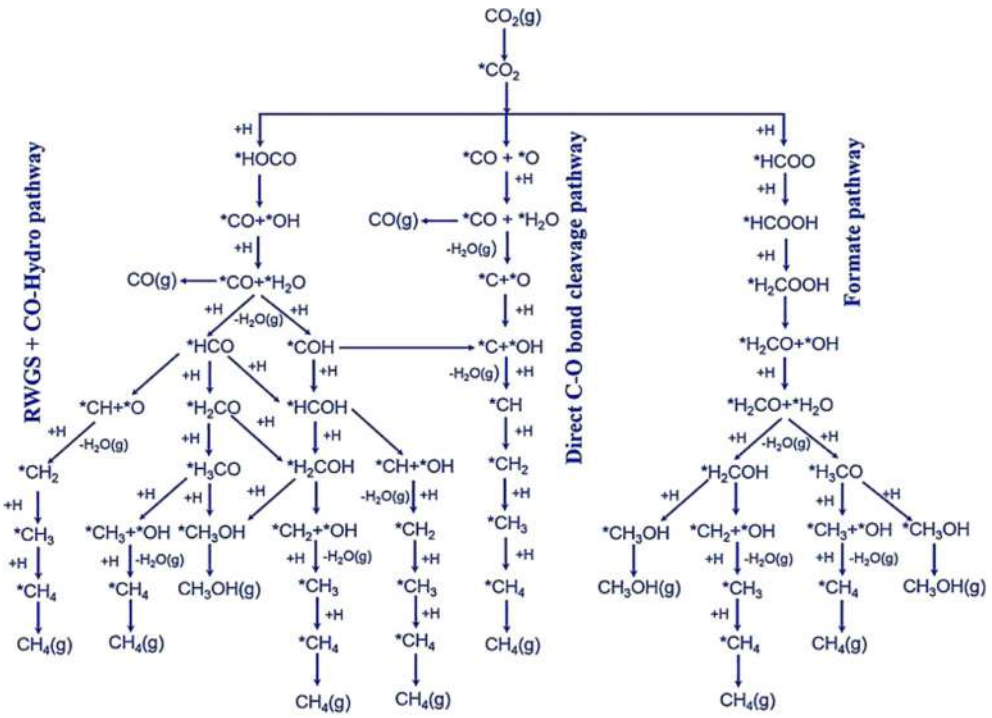

Fig. 25. Possible reaction pathways of CO_2 methantion to CH_4 along with CH_3OH and CO, (*) presents the adsorbed surface species. Reprinted with permission from [320]. Copyright (2017) American Chemical Society.

Table 6
Reaction energies (ΔE) and activation energies (*Ea*) of different elementary reactions of for direct C-O bond cleavage pathway during CO_2 methanation [322].

No.	Reaction steps	ΔE (kJ/mol)	E_a (kJ/mol)
1	$CO_2^* \rightarrow CO^* + O^*$	−73.09	13.60
2	$CO^* + O^* + H_2 \rightarrow CO^* + O^* + H_2^*$	−36.73	–
3	$CO^* + O^* + H_2^* \rightarrow CO^* + H_2O^*$	78.26	319.60
4	$CO^* + H_2O^* \rightarrow CO^* + H_2O\uparrow$	58.90	–
5	$CO^* \rightarrow C^* + O^*$	76.92	132.18
6	$C^* + O^* + H_2 \rightarrow C^* + O^* + H_2^*$	−216.39	–
7	$C^* + O^* + H_2^* \rightarrow C^* + OH^* + H^*$	16.35	113.67
8	$C^* + OH^* + H^* \rightarrow C^* + H_2O^*$	−78.56	58.02
9	$C^* + H_2O^* \rightarrow C^* + H_2O\uparrow$	121.68	–
10	$C^* + H_2 \rightarrow C^* + H_2^*$	−88.52	–
11	$C^* + H_2^* \rightarrow CH^* + H^*$	−88.61	12.82
12	$CH^* + H^* \rightarrow CH_2^*$	−45.12	39.64
13	$CH_2^* + H_2 \rightarrow CH_2^* + H_2^*$	−108.06	–
14	$CH_2^* + H_2^* \rightarrow CH_3^* + H^*$	−47.02	102.23
15	$CH_3^* + H^* \rightarrow CH_4^*$	15.70	135.86

were obtained, which have significantly improved the catalytic performance for carbon oxides. The summary of the representative catalysts for CO_2 methanation has been shown in Table 4.

6. Main challenges in CO_2 methanation

6.1. Deactivation of the catalysts

The methanation catalysts undergo rapid and severe deactivation due to different physicochemical changes, such as thermal degradation of the support material, metal sintering, oxidation of the metallic phase, particularly, the coke formation. The deactivation of the catalysts can be classified into two major types: (i) physical deactivation and (ii) chemical deactivation. Fouling (coke deposition), thermal degradation (sintering), and attrition are the major factors of the catalyst's physical deactivation. While in the chemical deactivation, the catalysts are typically deactivated by poisoning and vapor–solid reactions [38], these deactivation phenomena are summarized in Table 5 with schematic representations, as shown in Fig. 24. The deactivation of the catalysts depends on the structure and the composition of the catalysts, and operating conditions during the catalytic performance, including feed ratio, temperature, and pressure, which could promote the sintering, attrition, or coke deposition [11]. The physical deposition of gas-phase species onto the active surface of the catalyst is called fouling, which causes blockage of the pores and active sites of the catalysts, as shown in Fig. 24A. For example, the decomposition of CO_2 produces CO molecules, which further generate solid carbon and CO_2 through Boudouard reaction or CO disproportionation:

Table 7
Reaction energies (Δ*E*) and activation energies (*Ea*) of different elementary reactions of for formate pathway during CO_2 methanation [322].

No.	Reaction steps	Δ*E* (kJ/mol)	E_a (kJ/mol)
1	$CO_2^* + H_2 \rightarrow CO_2^* + H_2^*$	−94.32	–
2	$CO_2^* + H_2^* \rightarrow HCOO^* + H^*$	30.29	88.61
3	$HCOO^* + H^* \rightarrow HCOOH^*$	17.03	172.45
4	$HCOOH^* + H_2 \rightarrow HCOOH^* + H_2^*$	−53.65	–
5	$HCOOH^* + H_2^* \rightarrow H_2COOH^* + H^*$	−47.02	70.92
6	$H_2COOH^* + H^* \rightarrow H_2CO^* + H_2O^*$	−44.75	283.67
7	$H_2CO^* + H_2O^* \rightarrow H_2CO^* + H_2O\uparrow$	46.10	–
8	$H_2CO^* + H_2 \rightarrow H_2CO^* + H_2^*$	−103.64	–
9	$H_2CO^* + H_2^* \rightarrow H_2COH^* + H^*$	112.24	254.90
10	$H_2COH^* + H^* \rightarrow CH_2^* + OH^* + H^*$	−144.87	160.99
11	$CH_2^* + OH^* + H^* \rightarrow CH_2^* + H_2O^*$	9.39	65.45
12	$CH_2^* + H_2O^* \rightarrow CH_2^* + H_2O\uparrow$	64.07	–
13	$CH_2^* + H_2 \rightarrow CH_2^* + H_2^*$	−73.27	–
14	$CH_2^* + H_2^* \rightarrow CH_3^* + H^*$	−18.61	25.92
15	$CH_3^* + H^* \rightarrow CH4^*$	45.48	118.91
16	$H_2CO^* + H_2^* \rightarrow H_3CO^* + H^*$	−10.28	116.72
17	$H_3CO^* + H^* \rightarrow CH_3^* + OH^*$	87.27	321.96
18	$CH_3^* + OH^* + H_2 \rightarrow CH_3^* + OH^* + H_2^*$	−38.23	–
19	$CH_3^* + OH^* + H_2^* \rightarrow CH_3^* + H_2O^* + H^*$	49.90	128.40
20	$CH_3^* + H_2O^* + H^* \rightarrow CH_3^* + H^* + H_2O\uparrow$	53.96	–
21	$CH_3^* + H^* \rightarrow CH_4^*$	30.55	127.89

2CO (g) ⇌CO_2 (g) + C (s) [308]. This problem can be solved by increasing the H_2/CO ratio or adding the steam during the methanation reaction because solid carbon can react with water and hydrogen to inhibit carbon deposition [309,313].

This type of deactivation process mainly depends on catalyst particle shape and the operating conditions. Typically, it proceeds when the feedstock passes through methanation reactors, including, fixed-bed, fluidized-bed, and slurry-bed reactors, it carryover of dust and fines produced after attrition, as shown in Fig. 24B. To solve this issue, process conditions and structural properties of catalysts are optimized and tuned, respectively with minimum impacts of attrition. Besides, new technology has been introduced by DuPont, which could encapsulate the active phase in a porous silica shell to permit unhindered diffusion of the reactants and products, without affecting selectivity and conversion [308,309].

Another type of deactivation of catalysts is the sintering of metal particles due to growing the surface metal particles or metal crystallite size. This phenomenon can lead to the loss of the active surface area of the catalysts, resulting in decreases in the activity per gram of catalyst (less accessible active sites) [310], as shown in Fig. 24C. The high temperature (above 500 °C) and the exothermicity nature of the methanation reaction are somehow also responsible for the sintering effect. Therefore, some catalysts have been designed for high temperatures methanation (<700 °C) [314].

In addition, poisoning is another major issue that causes the deactivation of the Ni-based catalysts. Ni metal is highly active towards impurities, which are inherently present in the CO_2 stream, such as biogas and flue gas, or atmosphere. Contaminants such as tars, ammonia, chlorine compounds, alkalis, particles, or sulfur compounds can react sensitively to active sites of the methanation catalysts during methanation reactions. This issue is tackled by additional care in operating or planning CO_2 methanation plants with sulfur-containing CO_2 derived from anaerobic biogas plants because the sulfur gradient is readily formed along the reactor axis [315,316]. For this purpose, the CO_2 methanation reactors must be installed with a suitable sulfur elimination system to avoid sulfur poising. Generally, a Rectisol wash process is conducted with adsorption of zinc oxide or low-temperature methanol [317]. The state-of-the-art Ni-supported catalysts can sustain the stability and activity over hundreds of hours if the concentration of sulfur content is present in the feedstock in parts per billion (ppb) [318]. Hydrogen sulfide (H_2S) can react quickly with nickel oxide (NiO) to form water and nickel sulfide (NiS), leading to a decrease in the activity of Ni-based catalysts during the chemical reaction as shown in Table 5 and Fig. 24D [311]. Many chemical reactions, such as vapor phase reactions that can react with the catalysts' surface to produce inactive surface species, lead to catalyst deactivation. Typically, in methanation reactors, CO (g) reacts with Ni (s) to form a nickel tetracarbonyl compound (Ni $(CO)_4$ (g)) at temperatures below approximately 230 °C [312], as mentioned in Fig. 24E and Table 5. To solve this issue, the methanation reaction should not run over commercial Ni-based catalysts below 250 °C [319].

Table 8
Reaction energies (ΔE) and activation energies (Ea) of different elementary reactions of for RWGS + CO hydrogenation pathway during CO_2 methanation [322].

No.	Reaction steps	ΔE (kJ/mol)	E_a (kJ/mol)
1	$CO_2^* + H_2 \rightarrow CO_2^* + H_2^*$	−94.32	–
2	$CO_2^* + H_2^* \rightarrow COOH^* + H^*$	38.05	151.75
3	$COOH^* + H^* \rightarrow CO^* + H_2O^*$	29.82	228.90
4	$CO^* + H_2O^* \rightarrow CO^* + H_2O\uparrow$	64.46	-
5	$CO^* + H_2 \rightarrow CO^* + H_2^*$	−97.59	-
6	$CO^* + H_2^* \rightarrow HCO^* + H^*$	−51.28	110.43
7	$HCO^* + H^* \rightarrow CH^* + OH^*$	54.83	210.01
8	$CH^* + OH^* + H_2^* \rightarrow CH^* + H_2O^* + H^*$	−105.68	-
9	$CH^* + OH^* + H_2 \rightarrow CH^* + OH^* + H_2^*$	100.04	172.30
10	$CH^* + H_2O^* + H^* \rightarrow CH^* + H^* + H_2O\uparrow$	24.79	–
11	$CH^* + H^* \rightarrow CH_2^*$	65.85	237.15
12	$CH_2^* + H_2 \rightarrow CH_2^* + H_2^*$	−140.39	-
13	$CH_2^* + H_2^* \rightarrow CH_3^* + H^*$	−77.99	101.97
14	$CH_3^* + H^* \rightarrow CH_4^*$	17.84	70.26
15	$HCO^* + H^* \rightarrow H_2CO^*$	−97.32	36.06
16	$H_2CO^* + H_2 \rightarrow H_2CO^* + H_2^*$	−100.62	-
17	$H_2CO^* + H_2^* \rightarrow H_3CO^* + H^*$	4.68	97.81
18	$H_3CO^* + H^* \rightarrow CH_3^* + OH^*$	173.77	368.32
19	$CH_3^* + OH^* + H_2 \rightarrow CH_3^* + OH^* + H_2^*$	−146.45	-
20	$CH_3^* + OH^* + H_2^* \rightarrow CH_3^* + H_2O^* + H^*$	22.58	51.21
21	$CH_3^* + H_2O^* + H^* \rightarrow CH_3^* + H^* + H_2O\uparrow$	64.81	-
23	$CO^* + H_2^* \rightarrow COH^* + H^*$	141.51	153.96
24	$COH^* + H^* \rightarrow HCOH^*$	−20.79	196.62
25	$HCOH^* \rightarrow CH^* + OH^*$	−45.02	196.24
26	$CH^* + OH^* + H_2 \rightarrow CH^* + OH^* + H_2^*$	−48.18	-
27	$CH^* + OH^* + H_2^* \rightarrow CH_2^* + H_2O^*$	7.46	243.43
28	$CH_2^* + H_2O^* \rightarrow CH_2^* + H_2O\uparrow$	53.57	-
29	$CH_2^* + H_2 \rightarrow CH_2^* + H_2^*$	−140.39	-
32	$HCOH^* + H_2 \rightarrow HCOH^* + H_2^*$	−123.28	-
33	$HCOH^* + H_2^* \rightarrow H_2COH^* + H^*$	−47.08	145.86
34	$H_2COH^* + H^* \rightarrow CH_3^* + OH^*$	−21.13	99.76

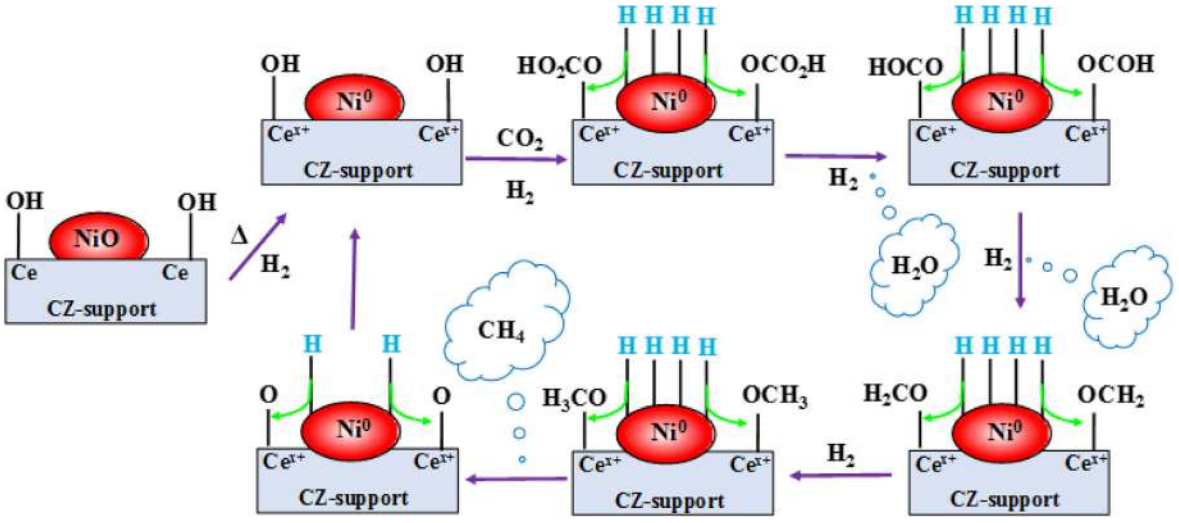

Fig. 26. Proposed reaction mechanism via formate pathway during CO_2 methanation over Ni/CZ-AE catalyst. Adapted from [346].

6.2. Reaction mechanisms of CO_2 methanation

In order to design superior catalytic systems rationally, reaction mechanisms during CO_2 methanation must be investigated. Although CO_2 methanation is relatively a simple reaction, there are several challenges to establish the arguments on the nature of the intermediate surface species, and their role in forming methane is still debatable. The CO_2 methanation mechanisms can be categorized into three major routes based on CO_2 initial hydrogenation: (i) CO_2 direct dissociation pathway (CO_2 direct dissociation into CO*), (ii) the formate pathway (CO_2 C-terminal hydrogenation to HCOO* species), and (iii) RWGS + CO Hydro pathway (CO_2 O-terminal hydrogenation to COOH* species) [320–322], as shown in Fig. 25. Typically, the multiple active sites available at the surface of catalysts facilitate the activation and dissociation of reactants to produce the desired product via different reaction intermediate species. Recently, several in situ, operando experimental techniques and theoretical studies of CO_2 methanation were elucidated [322–332] and reaction intermediate species and elementary steps were discussed.

6.2.1. CO_2 direct dissociation pathway

In this pathway, CO_2* dissociates into CO* and O* first; the subsequent steps are the same as those of CO methanation. This process is exothermic with the reaction energy of −73.09 kJ/mol and needs to overcome a barrier of 13.60 kJ/mol on Rh/TiO_2 catalyst, as mentioned in Table 6. This specifies that the Rh/TiO_2 catalyst dissociated CO_2* into CO* with high activation energy barrier (51.00 kJ/mol) [322,323], which reveals that the Rh/TiO_2 catalyst is much more active for CO_2 activation than Ni-based catalysts. The *CO undergoes dissociation reaction to form *O and *C, which subsequently converted to CH_4 on hydrogenation [322,324,333]. The reaction energies (ΔE) and activation energy barriers (Ea) of different elementary reactions have been listed in Table 6.

Methanation of CO_2 was conducted over Ni (110), and Ni (100) surfaces by density functional theory (DFT) observations. The CO was found one of the main intermediates in this process by comparison of the energy barrier. Some of the other intermediates were also observed, including carbonyl, hydroxyl, and HCOO during CO_2 methanation [334–336]. It was found that the reaction rates for CH_4 formation and activation energy for CO_2 were close to the values for methanation of CO under the same circumstances. Falconer et al. [337] performed CO_2 methanation over a Ni/Si catalyst through temperature-programmed reduction and temperature-programmed desorption. They found that the CO_2 was dissociated CO and O atoms at high temperatures. In other mechanistic studies of CO_2 methanation, it has also been reported that CO as an intermediate was produced not only on Ni-based catalysts, but on other catalysts as well, such as Pt and, Rh and Ru [338–342].

6.2.2. Formate pathway

The formation of methane via the CO bond cleavage in H_2COH or H_3CO is termed a formate pathway [111]. According to some CO_2 methanation studies, the associative pathways with formate are important in the formation of methane [343,344]. Yang et al. [322] investigated the reaction mechanism over an Rh/TiO_2 catalyst. They found the reaction energies (ΔE) and activation energy barriers (Ea) of different elementary reactions have been listed in Table 7. They reported that the H_2 molecule was adsorbed and spontaneously dissociates on the interfacial Rh site. Subsequently, CO_2* was hydrogenated to HCOO* (30.29 kJ/mol) and HCOOH* (17.03 kJ/mol). The HCOOH* further converted into H_2COOH* species, which is an exothermic process, as listed in Table 7. The H_2COOH* species decomposed into H_2CO* and H_2O* by reacting with H*; however, the decomposition of H_2COOH* was a kinetically unfavorable process (Ea = 283.67 kJ/mol). The H_2CO* species further hydrogenated to H_3CO* or H_2COH* after H_2O* desorption. Subsequently, the CH_2* and OH* were formed by the decomposition of H_2COH*. The H_2O* species were formed by the reaction of OH* and H* to desorbs from the catalyst surface. While after H_2O* desorption, the H_2COH* species decomposed to produce CH_2*, which was hydrogenated to CH_4*. Bian et al. [345] investigated kinetic and mechanistic study CO_2 methanation over the

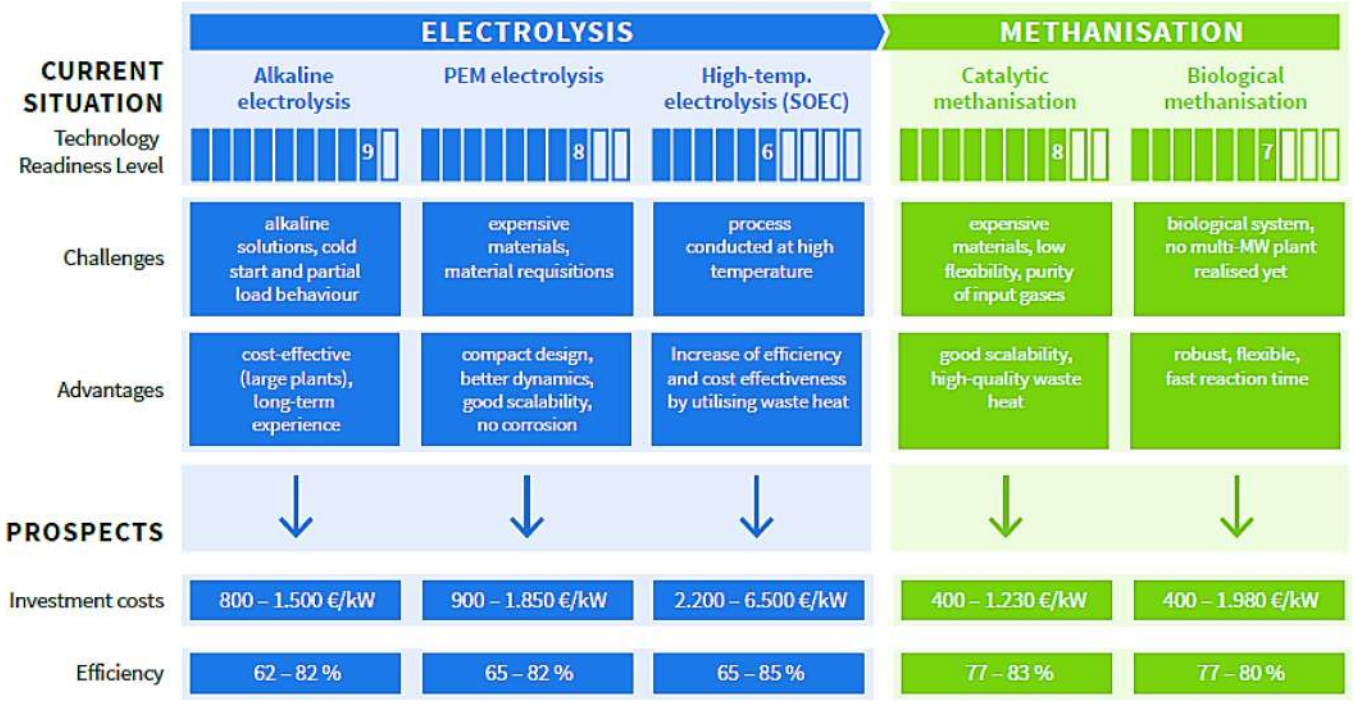

Fig. 27. Methantion to methane technology: current state and perspectives. Adapted from [365].

Ni/CeO_2; they found that methane formation followed the formate pathway over oxygen vacancies, which acted as active sites for the formate formation. Ashok et al. [346] examined CO_2 methanation over a Ni/CeO_2-ZrO_2 catalyst. According to DRIFTS observations, they concluded that the main reaction pathway does not involve CO as an intermediate; most of the CO_2 part was converted to methane via a formate pathway. They reported that the CO_2 could linearly adsorb onto catalyst support as mono or bidentate carbonate, which reacted with dissociated hydrogen to form hydrogenated carbonates. Hydrogen was dissociated on the surface of Ni0 and then spilled over to Ce_x^+ species present in the catalyst support. On further increasing the temperature (250°C), these hydrogenated carbonate species converted into monodentate formats by reaction with the dissociated hydrogen. These formate intermediates converted into formaldehyde-like species and subsequently methoxy species, which finally dissociated to release CH_4, as shown in Fig. 26. Similar results were reported in other studies [118,347–351]. Nevertheless, few studies are available in the literature, which suggests that the intermediate formate species are spectators during the CO_2 methanation activity; they can block the active sites on catalysts surfaces [352–353].

6.2.3. RWGS + CO-Hydro pathway

The formation of methane from CO_2 methanation can also occur via the RWGS + CO hydrogenation pathway. The RWGS + CO-Hydro pathway is also called the carboxyl pathway, which is initiated by the hydrogenation of adsorbed CO_2 to COOH or the C-O bond scission of $^*HCOH$, $^*H_2COH$, $^*H_3CO$ leads to the formation of CH_x species which undergo subsequent hydrogenation reactions to form CH_4 [117,322,342]. Different intermediates have been shown in Table 8 with their *Ea and ⊿E* values of different elementary reactions via the RWGS + CO hydrogenation pathway over the Rh/TiO_2 catalyst. In RWGS + CO hydrogenation pathway, methane is formed through the channel:

$$CO_2^* \rightarrow COOH^* \rightarrow CO^* \rightarrow COH^* \rightarrow HCOH^* \rightarrow H_2COH^* \rightarrow CH_3^* \rightarrow CH_4^* ().$$

In this route, the $COOH^*$ species dissociated into CO^*, which was known as the rate-determining [322]. In some studies, CO and CHO were considered crucial intermediates in the RWGS + CO-Hydro pathway [354–357].

7. The state-of-the-art commercial aspects of CO_2 methanation

Based on the findings of this review, it is clear that catalyst development is a critical step towards the large-scale commercialization of CO_2 methanation. In the current state of technological developments, CO_2 methanation is the most compatible approach to produce substitute natural gas compared to photocatalytic, electrocatalytic, or biological ways. These systems are still far from being a practical consideration compared to CO_2 methanation due to lower volumetric mass transfer coefficient and a lower reaction rate. To produce SNG, CO_2 can be obtained directly from the air or the exhaust gas of the industrial plants and power plants. While H_2 is produced through water electrolysis using renewable methods, including hydroelectric generators, wind turbines, tide, wave, geothermal, solar panels, or photovoltaic cells [31–34]. More efforts to develop reactors, suitable operating conditions, and electrolytic systems for the generation of H_2 from water are expected in the near future, leading to the realistic implementation of large-scale CO_2 methanation.

In the light of international protocols and policies on environmental protection, such as Sustainable Development Goals (SDGs), Kyoto Protocol the Paris Agreement [358–360], the catalytic CO_2 methanation has a great potential to reduce CO_2 and fulfill energy demands. The European Union (EU) aspires to be carbon neutral by 2050, and this goal is at the heart of the European Green Deal [361]. As demonstrated throughout this paper, the development of substitute natural gas emerges as a viable choice for meeting this demand. Taking into account all of the methane's benefits, and with EU policies supporting low CO_2 emission scenarios in the near future, CO_2 methanation appears to be a positive paradigm change that will play a key role in a new energy model. Several EU countries are developing power-to-gas (P2G) technology to produce substitute natural gas. Since 2009, Germany tends to be at the forefront of P2G technology, which offers substitute natural gas. In Stuttgard, there is a well-established industrial-scale Power-to-methane plant of 6300 kW capacity, which supplies methane to Audi (250 kW). This power plant project was launched by "ETOGAS GmbH. ETOGAS" through "ZSW: The Center for Solar Energy and Hydrogen Research" in Wertle, Germany. Another project, the Karlsruhe Institute of Technology (KIT) co-financed by the EU's Seventh Framework Program, has been working on methanation with thermally integrating high-temperature electrolysis (SOEC Technology). This industrial project's predictable hydrogen generation efficiency is 85% higher than that of traditional water electrolysis. In practice, methanation (exothermic) coupled with high-temperature electrolysis (endothermic) provides superior conversion efficiency [362]. Another project was initiated by the Electrochaea Company using a microorganism (methanogenic archaea) as a biocatalyst for a methanation technology [363]. Archaea BioCat has a high mass conversion efficiency and is resistant to a variety of pollutants found in industrial CO_2 sources, such as particulates, H_2S, and O_2. In addition, archaea is highly selective for methane formation, so minimal post-reaction gas treatment is required before injecting the produced gas into the gas grid. Kristjanpoller et al. [364] have published a fascinating paper on the evaluation of biomethanation plants. The work outlines two critical principles that will direct research and generate proposals for the improvement of industrial plants: performance and effectiveness. The first is a measure of the economy in which the company's products are used, including the cost of the catalyst; the second is a measure of the economy in which the company's resources are used, including the cost of the catalyst.

A state-of-the-art perspective on methane production is shown in Fig. 27. According to recent reports, methanation cost is expected to drop from > €1000/kW_{el} by up to 75% below 500 €/kW_{el} by 2050 [41,365]. This decrease in costs is an obvious sign that catalytic CO_2 methanation is being introduced on the market. It is estimated that investment costs for electrolysis and methanation technologies will fall from more than 1000 € $kWel^{-1}$ nowadays to around 500 € $kWel^{-1}$ in the future. This cost reduction is clearly indicated that the market implementation of the CO_2 methanation concept is underway.

8. Conclusions and outlook

The CO_2 methanation reaction has been a topic of significant research interest since the early 1900 s. In recent times, for full-fledged commercialization of CO_2 methanation to produce substituted natural gas, the development of economical, robust, viable, and sustainable catalysts with high activity has been a great challenge due to its strongly exothermic nature, low catalytic performance and coke formation. Previously, several top-notch efforts have been made to resolve these issues; thermodynamics, reactor design, and process configuration aspects have been studied extensively in many reviews. However, reports on robust catalyst systems, which are the perquisites for high CO_2 methanation activity, are somewhat scattered. Here we have carefully examined emerging novel catalysts; especially those fabricated using new generation manufacturing methods, supporting materials and pro-

moters, a subject that has been largely unexplored to date. We have analytically reviewed aspects of robust catalyst systems with identifying opportunities and the critical challenges for enhanced CO_2 methanation. We have also critically reviewed the comprehensive understandings of synergistic interactions of catalyst components (active metal, support, promoter, etc.) for enhanced catalytic performance and stability during CO_2 methanation reaction. We have carefully scrutinized the new emerging novel catalysts, specifically those made-up using new preparation methods, which were unexplored to date. For example, Metal-organic framework (MOF), carbons, and core–shell structure support materials, which are a powerful platform for the design of multifunctional, efficient, and stable catalysts for CO_2 methanation. We discovered that using the right combination of active metals, supporting materials, promoters, and preparation methods is an excellent way to tune the interactions between surface area, electronic/redox properties, structural properties, basicity, metal-support interaction, oxygen vacancies, and reducibility for improved CO_2 methanation. For CO_2 methanation, catalytic stability is also a critical factor because harsh conditions can cause chemical and physical deactivation of the catalysts. The deactivation of CO_2 methanation catalysts was studied with emphasis on their source, effects, development, and control. The main reason for deactivating CO_2 methanation catalysts was coke formation due to side reactions, especially cracking of methane (CH_4 (g) ⇌C + $2H_2$ (g)) and boudouard (2CO (g)⇌ C + CO_2 (g)) reactions. Different techniques such as optimizing reaction conditions, the addition of promoters, and catalyst preparation methods have been explored to avoid this issue. In spite of catalysts deactivation and energy consumption, higher CH_4 selectivity (≤100%) with CO_2 conversion (≤99%) was achieved at temperatures around 250–350 °C. The CO_2 methanation reaction occurs in a complex system of multiple side reactions, thereby elucidating the reaction mechanism a challenging task and will probably require the development of new approaches and techniques. We reviewed several experimental and theoretical studies in order to elucidate the reaction mechanisms for CO_2 methanation. The critical exploration of the catalytic system and mechanism are significant breakthroughs of great importance in the CO_2 methanation for tackling the climate change issues, global energy crisis, and for sustainable development of our world.

Declaration of Competing Interest

The authors declare that they have no known competing financial interests or personal relationships that could have appeared to influence the work reported in this paper.

Acknowledgments

This research work was made possible by a Transdisciplinary Research Grant from Universiti Teknologi Malaysia (Grant No. 06G52 and 06G53).

References

[1] E.S. Sanz-Perez, C.R. Murdock, S.A. Didas, C.W. Jones, Chem. Rev. 116 (2016) 11840–11876.
[2] W. Zhang, H. Machida, H. Takano, K. Izumiya, K. Norinaga, Chem. Eng. Sci. 211 (2020) 115276..
[3] N.S. Spinner, J.A. Vega, W.E. Mustain, Catal, Sci. Technol. 2 (2012) 19–28.
[4] N.A.A. Fatah, A.A. Jalil, A.F.A. Rahman, H.U. Hambali, I. Hussain, J. Energy. Saf. Technol. 2 (2019) 49–53.
[5] M. Ozturk, I. Dincer, Int. J. Hydrog. Energy 44 (2019) 5043–5053.
[6] A.H.K. Owgi, A.A. Jalil, I. Hussain, N.S. Hassan, H.U. Hambali, T.J. Siang, D.V.N. Vo, Environ. Chem. Lett. (2021) 1–27.
[7] J.B. Shukla, M. Verma, A.K. Misra, Ecol. Complex. 32 (2017) 99–110.
[8] C.P.C. Bong, L.Y. Lim, W.S. Ho, J.S. Lim, J.J. Klemes, S. Towprayoon, C.S. Ho, C.T. Lee, J. Clean. Prod. 146 (2017) 149–157.
[9] A. Galadima, O. Muraza, Renew. Sust. Energ. Rev. 115 (2019) 109333.
[10] IEA, Global Energy & CO2 Status Report, 2018. https://webstore.iea.org/global-energy-co2-status-report-2018 (accessed 12 March 2021).
[11] I. Ganesh, Renew. Sust. Energ. Rev. 31 (2014) 221–257.
[12] H. Arakawa, M. Aresta, J.N. Armor, M.A. Barteau, E.J. Beckman, A.T. Bell, J.E. Bercaw, C. Creutz, E. Dinjus, D.A. Dixon, K. Domen, Chem. Rev. 101 (2001) 953–996.
[13] M. Jacquemin, A. Beuls, P. Ruiz, Catal. Today 157 (2010) 462–466.
[14] G. Mohanakrishna, K. Vanbroekhoven, D. Pant, React Chem. Eng. 3 (2018) 371–378.
[15] S. Bai, Q. Shao, P. Wang, Q. Dai, X. Wang, X. Huang, J. Am. Chem. Soc. 139 (2017) 6827–6830.
[16] W. Wei, G. Jinlong, Front. Chem. Sci. Eng. 5 (2011) 2–10.
[17] C. Song, Catal. Today 115 (2006) 2–32.
[18] T. Sakakura, J.C. Choi, H. Yasuda, Chem. Rev. 107 (2007) 2365–2387.
[19] M. Aresta, A. Dibenedetto, Dalton Trans. 28 (2007) 2975–2992.
[20] M. Mikkelsen, M. Jorgensen, F.C. Krebs, Energy Environ. Sci. 3 (2010) 43–81.
[21] E.A. Quadrelli, G. Centi, J.L. Duplan, S. Perathoner, ChemSusChem 4 (2011) 1194–1215.
[22] M. Aresta, A. Dibenedetto, A. Angelini, Chem. Rev. 114 (2014) 1709–1742.
[23] M. Aresta, A. Dibenedetto, E. Quaranta, J. Catal. 343 (2016) 2–45.
[24] A.C. Faria, C.V. Miguel, L.M. Madeira, J. CO_2 Util. 26 (2018) 271–280.
[25] I. Hussain, A.A. Jalil, N.A.A. Fatah, M.Y.S. Hamid, M. Ibrahim, M.A.A. Aziz, H.D. Setiabudi, Energy Convers. Manage. 211 (2020) 112754.
[26] P. Frontera, A. Macario, M. Ferraro, P. Antonucci, Catalysts 7 (2017) 59.
[27] I. Hussain, A.A. Jalil, C.R. Mamat, T.J. Siang, M.S. Azami, H.U. Hambali, J. Energy. Saf. Technol. 2 (2019) 15–20.
[28] K. Lars, T. Jorg, Chem. Eng. Sci. 132 (2015) 59–71.
[29] A. Goeppert, M. Czaun, J.P. Jones, G.S. Prakash, G.A. Olah, Chem. Soc. Rev. 43 (2014) 7995–8048.
[30] C.J. Quarton, S. Samsatli, Renew. Sustain. Energy Rev. 98 (2018) 302–316.
[31] H.L. Huynh, W.M. Tucho, X. Yu, Z. Yu, J. Clean. Prod. 264 (2020) 121720.
[32] E.V. Kondratenko, G. Mul, J. Baltrusaitis, G.O. Larrazabal, J. Perez-Ramirez, Energy Enviro. Sci. 6 (2013) 3112–3135.
[33] M. Peters, B. Koehler, W. Kuckshinrichs, W. Leitner, P. Markewitz, T.E. Muller, ChemSusChem 4 (2011) 1216–1240.
[34] A. Goeppert, M. Czaun, G.S. Prakash, G.A. Olah, Energy Environ. Sci. 5 (2012) 7833–7853.
[35] I. Hussain, A.A. Jalil, S.M. Izan, M.S. Azami, K. Kidam, N. Ainirazali, A. Ripin, Chem. Eng. Sci. 229 (2021) 116015.
[36] S. Rönsch, J. Schneider, S. Matthischke, M. Schlüter, M. Götz, J. Lefebvre, P. Prabhakaran, S. Bajohr, Fuel 166 (2016) 276–296.
[37] I. Kuznecova, J. Gusca, Energy Procedia 128 (2017) 255–260.
[38] C. Mebrahtu, F. Krebs, S. Abate, S. Perathoner, G. Centi, R. Palkovits, Stud. Surf. Sci. Catal. 178 (2019) 85–103.
[39] X. Su, J. Xu, B. Liang, H. Duan, B. Hou, Y. Huang, J. Energy Chem. 25 (2016) 553–565.
[40] K. Ghaib, K. Nitz, F.Z. Ben-Fares, Chem. Bio. Eng. Rev. 3 (2016) 266–275.
[41] M. Thema, F. Bauer, M. Sterner, Renew. Sust. Energ. Rev. 112 (2019) 775–787.
[42] M. Younas, L. Loong Kong, M.J. Bashir, H. Nadeem, A. Shehzad, S. Sethupathi, Energy Fuels 30 (2016) 8815–8831.
[43] M. Gotz, J. Lefebvre, F. Mors, A.M. Koch, F. Graf, S. Bajohr, R. Reimert, T. Kolb, Renew. Energy 85 (2016) 1371–1390.
[44] K. Ghaib, F.Z. Ben-Fares, Renew. Sust. Energ. Rev. 81 (2018) 433–446.
[45] J. Gao, Q. Liu, F. Gu, B. Liu, Z. Zhong, F. Su, RSC Adv. 5 (2015) 22759–22776.
[46] M.A.A. Aziz, A.A. Jalil, S. Triwahyono, A. Ahmad, Green Chem. 17 (2015) 2647–2663.
[47] B. Miao, S.S.K. Ma, X. Wang, H. Su, S.H. Chan, Catal. Sci. 6 (2016) 4048–4058.
[48] V. Ponec, Catal. Rev. Sci. Eng. 18 (1978) 151–171.
[49] M.C. Bacariza, I. Graça, J.M. Lopes, C. Henriques, ChemCatChem 11 (2019) 2388–2400.
[50] I. Hussain, A.A. Jalil, N.A.A. Fatah, M. Ibrahim, M.S. Azami, W. Fadlun, M.A.H. Aziz, H.U. Hambali, Mater. Sci. Eng. 808 (2020) 012037.
[51] M.A.A. Aziz, A.A. Jalil, S. Triwahyono, R.R. Mukti, Y.H. Taufiq-Yap, M.R. Sazegar, Appl. Catal. B. 147 (2014) 359–368.
[52] K. Kaltenmaier, Untersuchungen zur Kinetik der Methanisierung von CO_2-reichen Gasen bei höheren Drücken, Doctoral dissertation, Universität Karlsruhe (1988).
[53] G.D. Weatherbee, C.H. Bartholomew, J. Catal. 68 (1981) 67–76.
[54] K. Hashimoto, M. Yamasaki, K. Fujimura, T. Matsui, K. Izumiya, M. Komori, A. A. El-Moneim, E. Akiyama, H. Habazaki, N. Kumagai, A. Kawashima, Mater. Sci. Eng. A. 267 (1999) 200–206.
[55] M. Sterner, Bioenergy and renewable power methane in integrated 100% renewable energy systems limiting global warming by transforming energy systems Doctoral dissertation, University of Kassel, 2009.
[56] J. Gao, Y. Wang, Y. Ping, D. Hu, G. Xu, F. Gu, F. Su, RSC Adv. 2 (2012) 2358–2368.
[57] C.V. Miguel, M.A. Soria, A. Mendes, L.M. Madeira, J. Nat. Gas Sci. Eng. 22 (2015) 1–8.
[58] F. Meng, X. Li, X. Lv, Z. Li, Int. J. Coal. Sci. Technol. 5 (2018) 439–451.
[59] W. Ahmad, A. Al-Matar, R. Shawabkeh, A. Rana, J. Environ. Chem. Eng. 4 (2016) 2725–2735.
[60] D. Chaconas, P. Pichardo, I.V. Manousiouthakis, V.I. Manousiouthakis, AIChE J. 67 (2021) 17052.
[61] R. Kaczmarczyk, A. Mlonka-Medrala, S. Gurgul, E3S Web Conf. 14 (2017) 02041.

[62] Z. Pan, W.P. Chan, A. Veksha, A. Giannis, X. Dou, H. Wang, G. Lisak, T.T. Lim, Energy Convers. Manag. 202 (2019) 112160.
[63] A. Molino, G. Braccio, Fuel 139 (2015) 425–429.
[64] M.M. Jaffar, M.A. Nahil, P.T. Williams, Energy Technol. 7 (2019) 1900795.
[65] W.R. Kang, K.B. Lee, Korean J. Chem. Eng. 30 (2013) 1386–1394.
[66] C.W. Hu, J. Yao, H.Q. Yang, Y. Chen, A.M. Tian, J. Catal. 166 (1997) 1–7.
[67] P. Garbis, C. Kern, A. Jess, Energies 12 (2019) 469.
[68] A. Swapnesh, V.C. Srivastava, I.D. Mall, Chem. Eng. Tech. 37 (2014) 1765–1777.
[69] K. Stangeland, D. Kalai, H. Li, Z. Yu, Energy Procedia 105 (2017) 2022–2027.
[70] B. Castellani, A.M. Gambelli, E. Morini, B. Nastasi, A. Presciutti, M. Filipponi, A. Nicolini, F. Rossi, Energies 10 (2017) 855.
[71] D.J. Goodman, Methanation of Carbon Dioxide Master dissertation, University of California, Los Angeles, 2013.
[72] J.N. Park, E.W. McFarland, J. Catal. 266 (2009) 92–97.
[73] G.A. Mills, F.W. Steffgen, Catal. Rev. 8 (1974) 159–210.
[74] T. Burger, F. Koschany, O. Thomys, K. Köhler, O. Hinrichsen, Appl. Catal. A Gen. 558 (2018) 44–54.
[75] S. Tada, I. Thiel, H.K. Lo, C. Coperet, Chimia 69 (2015) 759–764.
[76] I. Fechete, J.C. Vedrine, Molecules 20 (2015) 5638–5666.
[77] H.L. Huynh, Z. Yu, Z., 2020, Energy Technol. 8 (2020) 1901475.
[78] W. Wang, S. Wang, X. Ma, J. Gong, Chem. Soc. Rev. 40 (2011) 3703–3727.
[79] F. Fischer, H. Tropsch, P. Dilthey, Brennst.-Chem. 6 (1925) 265–271.
[80] M.A. Vannice, Catal. Rev. 14 (1976) 153–191.
[81] C. Italiano, J. Llorca, L. Pino, M. Ferraro, V. Antonucci, A. Vita, Appl. Catal. B Environ. 264 (2020) 118494.
[82] E. Moioli, A. Zuttel, Sustain, Energy Fuels 4 (2020) 1396–1408.
[83] L. Falbo, C.G. Visconti, L. Lietti, J. Szanyi, Appl. Catal. B Environ. 256 (2019) 117791.
[84] I. Fuentes, C. Ulloa, R. Jiménez, X. Garcia, J. Hazard. Mater. 387 (2020) 121693.
[85] C. de Vries, M. Claeys, G. Schaub, Catal. Today 242 (2015) 184–192.
[86] S.E. Olesen, K.J. Andersson, C.D. Damsgaard, I. Chorkendorff, J. Phys. Chem. C. 121 (2017) 15556–15564.
[87] X. Jia, N. Rui, X. Zhang, X. Hu, C.J. Liu, Catal. Today 334 (2019) 215–222.
[88] I. Czekaj, F. Loviat, F. Raimondi, J. Wambach, S. Biollaz, A. Wokaun, Appl. Catal. A Gen. 329 (2007) 68–78.
[89] J. Zhou, H. Ma, C. Liu, H. Zhang, W. Qian, W. Ying, Catal. Lett. 149 (2019) 2563–2574.
[90] A.L. Kustov, A.M. Frey, K.E. Larsen, T. Johannessen, J.K. Norskov, C.H. Christensen, Appl. Catal. A Gen. 320 (2007) 98–104.
[91] E. de Smit, B.M. Weckhuysen, Chem. Soc. Rev. 37 (2008) 2758–2781.
[92] C.K. Poh, S.W.D. Ong, Y. Du, H. Kamata, K.S.C. Choong, J. Chang, Y. Izumi, K. Nariai, N. Mizukami, L. Chen, A. Borgna, Catal. Today 342 (2020) 21–31.
[93] Z. Bian, X. Meng, M. Tao, Y. Lv, Z. Xin, Fuel 179 (2016) 193–201.
[94] E. Kok, J. Scott, N. Cant, D. Trimm, Catal. Today 164 (2011) 297–301.
[95] M. Saito, R.B. Anderson, J. Catal. 63 (1980) 438–446.
[96] T. Bligaard, J.K. Norskov, S. Dahl, J. Matthiesen, C.H. Christensen, J. Sehested, J. Catal. 224 (2004) 206–217.
[97] M. Mihet, M.D. Lazar, Catal. Today 306 (2018) 294–299.
[98] G. Ertl, H. Knözinger, J. Weitkamp (Eds.), Handbook of heterogeneous catalysis, Weinheim, 1997, pp. 427–440.
[99] C.J. Jacobsen, S. Dahl, B.S. Clausen, S. Bahn, A. Logadottir, J.K. Norskov, J. Am. Chem. Soc. 123 (2001) 8404–8405.
[100] H. Toulhoat, P. Raybaud, J. Catal. 216 (2003) 63–72.
[101] R. Mutschler, E. Moioli, W. Luo, N. Gallandat, A. Züttel, J. Catal. 366 (2018) 139–149.
[102] G. Garbarino, T. Cavattoni, P. Riani, G. Busca, Catal. Today 345 (2020) 213–219.
[103] G. Garbarino, P. Riani, L. Magistri, G. Busca, Int. J. Hydrog Energy 39 (2014) 11557–11565.
[104] M. Bersani, K. Gupta, A.K. Mishra, R. Lanza, S.R. Taylor, H.U. Islam, N. Hollingsworth, C. Hardacre, N.H. De Leeuw, J.A. Darr, ACS Catal. 6 (2016) 5823–5833.
[105] P. Panagiotopoulou, Appl. Catal. A Gen. 542 (2017) 63–70.
[106] N.M. Martin, P. Velin, M. Skoglundh, M. Bauer, P.A. Carlsson, Catal Sci. Technol. 7 (2017) 1086–1094.
[107] L.R. Winter, E. Gomez, B. Yan, S. Yao, J.G. Chen, Appl. Catal. B Environ. 224 (2018) 442–450.
[108] G.D. Weatherbee, C.H. Bartholomew, J. Catal. 87 (1984) 352–362.
[109] J. Zhu, G. Zhang, W. Li, X. Zhang, F. Ding, C. Song, X. Guo, ACS Catal. 10 (2020) 7424–7433.
[110] X. Chen, X. Su, B. Liang, X. Yang, X. Ren, H. Duan, Y. Huang, T. Zhang, J. Energy Chem. 25 (2016) 1051–1057.
[111] S. Kattel, B. Yan, J.G. Chen, P. Liu, J. Catal. 343 (2016) 115–126.
[112] S.S. Kim, H.H. Lee, S.C. Hong, Appl. Catal. A Gen. 423 (2012) 100–107.
[113] N.M. Martin, F. Hemmingsson, X. Wang, L.R. Merte, U. Hejral, J. Gustafson, M. Skoglundh, D.M. Meira, A.C. Dippel, O. Gutowski, M. Bauer, Catal, Sci. Technol. 8 (2018) 2686–2696.
[114] A. Beuls, C. Swalus, M. Jacquemin, G. Heyen, A. Karelovic, P. Ruiz, Appl. Catal. B Environ. 113 (2012) 2–10.
[115] A. Petala, P. Panagiotopoulou, Appl. Catal. B Environ. 224 (2018) 919–927.
[116] S. Tada, O.J. Ochieng, R. Kikuchi, T. Haneda, H. Kameyama, Int. J. Hydrog. Energy. 39 (2014) 10090–10100.
[117] T. Avanesian, G.S. Gusmão, P. Christopher, J. Catal. 343 (2016) 86–96.
[118] P.U. Aldana, F. Ocampo, K. Kobl, B. Louis, F. Thibault-Starzyk, M. Daturi, P. Bazin, S. Thomas, A.C. Roger, Catal. Today 215 (2013) 201–207.
[119] D.C. da Silva, S. Letichevsky, L.E. Borges, L.G. Appel, Int. J. Hydrog Energy 37 (2012) 8923–8928.
[120] R. Zhou, N. Rui, Z. Fan, C.J. Liu, Int. J. Hydrog. Energy 41 (2016) 22017–22022.
[121] Q. Pan, J. Peng, T. Sun, S. Wang, S. Wang, Catal. Commun. 45 (2014) 74–78.
[122] T. Iizuka, Y. Tanaka, K. Tanabe, J. Catal. 76 (1982) 1–8.
[123] S. Tada, T. Shimizu, H. Kameyama, T. Haneda, R. Kikuchi, Int. J Hydrog. Energy 37 (2012) 5527–5531.
[124] A. Alvarez, A. Bansode, A. Urakawa, A.V. Bavykina, T.A. Wezendonk, M. Makkee, J. Gascon, F. Kapteijn, Chem. Rev. 117 (2017) 9804–9838.
[125] H.L. Huynh, Z. Yu, Energy Technol. 8 (2020) 1901475.
[126] M. Cai, J. Wen, W. Chu, X. Cheng, Z. Li, J. Nat. Gas. Chem. 20 (2011) 318–324.
[127] W. Gac, W. Zawadzki, M. Rotko, G. Slowik, M. Greluk, Top. Catal. 62 (2019) 524–534.
[128] Q. Zheng, R. Farrauto, A. Chau Nguyen, Ind. Eng. Chem. 55 (2016) 6768–6776.
[129] J. Liu, C. Li, F. Wang, S. He, H. Chen, Y. Zhao, M. Wei, D.G. Evans, X. Duan, Catal Sci. Technol. 3 (2013) 2627–2633.
[130] X. Jia, X. Zhang, N. Rui, X. Hu, C.J. Liu, Appl. Catal. B Environ. 244 (244) (2019) 159–169.
[131] H. Liu, X. Zou, X. Wang, X. Lu, W. Ding, J. Nat. Gas. Chem. 21 (2012) 703–707.
[132] R.P. Ye, Q. Li, W. Gong, T. Wang, J.J. Razink, L. Lin, Y.Y. Qin, Z. Zhou, H. Adidharma, J. Tang, A.G. Russell, Appl. Catal. B Environ. 268 (2020) 118474.
[133] F. Ocampo, B. Louis, L. Kiwi-Minsker, A.C. Roger, Appl. Catal. A Gen. 392 (2011) 36–44.
[134] E. Marconi, S. Tuti, I. Luisetto, Catalysts 9 (2019) 375.
[135] S. Hwang, U.G. Hong, J. Lee, J.H. Baik, D.J. Koh, H. Lim, I.K. Song, Catal. Lett. 142 (2012) 860–868.
[136] A. Taguchi, F. Schuth, Micropor Mesopor. Mat. 77 (2005) 1–45.
[137] W.J. Roth, J. Cejka, Catal Sci. Technol. 1 (2011) 43–53.
[138] H. Zheng, C. Gao, B. Peng, M. Shu, S. Che, J. Phys. Chem. C 115 (2011) 7230–7237.
[139] M. Liong, S. Angelos, E. Choi, K. Patel, J.F. Stoddart, J.I. Zink, J. Mater. Chem. 119 (2009) 6251–6257.
[140] J. Dou, H.C. Zeng, J. Am. Chem. Soc. 134 (2012) 16235–16246.
[141] V. Hulea, D. Brunel, A. Galarneau, K. Philippot, B. Chaudret, P.J. Kooyman, F. Fajula, Micropor. Mesopor. Mat. 79 (2005) 185–194.
[142] M.A.A. Aziz, A.A. Jalil, S. Triwahyono, M.W.A. Saad, Chem. Eng. 260 (2015) 757–764.
[143] M.A.A. Aziz, A.A. Jalil, S. Triwahyono, S.M. Sidik, Appl. Catal. A Gen. 486 (2014) 115–122.
[144] H. Zhang, J. Nai, L. Yu, X.W.D. Lou, Joule 1 (2017) 77–107.
[145] G. Zhou, T. Wu, H. Xie, X. Zheng, Int. J. Hydrog. Energy 38 (2013) 10012–10018.
[146] W. Zhen, B. Li, G. Lu, J. Ma, Chem. Commun 51 (2015) 1728–1731.
[147] Y.Z. Chen, R. Zhang, L. Jiao, H.L. Jiang, Coord. Chem. Rev. 362 (2018) 1–23.
[148] Q. Wang, D. Astruc, Chem. Rev. 120 (2020) 1438–1511.
[149] R. Lippi, S.C. Howard, H. Barron, C.D. Easton, I.C. Madsen, L.J. Waddington, C. Vogt, M.R. Hill, C.R. Sumby, C.J. Doonan, D.F. Kennedy, J. Mater. Chem. A 5 (2017) 12990–12997.
[150] H. Furukawa, K.E. Cordova, M. O'Keeffe, O.M. Yaghi, Science 341 (2013) 1230444.
[151] N.V. Maksimchuk, O.V. Zalomaeva, I.Y. Skobelev, K.A. Kovalenko, V.P. Fedin, O. A. Kholdeeva, Proc. R. Soc. A. 468 (2017) 2034.
[152] S. Horike, M. Dinca, K. Tamaki, J.R. Long, J. Am. Chem. Soc. 130 (2008) 5854–5855.
[153] K. Schlichte, T. Kratzke, S. Kaskel, Micropor. Mesopor. Mat. 73 (2004) 81–88.
[154] W. Xu, M. Dong, L. Di, X. Zhang, Nanomaterials 9 (2019) 1432.
[155] W. Li, A. Zhang, X. Jiang, C. Chen, Z. Liu, C. Song, X. Guo, A.C.S. Sustain, Chem. Eng. 5 (2017) 7824–7831.
[156] M. Mihet, O. Grad, G. Blanita, T. Radu, M.D. Lazar, Int. J. Hydrog. Energy 44 (2019) 13383–13396.
[157] M. Mihet, G. Blanita, M. Dan, L. Barbu-Tudoran, M.D. Lazar, J. Nanosci. Nanotechnol. 19 (2019) 3187–3196.
[158] T. Zhao, Y. Hui, Z. Li, Mol. Catal. 474 (2019) 110421.
[159] D. Jampaiah, D. Damma, A. Chalkidis, P. Venkataswamy, S.K. Bhargava, B.M. Reddy, Catal. Today 356 (2020) 519–526.
[160] W. Zhen, F. Gao, B. Tian, P. Ding, Y. Deng, Z. Li, H. Gao, G. Lu, J. Catal. 348 (2017) 200–211.
[161] H. Yang, C. Zhang, P. Gao, H. Wang, X. Li, L. Zhong, W. Wei, Y. Sun, Catal. Sci. 7 (2017) 4580–4598.
[162] T. Zurrer, K. Wong, J. Horlyck, E.C. Lovell, J. Wright, N.M. Bedford, Z. Han, K. Liang, J. Scott, R. Amal, Adv. Funct. Mater. 31 (2021) 2007624.
[163] H. Jiang, Q. Gao, S. Wang, Y. Chen, M. Zhang, J. CO_2 Util. 31 (2019) 167–172.
[164] E.S. Gutterod, S. Qien-Qdegaard, K. Bossers, A.E. Nieuwelink, M. Manzoli, L. Braglia, A. Lazzarini, E. Borfecchia, S. Ahmadigoltapeh, B. Bouchevreau, B.T. Lonstad-Bleken, Ind. Eng. Chem. 56 (2017) 13206–13218.
[165] M. Cabrero-Antonino, S. Remiro-Buenamanana, M. Souto, A.A. García-Valdivia, D. Choquesillo-Lazarte, S. Navalon, A. Rodriguez-Dieguez, G.M. Espallargas, H. García, Chem Commun 55 (2019) 10932–10935.
[166] M. Sanchez-Contador, A. Ateka, A.T. Aguayo, J. Bilbao, Fuel Process Technol. 179 (2018) 258–268.
[167] Q. Wang, X. Wang, J. Liu, Y. Yang, J. Nanoparticle Res. 19 (2017) 25.
[168] W. Hui, J.F. Zhang, Y.X. Bai, W.F. Wang, Y.S. Tan, Y.Z. Han, J. Fuel Chem. Technol. 44 (2016) 548–556.
[169] K.D. Gilroy, A. Ruditskiy, H.C. Peng, D. Qin, Y. Xia, Chem. Rev. 116 (2016) 10414–10472.

[170] J. Ilsemann, A. Strab-Eifert, J. Friedland, L. Kiewidt, J. Thöming, M. Bäumer, R. Güttel, ChemCatChem 11 (2019) 4884–4893.
[171] N. Almana, S.P. Phivilay, P. Laveille, M.N. Hedhili, P. Fornasiero, K. Takanabe, J. M. Basset, J. Catal. 340 (2016) 368–375.
[172] H. Lee, J. Kim, D. Lee, Appl. Catal. A Gen. 594 (2020) 117461.
[173] C. Xie, C. Chen, Y. Yu, J. Su, Y. Li, G.A. Somorjai, P. Yang, Nano letters 17 (2017) 3798–3802.
[174] J. Le TA, Kim, Y.R. Jeong, E.D. Park, Catalysts 9 (2019) 599.
[175] J. Kirchner, C. Zambrzycki, S. Kureti, R. Guttel, Chem. Ing. Tech. 92 (2020) 603–607.
[176] Y. Li, G. Lu, J. Ma, RSC Adv. 34 (2014) 17420–17428.
[177] S. Das, J. Pérez-Ramírez, J. Gong, N. Dewangan, K. Hidajat, B.C. Gates, S. Kawi, Chem. Soc. Rev. 49 (2020) (2020) 2937–3004.
[178] M.A. Lucchini, A. Testino, A. Kambolis, C. Proff, C. Ludwig, Appl. Catal. B Environ. 182 (2016) 94–101.
[179] W. Luc, C. Collins, S. Wang, H. Xin, K. He, Y. Kang, F. Jiao, J. Am. Chem. Soc. 139 (2017) 1885–1893.
[180] B.S. Kwak, N.K. Park, S.M. Park, J.P. Hong, J.I. Baek, S.J. Lee, H.J. Ryu, M. Kang, Sci Adv. Mater. 9 (2017) 1828–1836.
[181] J.K. Kesavan, I. Luisetto, S. Tuti, C. Meneghini, G. Iucci, C. Battocchio, S. Mobilio, S. Casciardi, R. Sisto, J. CO_2 Util. 23 (2018) 200–211.
[182] K. Shen, L. Chen, J. Long, W. Zhong, Y. Li, ACS Catal. 5 (2015) 5264–5271.
[183] H. Xie, S. Chen, F. Ma, J. Liang, Z. Miao, T. Wang, H.L. Wang, Y. Huang, Q. Li, A. C.S. Appl, Mater. Interfaces 10 (2018) 36996–37004.
[184] Y. Han, H. Xu, Y. Su, Z.L. Xu, K. Wang, W. Wang, J. Catal. 370 (2019) 70–78.
[185] I. Hussain, A.A. Jalil, N.S. Hassan, H.U. Hambali, N.W.C. Jusoh, Chem. Eng. Sci. 228 (2020) 115978.
[186] V. Polshettiwar, D. Cha, X. Zhang, J.M. Basset, Angew. Chem. Int. Ed. 49 (2010) 9652–9656.
[187] B. Singh, V. Polshettiwar, J. Mat. Chem. A. 4 (2016) 7005–7019.
[188] A. Fihri, D. Cha, M. Bouhrara, N. Almana, V. Polshettiwar, ChemSusChem 5 (2012) 85–89.
[189] A. Fihri, M. Bouhrara, U. Patil, D. Cha, Y. Saih, V. Polshettiwar, ACS Catal. 2 (2012) 1425–1431.
[190] M. Dhiman, B. Chalke, V. Polshettiwar, A.C.S. Sustain, Chem. Eng. 3 (2015) 3224–3230.
[191] R. Singh, R. Bapat, L. Qin, H. Feng, V. Polshettiwar, ACS Catal. 6 (2016) 2770–2784.
[192] D.S. Moon, J.K. Lee, Langmuir 28 (2012) 12341–12347.
[193] U. Patil, A. Fihri, A.H. Emwas, V. Polshettiwar, Chem. Sci. 3 (2012) 2224–2229.
[194] M.Y.S. Hamid, M.L. Firmansyah, S. Triwahyono, A.A. Jalil, R.R. Mukti, E. Febriyanti, V. Suendo, H.D. Setiabudi, M. Mohamed, W. Nabgan, Appl. Catal. A Gen. 532 (2017) 86–94.
[195] A.K. Mishra, R. Belgamwar, R. Jana, A. Datta, V. Polshettiwar, PNAS 117 (2020) 6383–6390.
[196] M.Y.S. Hamid, S. Triwahyono, A.A. Jalil, N.W. Che Jusoh, S.M. Izan, T.A. Tuan Abdullah, Inorg Chem. 57 (2018) 5859–5869.
[197] M. Shamzhy, M. Opanasenko, P. Concepcion, A. Martinez, Chem. Soc. Rev. 48 (2019) 1095–1149.
[198] I. Graca, L.V. Gonzalez, M.C. Bacariza, A. Fernandes, C. Henriques, J.M. Lopes, M.F. Ribeiro, Appl. Catal. B Environ. 147 (2014) 101–110.
[199] E. Jwa, S.B. Lee, H.W. Lee, Y.S. Mok, Fuel Process Technol. 108 (2013) 89–93.
[200] R. Delmelle, R.B. Duarte, T. Franken, D. Burnat, L. Holzer, A. Borgschulte, A. Heel, Int J. Hydrog. Energy 41 (2016) 20185–20191.
[201] M.C. Bacariza, I. Graca, J.M. Lopes, C. Henriques, Micropor. Mesopor. Mat. 267 (2018) 9–19.
[202] A. Quindimil, U. De-La-Torre, B. Pereda-Ayo, J.A. Gonzalez-Marcos, J.R. Gonzalez Velasco, Appl. Catal. B Environ. 238 (2018) 393–403.
[203] M. Stöcker, Micropor Mesopor Mater. 82 (2005) 257–292.
[204] M. Guisnet, L. Costa, F.R. Ribeiro, J. Mol. Catal. A Chem. 305 (2009) 69–83.
[205] D. Murphy, P. Massiani, R. Franck, D. Barthomeuf, J. Phys. Chem. 100 (1996) 6731–6738.
[206] J. Weitkamp, Solid State Ion. 131 (2000) 175–188.
[207] A. Borgschulte, E. Callini, N. Stadie, Y. Arroyo, M.D. Rossell, R. Erni, H. Geerlings, A. Zuttel, D. Ferri, Catal, Sci. Technol. 5 (2000) 4613–4621.
[208] L. Wei, W. Haije, N. Kumar, J. Peltonen, M. Peurla, H. Grenman, W. de Jong, Catal. Today 362 (2020) 35–46.
[209] M.C. Bacariza, R. Bertolo, I. Graca, J.M. Lopes, C. Henriques, J. CO_2 Util. 21 (2017) 280–291.
[210] J. Tan, J. Wang, Z. Zhang, Z. Ma, L. Wang, Y. Liu, Appl. Surf. Sci. 481 (2019) 1538–1548.
[211] Y. Feng, W. Yang, W. Chu, Integr. Ferroelectr. 172 (2016) 40–48.
[212] X. Wang, L. Zhu, Y. Liu, S. Wang, Sci. Total. Environ. 625 (2018) 686–695.
[213] W.A.W.A. Bakar, R. Ali, N.S. Mohammad, Arab. J. Chem. 8 (2015) 632–643.
[214] H. Liu, S. Xu, G. Zhou, K. Xiong, Z. Jiao, S. Wang, Fuel 217 (2018) 570–576.
[215] A. Aljishi, G. Veilleux, J.A.H. Lalinde, J. Kopyscinski, Appl. Catal. A Gen. 549 (2018) 263–272.
[216] J.Y. Lim, J. McGregor, A.J. Sederman, J.S. Dennis, Chem. Eng. Sci. 141 (2016) 28–45.
[217] D. Pandey, G. Deo, J. Ind. Eng. Chem. 33 (2016) 99–107.
[218] J. Ren, X. Qin, J.Z. Yang, Z.F. Qin, H.L. Guo, J.Y. Lin, Z. Li, Fuel Process Technol. 137 (2015) 204–211.
[219] R. Buchel, A. Baiker, S.E. Pratsinis, Appl. Catal. A Gen. 477 (2014) 93–101.
[220] C. Yuan, N. Yao, X. Wang, J. Wang, D. Lv, X. Li, Chem. Eng. 260 (2015) 1–10.
[221] L. Bian, L. Zhang, R. Xia, Z. Li, J. Nat. Gas. Sci. Eng. 27 (2015) 1189–1194.
[222] N. Perkas, G. Amirian, Z. Zhong, J. Teo, Y. Gofer, A. Gedanken, Catal. Lett. 130 (2009) 455–462.
[223] M.C. Bacariza, I. Graça, S.S. Bebiano, J.M. Lopes, C. Henriques, Energy Fuel 31 (2017) 9776–9789.
[224] M.C. Bacariza, I. Graca, J.M. Lopes, C. Henriques, ChemCatChem 10 (2018) 2773–2781.
[225] F. Goodarzi, L. Kang, F.R. Wang, F. Joensen, S. Kegnæs, J. Mielby, ChemCatChem 10 (2018) 1566–1570.
[226] H. Chen, Y. Mu, Y. Shao, S. Chansai, S. Xu, C.E. Stere, H. Xiang, R. Zhang, Y. Jiao, C. Hardacre, X. Fan, Catal, Sci. Technol. 9 (2019) 4135–4145.
[227] K.K. Bando, K. Soga, K. Kunimori, N. Ichikuni, K. Okabe, H. Kusama, K. Sayama, H. Arakawa, Appl. Catal. A Gen. 173 (1998) 47–60.
[228] M.C. Bacariza, M. Maleval, I. Graca, J.M. Lopes, C. Henriques, Micropor. Mesopor. Mat. 274 (2019) 102–112.
[229] S. Scire, C. Crisafulli, R. Maggiore, S. Minico, S. Galvagno, Catal. Lett. 51 (1998) 41–45.
[230] A.V. Boix, M.A. Ulla, J.O. Petunchi, J. Catal. 162 (1996) 239–249.
[231] C. Swalus, M. Jacquemin, C. Poleunis, P. Bertrand, P. Ruiz, Appl. Catal. B. 125 (2012) 41–50.
[232] J.P. O'Byrne, R.E. Owen, D.R. Minett, S.I. Pascu, P.K. Plucinski, M.D. Jones, D. Mattia, Catal. Sci. 3 (2013) 1202–1207.
[233] W. Wang, W. Chu, N. Wang, W. Yang, C. Jiang, Int. J. Hydrog. Energy 41 (2016) 967–975.
[234] J. Li, Y. Zhou, X. Xiao, W. Wang, N. Wang, W. Qian, W. Chu, A.C.S. Appl, Mater. Interfaces 10 (2018) 41224–41236.
[235] W. Wang, C. Duong-Viet, H. Ba, W. Baaziz, G. Tuci, S. Caporali, L. Nguyen-Dinh, O. Ersen, G. Giambastiani, C. Pham-Huu, A.C.S. Appl, Energy Mater. 2 (2018) 1111–1120.
[236] L.M. Chew, P. Kangvansura, H. Ruland, H.J. Schulte, C. Somsen, W. Xia, G. Eggeler, A. Worayingyong, M. Muhler, Appl. Catal. A Gen. 482 (2014) 163–170.
[237] J. Wang, Z. You, Q. Zhang, W. Deng, Y. Wang, Catal. Today 215 (2013) 186–193.
[238] L. Roldan, Y. Marco, E. Garcia-Bordeje, ChemCatChem 7 (2015) 1347–1356.
[239] X. Wang, Y. Liu, L. Zhu, Y. Li, K. Wang, K. Qiu, N. Tippayawong, P. Aggarangsi, P. Reubroycharoen, S. Wang, J. CO_2 Util. 34 (2019) 733–741.
[240] W. Wang, C. Duong-Viet, Z. Xu, H. Ba, G. Tuci, G. Giambastiani, Y. Liu, T. Truong-Huu, J.M. Nhut, C. Pham-Huu, Catal. Today 357 (2020) 214–220.
[241] K. Liu, X. Xu, J. Xu, X. Fang, L. Liu, X. Wang, J. CO_2 Util. 38 (2020) 113–124.
[242] C. Zhao, F. Li, Y. Yang, R. Lippi, H. Li, W. Chen, Funct, Mater. Lett. 13 (2020) 2051019.
[243] S. Wang, T. Wu, J. Lin, Y. Ji, S. Yan, Y. Pei, S. Xie, B. Zong, M. Qiao, ACS Catal. 10 (2020) 6389–6401.
[244] J. Wu, Z. Jin, B. Wang, Y. Han, Y. Xu, Z. Liang, Z. Wang, Ind. Eng. Chem. Res. 58 (2019) 20536–20542.
[245] L. Roldan, Y. Marco, E. Garcia-Bordeje, ChemSusChem 10 (2017) 1139–1144.
[246] Y. Yang, K. Chiang, N. Burke, Catal. Today 178 (2011) 197–205.
[247] X. Wang, M. Yang, X. Zhu, L. Zhu, S. Wang, Appl. Energy 280 (2020) 115919.
[248] M.A. Paviotti, L.A.S. Hoyos, V. Busilacchio, B.M. Faroldi, L.M. Cornaglia, J. CO_2 Util. 42 (2020) 101328.
[249] Z. Gholami, Z. Tisler, V. Rubas, Catal. Rev. (2020) 1–84.
[250] S. Cimino, F. Boccia, L. Lisi, J. CO_2 Util. 37 (2020) 195–203.
[251] P. Panagiotopoulou, Appl. Catal. B Environ. 236 (2018) 162–170.
[252] T.K. Campbell, J.L. Falconer, Appl. Catal. 50 (1989) 189–197.
[253] D. Li, N. Ichikuni, S. Shimazu, T. Uematsu, Appl. Catal. A Gen. 172 (1998) 351–358.
[254] J. Ryczkowski, T. Borowiecki, Adsorpt. Sci. Technol. 9 (1998) 759–772.
[255] Z. Shi, H. Yang, P. Gao, X. Chen, H. Liu, L. Zhong, H. Wang, W. Wei, Y. Sun, Chinese, J. Catal. 39 (2018) 1294–1302.
[256] C. Vogt, J. Wijten, C.L. Madeira, O. Kerkenaar, K. Xu, R. Holzinger, B.M. Weckhuysen, M. Monai, ChemCatChem 12 (2020) 2792–2800.
[257] C. Liang, X. Hu, T. Wei, P. Jia, Z. Zhang, D. Dong, S. Zhang, Q. Liu, G. Hu, Int. J. Hydrog. Energy 44 (2019) 8197–8213.
[258] T.A. Le, T.W. Kim, S.H. Lee, E.D. Park, Catal. Today 303 (2018) 159–167.
[259] R.A. Iloy, K. Jalama, Catalysts 9 (2019) 807.
[260] M. Guo, G. Lu, RSC Adv. 4 (2014) 58171–58177.
[261] Z. Baysal, S. Kureti, Appl. Catal. B Environ. 262 (2020) 118300.
[262] X.F. Hu, W. Yang, N. Wang, S.Z. Luo, W. Chu, Adv. Mat. Res. 924 (2014) 217–226.
[263] X.L. Wang, Y.A.N.G. Meng, L.J. Zhu, X.N. Zhu, S.R. Wang, J. Fuel Chem. Technol. 48 (2020) 456–465.
[264] H. Lu, X. Yang, G. Gao, J. Wang, C. Han, X. Liang, C. Li, Y. Li, W. Zhang, X. Chen, Fuel 183 (2016) 335–344.
[265] J. Lin, C. Ma, Q. Wang, Y. Xu, G. Ma, J. Wang, H. Wang, C. Dong, C. Zhang, M. Ding, Appl. Catal. B Environ. 243 (2019) 262–272.
[266] X. Guo, H. He, A. Traitangwong, M. Gong, V. Meeyoo, P. Li, C. Li, Z. Peng, S. Zhang, Catal. Sci. 9 (2019) 5636–5650.
[267] J.M. Rynkowski, T. Paryjczak, A. Lewicki, M.I. Szynkowska, T.P. Maniecki, W.K. Jozwiak, React. Kinet, Catal. Lett. 71 (2000) 55–64.
[268] A. Alarcon, J. Guilera, R. Soto, T. Andreu, Appl. Catal. B Environ. 363 (2020) 118346.
[269] L. Zhang, L. Bian, Z. Zhu, Z. Li, Int. J. Hydrog. Energy 43 (2018) 2197–2206.
[270] G. Zhi, X. Guo, Y. Wang, G. Jin, X. Guo, Catal. Commun. 16 (2011) 56–59.

[271] X. Wang, L. Zhu, Y. Zhuo, Y. Zhu, S. Wang, A.C.S. Sustain, Chem. Eng. 7 (2019) 14647–14660.
[272] X. Lu, F. Gu, Q. Liu, J. Gao, Y. Liu, H. Li, L. Jia, G. Xu, Z. Zhong, F. Su, Fuel Process Technol. 135 (2015) 34–46.
[273] M.Y.S. Hamid, A.A. Jalil, A.F.A. Rahman, T.A.T. Abdullah, React, Chem. Eng. 4 (2019) 1126–1135.
[274] G. Wang, R. Luo, C. Yang, J. Song, C. Xiong, H. Tian, Z.J. Zhao, R. Mu, J. Gong, Sci China. Chem. 62 (2019) 1710–1719.
[275] T. Burger, F. Koschany, A. Wenng, O. Thomys, K. Kohler, O. Hinrichsen, Catal, Sci. Technol. 8 (2018) 5920–5932.
[276] S.V. Moghaddam, M. Rezaei, F. Meshkani, R. Daroughegi, Int. J. Hydrog. Energy 43 (2018) 16522–16533.
[277] K. Zhao, Z. Li, L. Bian, Front. Chem. Sci. Eng. 10 (2016) 273–280.
[278] W.L. Vrijburg, G. Garbarino, W. Chen, A. Parastaev, A. Longo, E.A. Pidko, E.J. Hensen, J. Catal. 382 (2020) 358–371.
[279] M. Guo, G. Lu, React. Kinet. Mech. Cat. 113 (2014) 101–113.
[280] H. Zhu, R. Razzaq, C. Li, Y. Muhmmad, S. Zhang, AIChE J. 59 (2013) 2567–2576.
[281] A. Isah, I. Akanyeti, A.A. Oladipo, React. Kinet. Mech. Cat. 130 (2020) 217–228.
[282] D.A. Ward, E.I. Ko, Ind. Eng. Chem 34 (1995) 421–433.
[283] D.P. Debecker, Chem. Rec. 18 (2018) 662–675.
[284] A.E. Danks, S.R. Hall, Z.J.M.H. Schnepp, Mater. Horiz. 3 (2016) 91–112.
[285] N.A. Buang, W.A. Bakar, F.M. Marsin, M.H. Razali, Malaysian J, Anal. Sci. 12 (2008) 217–223.
[286] M.A. Cauqui, J.M. Rodriguez-Izquierdo, J. Non-Cryst, Solids 147 (1992) 724–738.
[287] A. Kim, C. Sanchez, B. Haye, C. Boissiere, C. Sassoye, D.P. Debecker, A.C.S. Appl, Nano Mater. 2 (2019) 3220–3230.
[288] M. Campanati, G. Fornasari, A. Vaccari, Catal. Today 77 (2003) 299–314.
[289] T. Das, G. Deo, Catal. Today 198 (2012) 116–124.
[290] F.W. Chang, M.S. Kuo, M.T. Tsay, M.C. Hsieh, Appl. Catal. A Gen. 247 (2003) 309–320.
[291] Q. Pan, J. Peng, T. Sun, D. Gao, S. Wang, S. Wang, Fuel process Technol. 123 (2014) 166–171.
[292] H. Dong, Q. Liu, A.C.S. Sustain, Chem. Eng. 8 (2020) 6753–6766.
[293] M. Guo, G. Lu, Catal. Commun. 54 (2014) 55–60.
[294] A.J. Zarur, J.Y. Ying, Nature 403 (2000) 65–67.
[295] S. Shojaei, S.A. Hassanzadeh-Tabrizi, M. Ghashang, Ceram. Int. 40 (2014) 9609–9613.
[296] C. Stubenrauch, T. Wielputz, T. Sottmann, C. Roychowdhury, F.J. DiSalvo, Colloids Surf. A 317 (2008) 328–338.
[297] M.L. Firmansyah, A.A. Jalil, S. Triwahyono, H. Hamdan, M.M. Salleh, W.F.W. Ahmad, G.T.M. Kadja, Catal, Sci. Technol. 6 (2016) 5178–5182.
[298] M. Schwarze, T. Pogrzeba, I. Volovych, R. Schomäcker, Catal, Sci. Technol. 5 (2015) 24–33.
[299] D. Kumar, K.E. Neo, M.A. Rub, J. Surfactants Deterg. 19 (2016) 101–109.
[300] M.A. Rub, N. Azum, A.M. Asiri, J. Mol. Liq. 218 (2016) 595–603.
[301] T. Sheth, S. Seshadri, T. Prileszky, M.E. Helgeson, Nat. Rev. Mater. 5 (2020) 1–15.
[302] S. Hwang, U.G. Hong, J. Lee, J.G. Seo, J.H. Baik, D.J. Koh, H. Lim, I.K. Song, Ind. Eng. Chem. 19 (2013) 2016–2021.
[303] S. He, C. Li, H. Chen, D. Su, B. Zhang, X. Cao, B. Wang, M. Wei, D.G. Evans, X. Duan, Chem. Mater. 25 (2013) 1040–1046.
[304] L. He, Q. Lin, Y. Liu, Y. Huang, J. Energy Chem. 23 (2014) 587–592.
[305] R. Dębek, F. Azzolina-Jury, A. Travert, F. Mauge, F. Thibault-Starzyk, Catal. Today 337 (2019) 182–194.
[306] C.J. Lee, D.H. Lee, T. Kim, Catal. Today 293 (2017) 97–104.
[307] Z. Fan, K. Sun, N. Rui, B. Zhao, C.J. Liu, J. Energy Chem. 24 (2015) 655–659.
[308] C.H. Bartholomew, Appl. Catal. A Gen. 212 (2001) 17–60.
[309] M. Gotz, Methanisierung im Dreiphasen-Reaktor, Doctoral dissertation, Karlsruher Institut für Technologie (2014).
[310] G. Zhang, T. Sun, J. Peng, S. Wang, S. Wang, Appl. Catal A Gen. 462 (2013) 75–81.
[311] R.P. Struis, T.J. Schildhauer, I. Czekaj, M. Janousch, S.M. Biollaz, C. Ludwig, Appl. Catal A Gen. 362 (2009) 121–128.
[312] H. Harms, B. Hohlein, A. Skov, Chem. Ing. Tech. 52 (1980) 504–515.
[313] I. Hussain, A.A. Jalil, C.R. Mamat, T.J. Siang, A.F.A. Rahman, M.S. Azami, R.H. Adnan, Energy Convers. Manag. 199 (2019) 112056.
[314] J.R. Rostrup-Nielsen, K. Pedersen, J. Sehested, Appl. Catal. A Gen. 330 (2007) 134–138.
[315] C. Baumhakl, Substitute natural gas production with direct conversion of higher Hydrocarbons, Doctoral dissertation, Friedrich-Alexander-Universitat Erlangen-Nurnberg (2014).
[316] M.D. Argyle, C.H. Bartholomew, Catalysts 5 (2015) 145–269.
[317] C. Higman, B.G. Miller, D.A. Tillman (Eds.), Gasification in Combustion Engineering Issues for Solid Fuel Systems, Academic Press, Amsterdam, 2008, pp. 423–468.
[318] W. Boll, G. Hochgesand, W.D. Muller (Eds.), Methanation and methane synthesis, Ullmann's encyclopedia of industrial chemistry, Wiley-VCH Verlag GmbH & Co. KGaA, Weinheim, 2006, p. 85.
[319] B. Mutz, H.W. Carvalho, S. Mangold, W. Kleist, J.D. Grunwaldt, J. Catal. 327 (2015) 48–53.
[320] S. Kattel, P. Liu, J.G. Chen, J. Am. Chem. Soc. 139 (2017) 9739–9754.
[321] H. Yuan, X. Zhu, J. Han, H. Wang, Q. Ge, J. CO_2 Util. 26 (2018) 8–18.
[322] Y. Yang, J. Liu, F. Liu, D. Wu, Fuel 276 (2020) 118093.
[323] C. Liu, T.R. Cundari, A.K. Wilson, J. Phys. Chem. C 116 (2012) 5681–5688.
[324] D. Li, N. Ichikuni, S. Shimazu, T. Uematsu, Appl. Catal. A Gen. 180 (1999) 227–235.
[325] J. Wang, S. Funk, U. Burghaus, Catal. Lett. 103 (2005) 219–223.
[326] R.F. Hicks, A.T. Bell, J. Catal. 90 (1984) 205–220.
[327] J. Graciani, K. Mudiyanselage, F. Xu, A.E. Baber, J. Evans, S.D. Senanayake, D.J. Stacchiola, P. Liu, J. Hrbek, J.F. Sanz, J.A. Rodriguez, Science 345 (2014) 546–550.
[328] X.F. Yang, S. Kattel, S.D. Senanayake, J.A. Boscoboinik, X.W. Nie, J. Graciani, J.A. Rodriguez, P. Liu, D.J. Stacchiola, J.G.G. Chen, J. Am. Chem. Soc. 137 (2015) 10104.
[329] S. Kattel, B. Yan, Y. Yang, J.G. Chen, P. Liu, J. Am. Chem. Soc. 138 (2016) 12440–12450.
[330] X. Chen, X. Su, H.Y. Su, X. Liu, S. Miao, Y. Zhao, K. Sun, Y. Huang, T. Zhang, ACS Catal. 7 (2017) 4613–4620.
[331] S.G. Wang, X.Y. Liao, J.Hu.D.B. Cao, Y.W. Li, J. Wang, H. Jiao, Surf. Sci. 601 (2007) 1271–1284.
[332] S.G. Wang, D.B. Cao, Y.W. Li, J. Wang, H. Jiao, J. Phys. Chem. B 109 (2005) 18956–18963.
[333] J. Ren, H. Guo, J. Yang, Z. Qin, J. Lin, Z. Li, Appl. Surf. Sci. 351 (2015) 504–516.
[334] P. Bothra, G. Periyasamy, S.K. Pati, Phys. Chem. Chem. Phys. 15 (2013) 5701–5706.
[335] E. Vesselli, L. De Rogatis, X. Ding, A. Baraldi, L. Savio, L. Vattuone, M. Rocca, P. Fornasiero, M. Peressi, A. Baldereschi, R. Rosei, J. Am. Chem. Soc. 130 (2008) 11417–11422.
[336] D.E. Peebles, D.W. Goodman, J.M. White, J. Phys. Chem. 87 (1983) 4378–4387.
[337] J.L. Falconer, A.E. Zagli, J. Catal. 62 (1980) 280–285.
[338] M. Marwood, R. Doepper, A. Renken, Appl. Catal. A Gen. 151 (1997) 223–246.
[339] M.C. Roman-Martinez, D. Cazorla-Amoros, A. Linares-Solano, C.S.M. de Lecea, Appl. Catal. A Gen. 134 (1996) 159–167.
[340] P. Panagiotopoulou, D.I. Kondarides, X.E. Verykios, Catal. Today 181 (2012) 138–147.
[341] F. Wang, S. He, H. Chen, B. Wang, L. Zheng, M. Wei, D.G. Evans, X. Duan, J. Am. Chem. Soc. 138 (2016) 6298–6305.
[342] A. Erdohelyi, Catalysts 10 (2020) 155.
[343] C. Liang, L. Zhang, Y. Zheng, S. Zhang, Q. Liu, G. Gao, D. Dong, Y. Wang, L. Xu, X. Hu, Fuel 262 (2020) 116521.
[344] C. Liang, Z. Ye, D. Dong, S. Zhang, Q. Liu, G. Chen, C. Li, Y. Wang, X. Hu, Fuel 254 (2019) 115654.
[345] Z. Bian, Y.M. Chan, Y. Yu, S. Kawi, Catal. Today 347 (2018) 31–38.
[346] J. Ashok, M.L. Ang, S. Kawi, Catal. Today 281 (2007) 304–311.
[347] A. Westermann, B. Azambre, M.C. Bacariza, I. Graca, M.F. Ribeiro, J.M. Lopes, C. Henriques, Appl. Catal. B Environ. 174 (2015) 120–125.
[348] Q. Pan, J. Peng, S. Wang, S. Wang, Catal, Sci. Technol. 4 (2014) 502–509.
[349] H.Y. Kim, H.M. Lee, J.N. Park, J. Phys. Chem. C 114 (2010) 7128–7131.
[350] Y. Yan, Y. Dai, Y. Yang, A.A. Lapkin, Appl. Catal. B Environ. 337 (2018) 504–512.
[351] J. Huang, X. Li, X. Wang, X. Fang, H. Wang, X. Xu, J. CO_2 Util. 33 (2019) 55–63.
[352] E. Vesselli, M. Rizzi, L. De Rogatis, X. Ding, A. Baraldi, G. Comelli, L. Savio, L. Vattuone, M. Rocca, P. Fornasiero, A. Baldereschi, J. Phys. Chem. Letters 1 (2010) 402–406.
[353] L. Dietz, S. Piccinin, M. Maestri, J. Phys. Chem. C 119 (2015) 4959–4966.
[354] S. Kattel, W. Yu, X. Yang, B. Yan, Y. Huang, W. Wan, P. Liu, J.P. Chen, Angew Chem. Int. Ed. 55 (2016) 7968–7973.
[355] L. Liu, H. Yao, Z. Jiang, T. Fang, Appl. Surf. Sci. 451 (2018) 333–345.
[356] T. Avanesian, P. Christopher, ACS Catal. 6 (2016) 5268–5272.
[357] F.M. Mota, D.H. Kim, Chem. Soc. Rev. 48 (2019) 205–259.
[358] N. Apergis, J.E. Payne, Energy Econ. 31 (2009) 211–216.
[359] Transforming our World: The 2030 Agenda for Sustainable Development (2015). https://www.un.org/ga/search/view_doc.asp?symbol=A/RES/70/1%26Lang=E
[360] UNFCCC (United Nations Framework Convention on Climate Change) Paris Agreement (2015). https://unfccc.int/sites/default/files/english_paris_agreement.pdf
[361] A. Haines, P. Scheelbeek, Lancet 395 (2020) 1327–1329.
[362] HELMETH Project. http://www.helmeth.eu/index.php/project
[363] Electrochaea. http://www.electrochaea.com/technology/
[364] F. Kristjanpoller, A. Crespo, L. Barberá, P. Viveros, Renew. Energy 101 (2017) 301–310.
[365] C. Golling, R. Heuke, H. Seidl, J. Uhlig. Roadmap power-to-gas 2017. Berlin, https://www.powertogas.info/fileadmin/dena/Dokumente/Pdf/9215_Broschuere_Baustein_einer_Integrierten_Energiewende_Roadmap_Power_to_Gas.pdf.